frontiers | Research Topics

Radiation therapy using MRI-LINAC - the right way to start: a guide for physicians and physicists, volume II

Edited by
Enis Ozyar and Merav Ben-David

Published in
Frontiers in Oncology

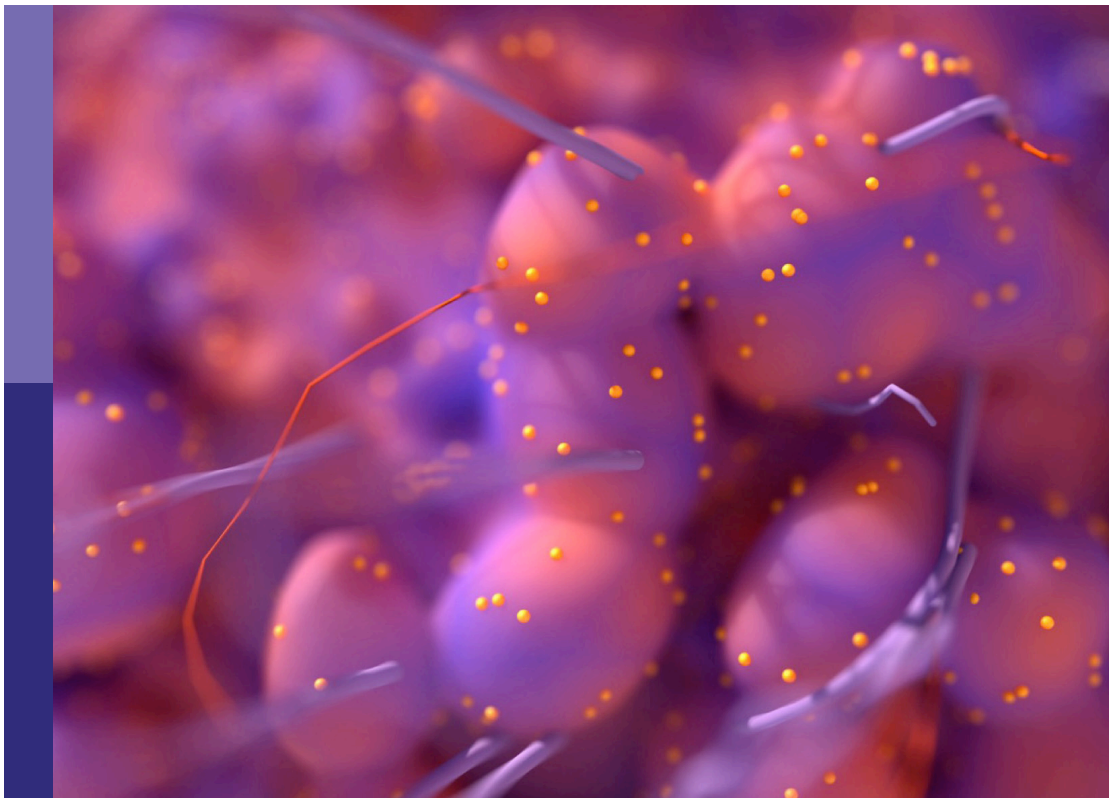

ISSN 1664-8714
ISBN 978-2-8325-5622-1
DOI 10.3389/978-2-8325-5622-1

About Frontiers

Frontiers is more than just an open access publisher of scholarly articles: it is a pioneering approach to the world of academia, radically improving the way scholarly research is managed. The grand vision of Frontiers is a world where all people have an equal opportunity to seek, share and generate knowledge. Frontiers provides immediate and permanent online open access to all its publications, but this alone is not enough to realize our grand goals.

Frontiers journal series

The Frontiers journal series is a multi-tier and interdisciplinary set of open-access, online journals, promising a paradigm shift from the current review, selection and dissemination processes in academic publishing. All Frontiers journals are driven by researchers for researchers; therefore, they constitute a service to the scholarly community. At the same time, the *Frontiers journal series* operates on a revolutionary invention, the tiered publishing system, initially addressing specific communities of scholars, and gradually climbing up to broader public understanding, thus serving the interests of the lay society, too.

Dedication to quality

Each Frontiers article is a landmark of the highest quality, thanks to genuinely collaborative interactions between authors and review editors, who include some of the world's best academicians. Research must be certified by peers before entering a stream of knowledge that may eventually reach the public - and shape society; therefore, Frontiers only applies the most rigorous and unbiased reviews. Frontiers revolutionizes research publishing by freely delivering the most outstanding research, evaluated with no bias from both the academic and social point of view. By applying the most advanced information technologies, Frontiers is catapulting scholarly publishing into a new generation.

What are Frontiers Research Topics?

Frontiers Research Topics are very popular trademarks of the *Frontiers journals series*: they are collections of at least ten articles, all centered on a particular subject. With their unique mix of varied contributions from Original Research to Review Articles, Frontiers Research Topics unify the most influential researchers, the latest key findings and historical advances in a hot research area.

Find out more on how to host your own Frontiers Research Topic or contribute to one as an author by contacting the Frontiers editorial office: frontiersin.org/about/contact

Radiation therapy using MRI-LINAC - the right way to start: a guide for physicians and physicists, volume II

Topic editors

Enis Ozyar — Acıbadem University, Türkiye

Merav Ben-David — Assuta Medical Center, Ramat-Hahayal, Israel

Citation

Ozyar, E., Ben-David, M., eds. (2024). *Radiation therapy using MRI-LINAC - the right way to start: a guide for physicians and physicists, volume II*.

Lausanne: Frontiers Media SA. doi: 10.3389/978-2-8325-5622-1

Table of contents

frontiers | Frontiers in Oncology

TYPE Editorial
PUBLISHED 17 October 2024
DOI 10.3389/fonc.2024.1487081

OPEN ACCESS

EDITED AND REVIEWED BY
Timothy James Kinsella,
Brown University, United States

*CORRESPONDENCE
Raphael M. Pfeffer
rephaelp@assuta.co.il

RECEIVED 27 August 2024
ACCEPTED 09 September 2024
PUBLISHED 17 October 2024

CITATION
Pfeffer RM, Oyzar E and David MAB (2024) Editorial: Radiation therapy using MRI-LINAC - the right way to start: a guide for physicians and physicists, volume II.
Front. Oncol. 14:1487081.
doi: 10.3389/fonc.2024.1487081

Editorial: Radiation therapy using MRI-LINAC - the right way to start: a guide for physicians and physicists, volume II

Raphael M. Pfeffer[1]*, Enis Oyzar[2] and Merav A. Ben David[1]

[1]Assuta Medical Center, Tel-Aviv, Israel, [2]Acıbadem University, Istanbul, Türkiye

KEYWORDS

stereotactic ablation body radiation therapy, MRgRT, radiation, oligometa, central lung tumors

Editorial on the Research Topic

Radiation therapy using MRI-LINAC - the right way to start: a guide for physicians and physicists, volume II

The second volume in this important series on applicating the novel MR guided radiotherapy technique follows on from the previous volume.

Editorial: Radiation therapy using MR-linac: Further studies

Image-guided radiation therapy (IGRT) based on 3-dimensional imaging has had a major impact on the advancement of radiotherapy in the past 50 years. Soon after the clinical introduction of computerized tomography (CT) it was employed in radiotherapy, in order to visualize internal organs and to calculate the volumes of the tumor target and internal organs close to the tumor which could be affected by the radiation dose (1). 3D imaging enabled the first studies of extracranial extreme hypofractionation, commonly called stereotactic body radiation therapy (SBRT) or stereotactic ablative radiation therapy (SABR). Timmerman et al. pioneered SBRT in early stage lung cancer (2). The success of SABR for lung cancer was made possible by the ability to accurately identify the tumor on CT imaging of the thorax. Further incremental improvements came with real-time imaging on the radiotherapy (RT) treatment table (e.g cone beam CT) ensuring control and accurate delivery of SBRT plans.

The application of SABR to mediastinal, abdominal and pelvic sites requires accurate and precise imaging of these areas as provided by magnetic resonance imaging (MRI). The first commercially available clinical MRI radiotherapy system began treating patients on a radioactive cobalt-based system in 2014 (3). Over the last 10 years there have been gradual developments in the delivery of MR guided RT, as the successful incorporation of Linac-based radiation into the ViewRay system and the development of rival machines such as the Elekta Unity. There are now over 100 installations of MR guided RT systems in the world. A PubMed search shows a steady increase in publications regarding MR Linac reaching over 200 per year in recent years.

This volume is the second in a series of frontiers dedicated to advances in the clinical use of MR guided radiotherapy. The articles can be divided into 2 overlapping broad categories, clinical experience and physics with quality assurance.

A single institution series of pancreatic cancer patients receiving MRgSBRT to the pancreas with 5- 10 Gy fractions shows the range of patients being treated today. The great majority have locally advanced inoperable disease. The series includes patients with locally recurrent disease following prior surgery or fractionated radiation and a few patients with oligo-progressive disease treated to both the primary and the oligometastasis. One of the difficulties of treating pancreatic tumors with MRgSBRT is the visualization of surrounding small bowel and real-time changes in organs at risk around the target tumor. Another paper reports on improved inter-observer contouring accuracy of pancreatic cancer MRI with the use of butylscopolamine prior to MRI.

A major advantage of MRguided radiotherapy is the ability to have real time tumor tracking to ensure coverage of the target and avoid toxicity of adjacent organs. Two papers describe novel methods of tracking. A case report of a nodal recurrence of endometrial cancer used real time tracking of isodose lines to deliver daily isotoxic doses. A single institute series of intrathoracic tumors who received MRgSBRT due to proximity to organs at risk showed the importance of real time tracking. A further study looked at gating protocols for apical lung lesions. Cardiac lesions close to the right ventricles are especially difficult to treat with focal radiotherapy and in this series there is a report of 2 patients safely treated with a dose of 30 Gy in 3 fractions of 10 Gy each.

A couple of papers described aspects in dosimetry of MR guided SBRT. One paper looked at techniques of delineation of gas packets and the impact of these gas packets using various dose and gas volume measurement protocols. Another paper reported on the benefits of online adaptation in the treatment of prostate cancer with MRgSBRT.

The addition of non-proprietary software upgrades to MRgRT planning programs requires meticulous QA. An online QA program to evaluate such upgrades is described.

In summary, the several papers in this volume describe a wide range of issues involved in implementing MRgSBRT and serve as an important addition to existing knowledge.

Author contributions

RP: Investigation, Writing – original draft, Writing – review & editing. EO: Investigation, Validation, Writing – original draft, Writing – review & editing. MD: Conceptualization, Writing – review & editing.

Conflict of interest

The authors declare that the research was conducted in the absence of any commercial or financial relationships that could be construed as a potential conflict of interest.

Publisher's note

References

1. Roberson PL, Lichter AS, Bodner A, et al. Dose to lung in primary breast irradiation. *Int J Radiat Oncol Biol Phys*. (1983) 9(1):97–102.

2. McGarry RC, Papiez L, Williams M, Whitford T, Timmerman RD. Stereotactic body radiation therapy of early-stage non-small-cell lung carcinoma: phase I study. *Int J Radiat Oncol Biol Phys*. (2005) 63(4):1010–5.

3. Mutic S, Dempsey JF. The viewray system: magnetic resonance-guided and controlled radiotherapy. *Semin Radiat Oncol*. (2014) 24:196–9.

frontiers | Frontiers in Oncology

TYPE Original Research
PUBLISHED 13 November 2023
DOI 10.3389/fonc.2023.1280836

OPEN ACCESS

EDITED BY
Enis Ozyar,
Acıbadem University, Türkiye

REVIEWED BY
Yoichi Watanabe,
University of Minnesota Twin Cities, United States
Gorkem Gungor,
Acibadem Maslak Hospital, Türkiye

*CORRESPONDENCE
Guenda Meffe
guenda.meffe@policlinicogemelli.it

RECEIVED 21 August 2023
ACCEPTED 27 October 2023
PUBLISHED 13 November 2023

CITATION
Nardini M, Meffe G, Galetto M, Boldrini L, Chiloiro G, Romano A, Panza G, Bevacqua A, Turco G, Votta C, Capotosti A, Moretti R, Gambacorta MA, Indovina L and Placidi L (2023) Why we should care about gas pockets in online adaptive MRgRT: a dosimetric evaluation. *Front. Oncol.* 13:1280836. doi: 10.3389/fonc.2023.1280836

Why we should care about gas pockets in online adaptive MRgRT: a dosimetric evaluation

Matteo Nardini[1], Guenda Meffe[1]*, Matteo Galetto[2], Luca Boldrini[1], Giuditta Chiloiro[1], Angela Romano[1], Giulia Panza[1], Andrea Bevacqua[1], Gabriele Turco[1], Claudio Votta[1], Amedeo Capotosti[1], Roberto Moretti[1], Maria Antonietta Gambacorta[1,2], Luca Indovina[1] and Lorenzo Placidi[1]

[1]Fondazione Policlinico Universitario "A. Gemelli" IRCCS, Rome, Italy, [2]Radiotherapy Department, Università Cattolica del Sacro Cuore, Rome, Italy

Introduction: Contouring of gas pockets is a time consuming step in the workflow of adaptive radiotherapy. We would like to better understand which gas pockets electronic densitiy should be used and the dosimetric impact on adaptive MRgRT treatment.

Materials and methods: 21 CT scans of patients undergoing SBRT were retrospectively evaluated. Anatomical structures were contoured: Gross Tumour Volume (GTV), stomach (ST), small bowel (SB), large bowel (LB), gas pockets (GAS) and gas in each organ respectively STG, SBG, LBG. Average HU in GAS was converted in RED, the obtained value has been named as Gastrointestinal Gas RED (GIGED). Differences of average HU in GAS, STG, SBG and LBG were computed. Three treatment plans were calculated editing the GAS volume RED that was overwritten with: air RED (0.0012), water RED (1.000), GIGED, generating respectively APLAN, WPLAN and the GPLAN. 2-D dose distributions were analyzed by gamma analysis. Parameter called active gas volume (AGV) was calculated as the intersection of GAS with the isodose of 5% of prescription dose.

Results: Average HU value contained in GAS results to be equal to -620. No significative difference was noted between the average HU of gas in different organ at risk. Value of Gamma Passing Rate (GPR) anticorrelates with the AGV for each plan comparison and the threshold value for GPR to fall below 90% is 41, 60 and 139 cc for WPLANvsAPLAN, GPLANvsAPLAN and WPLANvsGPLAN respectively.

Discussions: GIGED is the right RED for Gastrointestinal Gas. Novel AGV is a useful parameter to evaluate the effect of gas pocket on dose distribution.

KEYWORDS

gas pockets, relative electron density, MRgRT, online adaptive radiotherapy, dosimetry

1 Introduction

Online adaptive MRI-guided radiotherapy (MRgRT) has many advantages for the patient (1–5), one of the most important is the ability to provide a treatment plan that is best tailored to the daily anatomical situation of the patient. Online adaptive treatments involve a multidisciplinary approach in the MR-Linac treatment control room: Radiation Therapists (RTT) for positioning, Radiation Oncologists (RO) for recontouring and Medical Physicists (MP) for evaluating the eventual changes in electron density (ED) map that could affect plan recalculation, before re-optimize (if needed) the dose distribution. One of the tasks of MP is to verify the accuracy of the. This map is generated from the simulation CT and is used as a "ED-model" for the patient in the dose calculation process. The simulation CT, being performed a few days before the treatment, has a sensitivity to the day-to-day situation that can vary, as the patient may go through anatomical variations. Indeed, among the inter- and intra-fraction anatomical variations that may occur, the one that has the greatest effect on the electron density map, is the formation and displacement of abdominal and pelvic gas pockets. These can alter the patient's anatomy by displacing both targets and organs at risk (OAR) in their proximity (6), but most importantly creating interfaces with very different electron densities, affecting dose distribution (7–9). During the online adaptive workflow, MP is concerned, in the preliminary phase, with the recontouring volumes useful for dose optimization including gas pockets. In the current adaptive workflow, the simulation CT can be rigidly or deformably registered with the daily MRI scan to obtain the updated electron density map. In the rigid workflow it is obvious that the re-countouring of the gas pockets must be done manually, but this is also the case in the deformable workflow if the gas pockets deviate greatly in volume and position since the deformable image registration (DIR) algorithm cannot reproduce them correctly. Accurate and complete contouring of the gas pockets position and size plays an important role in the process of adaptive radiotherapy especially since its purpose is to provide a treatment plan that included the daily variation in electron densities due to daily anatomy changing. Contouring is still a time-consuming process, even with the aid of modern automatic contouring tools. Therefore, it is important to understand when contouring is necessary and when it can be overlooked. The present literature mainly focusing on the issue of the electron return effect (ERE) with phantoms studies, CTs with *ad-hoc* synthetic gas pockets and Monte Carlo simulations (7, 9–13). In the few clinical published papers, the authors describe the effect of gas pocket only varying the metrics of the dosimetric analysis in terms of gamma passing rate (GPR), or by conformation indices, or comparing dose volume histograms (DVHs) of targets and OARs, reporting also very different results (8, 14–16). With this study, we would like to gain a better understanding of the nature of electronic densities of gas pockets and their dosimetric impact on a MRgRT treatment in a hybrid 0.35 T MRI-Linac. The aims of this study are:

- to evaluate a CT-derived gas pockets RED, considering that in the clinical practice air RED is used for gas pockets RED override
- to evaluate the differences in gas pockets RED with the respect to the specific OARs in which they are contained
- to quantify the dosimetric impact (both on targets and OARs) of gastrointestinal (GI) gas pockets RED override with different REDs
- to define a quantitative parameter able to describe such dosimetric impact

2 Materials and methods

2.1 Evaluation of gas pockets relative electron density map

Twenty-one CT scans, one for each different patient undergoing SBRT for gastrointestinal lesion were retrospectively evaluated. All the scans were acquired using the radiotherapy department simulation CT scanner (Discovery Optima, GEhealthcare, Madison, WI) with the same standard GI protocol. Our center's protocol provides a CT acquisition with 120 kV, 135 mA, slice thickness 1.25 mm, in plane resolution 1.27 x 1.27 mm^2 and the maximum field of view for all GI patients. The following anatomical structures were contoured during the treatment planning process: Gross Tumour Volume (GTV) and relative 3 mm isotropic expansion (PTV), the Gastrointestinal Organs at Risk (GIOARs), including stomach (ST), small bowel (SB), large bowel (LB) and gas pockets in the abdominal cavity (GAS). Three additional specific volumes of gas pockets were also defined and contoured: the intersection of GAS volume with each GIOAR obtaining stomach gas volume (STG), small bowel gas volume (SBG) and large bowel gas volume (LBG) (Figure 1). We did not deem it appropriate to add the duodenum to the list of GIOARs containing gas pockets due to the scarcity of gases present within its lumen in the sample of patients analyzed. All contouring were performed by a radiation oncologist with at least 5 years of experience. The normality of the distribution of the mean values of the Hounsfield Units (HU) of pixels contained in GAS, STG, SBG and LBG volumes for all CT scans was tested singularly using a Kolmogorov-Smirnov test ($p=0.05$). Mean value of HU values of the pixels contained in GAS structure of all patients was converted in RED using the calibration curve of the CT scanner and the obtained value has been named as Gastrointestinal Gas relative Electron Density (GIGED). Finally, differences of mean values of HU of the pixels included in GAS, STG, SBG and LBG using a Wilcoxon-Mann-Whitney test for unpaired samples with a threshold p-value of 0.05 were computed.

2.2 Evaluation of dosimetric impact

For each patient, three different treatment plans were calculated starting from the same clinical plan. The same fluences of the clinical plan were re-computed without any plan optimization, only editing the GAS volume RED that was overwritten with:

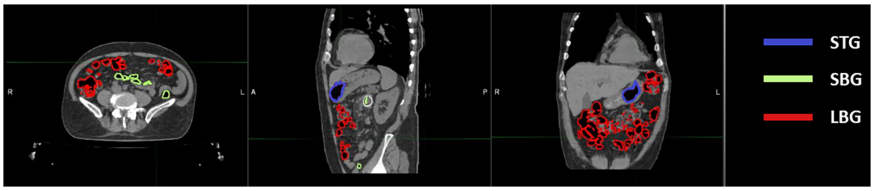

FIGURE 1
Location of abdominal gas volumes divided by the organ at risk in which they are located. A patient's CT is shown with gas pockets in the stomach highlighted in blue, those in the small bowel in green and those in the large bowel in red.

1 - the conventional AIR relative electron density value (0.0012, standard TPS value) (APLAN)

2 - the water electron density value (1.000) (WPLAN)

3 - the GIGED value (GPLAN)

generating respectively the APLAN, WPLAN and the GPLAN. WPLAN aims to simulate the extreme-case scenario of the patient presenting completely without air pockets. All clinical initial plans were calculated using the MRIdian (ViewRay Technologies Inc., Oakwood Village, OH) TPS by an experienced medical physicist. The planning was realized using the MRIdian Planning Technique (MPT) (17, 18) a particular technique for robust online adaptive planning. The plans were optimized using a standard template for the positioning and number of the Linac gantry angles. Twenty-four beams were equally distributed around the patient, except for two small sectors of about 20 degrees positioned at about 120 and 240 degrees where no radiation beams were present to avoid couch edges. All treatment plans dose prescriptions were at the 80% isodose and ranged from 35 to 40 Gy. Dose optimization for IMRT step-and-shoot treatments was then performed using the Kawrakow Monte Carlo (KMC) algorithm (19) on the MRIdian TPS (2500000 histories, dose grid 1.0 x 1.0 mm^2, 1% of recalculation uncertainty (20)). 2-D dose distributions obtained for APLAN, WPLAN and GPLAN were compared to each other in terms of gamma analysis (1%/1mm, threshold 10%) (21, 22).. The thresholds of the gamma analysis were chosen to be as tight as possible, being the calculation grid of both dose distributions of 1 mm and the recalculation error of the TPS being estimated at 1%. 2-D gamma analysis was performed separately for the three projections of dose on the three orthogonal planes passing through the centroid of the GTV. Mean value of the three relative gamma passing rates was then considered to evaluate differences in dose distribution. In addition, a parameter called active gas volume (AGV) was introduced and calculated as the intersection of the GAS structure with the isodose of 5% of prescription dose (Figure 2). AGV aims to evaluate and quantify the volume of gas invested by beam path. The Pearson correlation index was computed to verify the correlation between GPR values and the AGV parameter. Finally, DVH analysis was performed extracting the following values to assess dose distribution variation: the percentage volume of PTV covered by 95% of the prescription dose (PTV_V95), minimum dose to PTV as the isodose level that covers the 98% of the PTV volume (PTV_D98), the mean dose to PTV (PTV_D50) and the maximum dose to PTV as the isodose level that covers the 2% of the PTV volume (PTV_D2). Minimum, mean and maximum dose values were then extracted from DVH for the three GIOARs as done for the PTV. The differences of these extracted values for each plan comparison were computed and analyzed.

2.3 Dependence of electron return effect on relative electron density

In order to evaluate the dependence of the ERE on the electron density of the interfaces, we conducted a further in silico study. This evaluation better explain and support the obtained results. A Monte Carlo calculation was carried out using the MRIdian TPS (ViewRay Technologies Inc., Oakwood Village, OH) to evaluate the effect of a

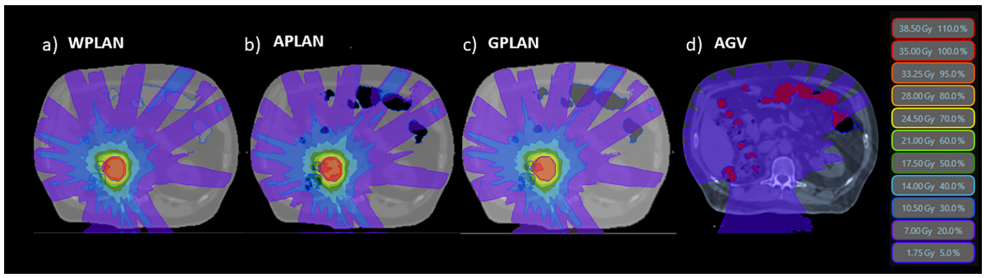

FIGURE 2
The three different dose distributions due to the recalculation of the treatment plan on the different electronic density maps generated by overwriting the volume of gas pockets with RED of water (**A** - WPLAN), RED of air (**B** - APLAN) and GIGED (**C** - GPLAN). In **D** we show the 5% prescription dose isodose intersecting the AIR structure defining the AGV parameter.

fixed conformal beam with a 10x10 cm^2 field size delivering 10 Gy at the isocentre onto a synthetic cubic phantom. The phantom consisted of a 30x30x30 cm^3 solid water block that has a medium interface inside which its relative electron density can be varied (Figure 3). The density-varying gap zone is located 7.5 cm from the top surface of the cubic phantom while the isocentre is 15 cm from the top surface. Eleven different dose distributions were calculated, with a dose grid resolution of 1.0x1.0 mm^2, by varying the relative electron density of the gap from air (0.0012) to water (1.0) in steps of 0.1. The axial projections of these dose distributions were compared to that obtained using the RED of air in terms of 2-D gamma analysis with 1%/1mm threshold. We also extracted the percentage dose depth (PDD) on the beam central axis for each calculated dose distribution in order to visualize the differences in terms of ERE.

3 Results

3.1 Evaluation of gas pockets relative electron density

The distribution of the mean values of the HU of pixels contained in both GAS, STG, SBG and LBG structures for all CT scans results to be normally distributed (p-values are 0.71, 0.46, 0.97, 0.94 respectively). Considering all 21 CT scans the mean HU value contained in of GAS structure results to be equal to -620 HU with a standard deviation (SD) of 90 HU. Regarding the different organs we have obtained (± SD in parenthesis) -610 (± 100) HU for LBG, -590 (± 180) HU for STG and -610 (± 80) HU for SBG. P-values of statistical test calculated for STG vs. LBG comparison is 0.62 while STG vs. SBG and SBG vs. LBG comparisons are 0.60 and 0.74 respectively (Figure 4).

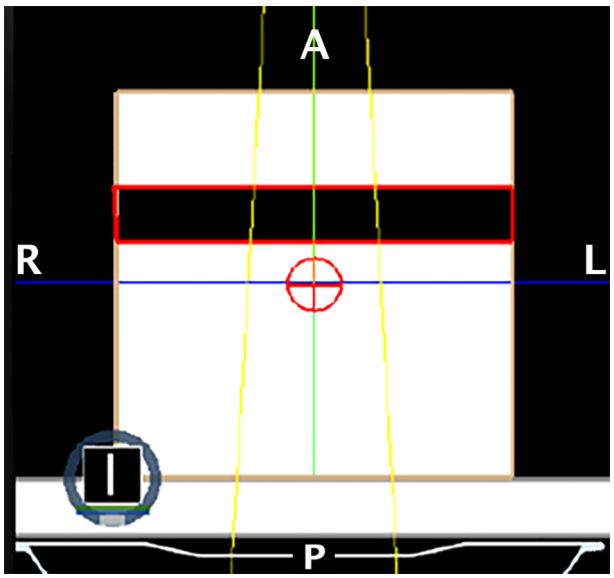

FIGURE 3
Setup of the phantom for the ERE dependency on the interface's RED experiment. The crosshair sign in red represents the isocenter of the single fixed conformal beam (in yellow). The dark zone contoured in red represents the gap with variable RED.

Linear fit of experimental data acquired in the calibration of the simulation CT scanner are reported in Figure 5 together with fit parameters. Only the part of the calibration curve between 0 and -1000 HU has been considered for this study. Linear fit was used to calculate the GIGED value that result to be equal to 0.38 for a HU value of -620.

3.2 Evaluation of dosimetric impact

Results for mean values of gamma passing rates (GPR) are summarized in Table 1 as well as the calculated values for AGV in cc. For the comparison of WPLAN and APLAN values of GPR range from 40% to 95% with a mean value of 81% while for WPLAN vs GPLAN values range from 69% to 100% with a mean value of 93%. For what concerns GPLAN vs APLAN we have a minimum value of GPR of 57% and a maximum of 96% for a mean value of 86%. Values are plotted in Figure 6 once sorted by increasing AGV value. In addition, we have added lines on the graph for a linear fit of the data for each comparison with the relative R squared value. Based on these linear fits, it's possible to interpolate, for each comparison, the threshold value of AGV for which the GPR falls below 90%, which is the GPR threshold value recommended by AAPM TG 218 for gamma tests for IMRT treatment plans with thresholds of 3% in dose difference and 2 mm distance to agreement (21). Those values result to be at least 41, 60 and 139 cc for WPLAN vs APLAN, GPLAN vs APLAN and WPLAN vs GPLAN respectively. Pearson's correlation coefficient between GPR and AGV results to be -0.97, -0.94 and -0.89 for WPLAN vs. GPLAN, WPLAN vs. APLAN and GPLAN vs. APLAN respectively, demonstrating a significant inverse correlation between the two variables. Differences in values extracted from DVH for each comparison of plans are summarized in Figures 7–9 (boxplot are shown without outliers). Figure 7 shows the DVH differences (D98, D50 and D2) in Gy for the three GIOARs evaluated that remain between -1.20 and 1.95 Gy. In Figure 8 are described the PTV's maximum, minimum and mean dose difference. In this case we find that difference values range from 0.50 to -4.13 Gy. Figure 9 shows difference in PTV coverage: values range between 1.01% to -21.75%. With regard to the patients analyzed, the GTV volume has an average value of 26.28 cc with a maximum of 74.7 cc and a minimum of 1.1 cc, the standard deviation is 18.66 cc. For the PTV we have an average of 42.67 cc with a maximum of 110.1 cc and a minimum of 3.0 cc, the standard deviation is 26.66 cc.

3.3 Dependence of electron return effect on relative electron density

The results of the gamma analysis performed are reported in Table 2. In the left column are reported the values of the density gap's RED in the phantom used for the study, while in the right column, the corresponding values of GPR for the comparison with

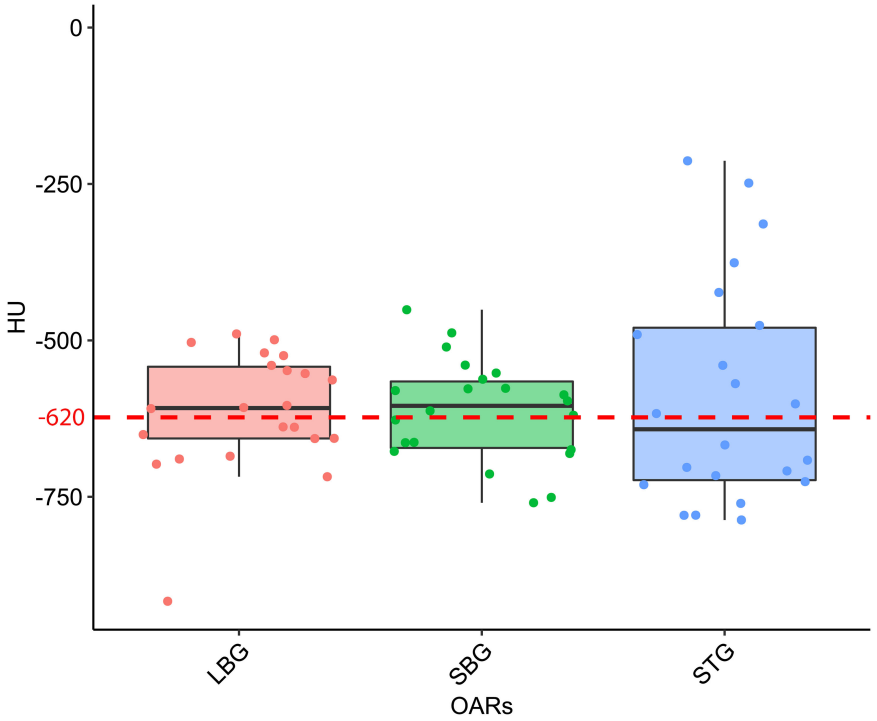

FIGURE 4
Boxplot distribution of the mean Hounsfield Units (HU) values distribution of the Large Bowel Gas (LBG), Small Bowel Gas (SBG) and Stomach Gas (STG) structures with their relative Wilcoxon test p-values. The dashed red line represents the mean HU value of the entire GAS structure, namely -620 HU.

the dose distribution calculated for the air's RED. The values change continuously from 68.3% for a RED of 0.1 to a value of 23.8% for a RED of 1.0. The trend of GPR values as a function of RED is plotted in panel "a" of Figure 10: the greatest variation in GPR occurs between the values of 0.1 and 0.3 of RED, with a difference of approximately 37%, while at higher RED values, GPR remains nearly constant. In panels "b" and "c" of Figure 10 are reported the axial projections of the dose distribution calculated for REDs of

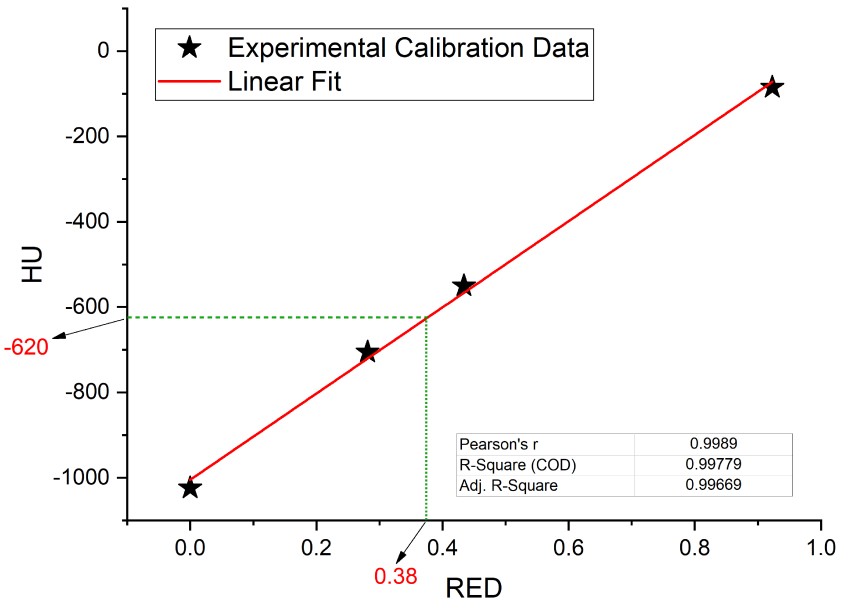

FIGURE 5
Interpolated value for relative electron densities (RED) from the mean value of Hounsfield Units (HU) contained in GAS volume, interpolation on linear fit (red line) of experimental data collected in the simulation CT calibration curve.

TABLE 1 Values of the average gamma passing rate (GPR) (1%, 1mm) for comparisons between plan calculated overwriting gas pockets electron density with water's one (WPLAN), air's one (APLAN) and the one calculated in this study (GPLAN) for all patients analyzed.

Mean GPR (1%,1mm)				
Patient ID	WPLAN vs APLAN	WPLAN vs GPLAN	GPLAN vs APLAN	AGV (cc)
Patient 1	73%	89%	83%	224.58
Patient 2	94%	100%	93%	0.36
Patient 3	94%	99%	92%	20.43
Patient 4	83%	96%	86%	62.47
Patient 5	78%	87%	85%	178.49
Patient 6	84%	94%	85%	58.44
Patient 7	90%	99%	91%	40.04
Patient 8	70%	88%	81%	135.64
Patient 9	79%	90%	86%	137.2
Patient 10	87%	98%	86%	24.26
Patient 11	87%	94%	90%	129.71
Patient 12	91%	98%	91%	35.44
Patient 13	95%	100%	92%	16.46
Patient 14	94%	98%	96%	20.94
Patient 15	70%	86%	81%	162.14
Patient 16	69%	86%	80%	183.48
Patient 17	75%	94%	83%	91.87
Patient 18	40%	69%	57%	432.63
Patient 19	92%	99%	91%	26.72
Patient 20	91%	95%	95%	49.09
Patient 21	70%	85%	79%	172.98

Mean GPR is the result of averaging the individual 2-D GPRs calculated in the three orthogonal planes passing through the centroid of the GTV. In the last column the value of the active gas volume (AGV) (in cc) parameter calculated as the intersection of the GAS structure with the 5% prescription dose isodose.

0.1 and 1.0, respectively, showing how ERE changes the dose distribution. Figure 11 shows the central axis dose rate (CAX), normalised to the global maximum value, as a function of the distance from the isocentre of the radiation beam. The various curves with different colours relate to the different RED values of the gap. For RED values between 0.0012 and 0.4 the distortions due to ERE are less evident as the RED increases, while for the value of 0.5 (dark blue solid line) the graph already overlaps almost exactly with the curve relative to the RED value of water (dashed orange line). Higher RED values are not plotted in the graph for clarity.

4 Discussion

4.1 Gas pockets RED

Considering the results obtained in the session on the evaluation of gas pockets RED, we demonstrated that the gas contained in the examined OARs does not show statistically significant difference in terms of RED. It therefore turns out to be a legitimate choice to treat the GAS volume as a single volume and to define its RED by taking the average value of the HUs relative to the pixels contained in the GAS volume. The result shows that the RED of the intestinal GAS pockets should not set equal to air's RED but a higher RED (0.38). All the previously published studies suggested to overwrite the electronic densities of the daily recontoured gas pockets with RED of air. Such approach increase the uncertainty in the daily adapted dose recalculation since the RED of air is an order of magnitude lower than that of the gas pockets (8, 14, 15). In Figure 6, the fits have no pretensions to assert that the model describing the trend of GPR vs. AGV is linear, although the trend has an acceptable R^2 in the case of WPLAN vs. GPLAN. Nevertheless, it graphically visualizes the decreasing trend of the GPR function when AGV increases. In the comparison between the recalculated plan with water RED (WPLAN) and the one overwriting the gas pockets RED with GIGED (GPLAN), it is found that the gamma passing rate drops below 90% when the AGV is greater than 139 cc. Therefore, considering the results of this study, it is our opinion that overwriting the RED of gas pockets with air RED can lead to a dosimetric error and should be better to

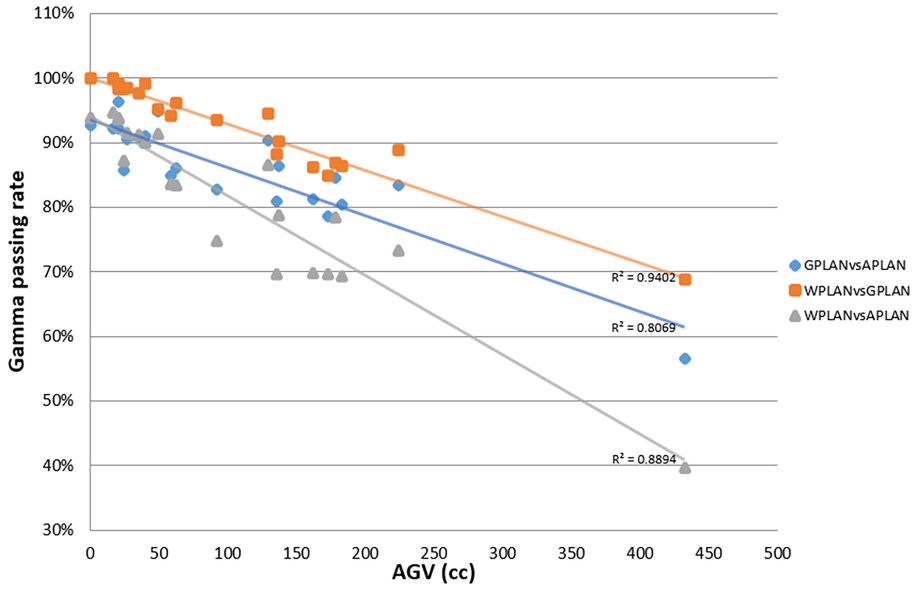

FIGURE 6
Plot of gamma passing rate (GPR) trend as a function of active gas volume (AGV) parameter (in cc) for comparisons between plan calculated overwriting gas pockets electron density with water's one (WPLAN), air's one (APLAN) and the one calculated in this study (GPLAN). The solid line represents the linear fit and the relative R2 values are shown (GPLAN vs. APLAN in blue, WPLAN vs. GPLAN in orange and WPLAN vs. APLAN in grey).

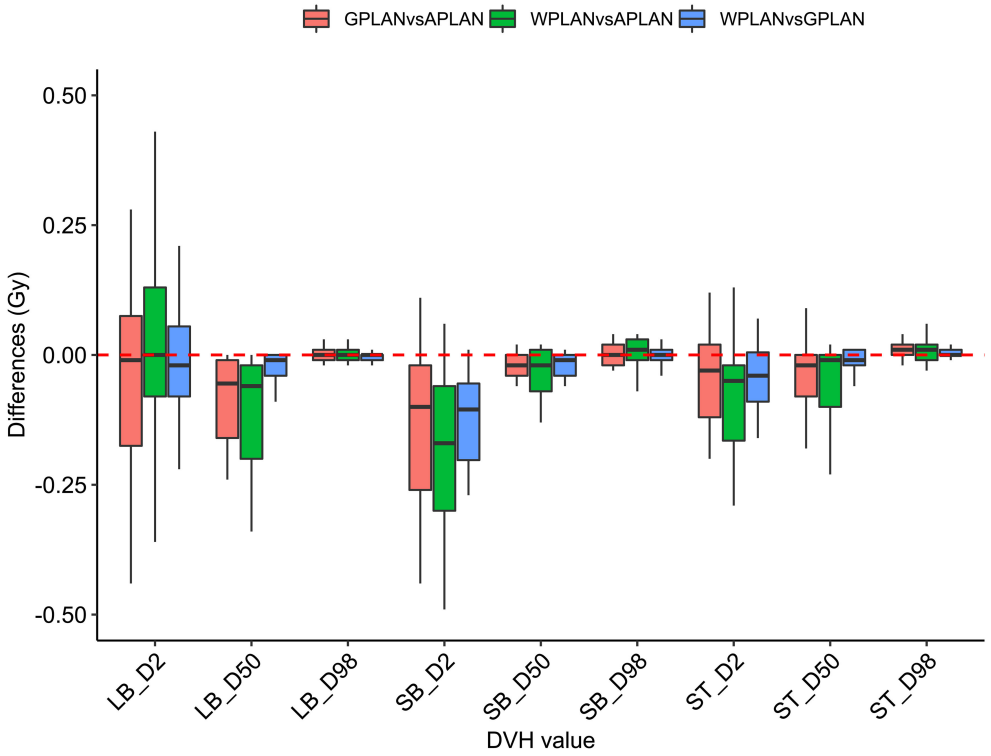

FIGURE 7
Boxplots of the distributions of the differences (in Gy) in the dose volume histogram (DVH) extracted values for D2, D50 and D98 of different organs at risk (large bowel (LB), small bowel (SB) and stomach (ST)) for different plan comparisons (in red GPLAN vs. APLAN, in green WPLAN vs. APLAN and in blue WPLAN vs. GPLAN).

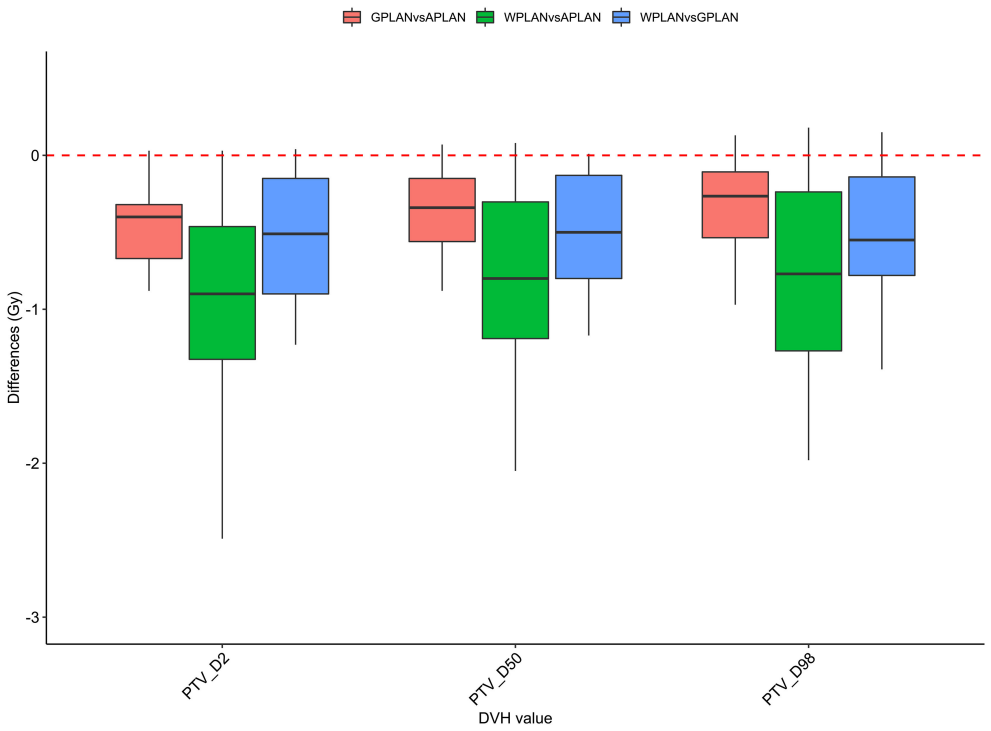

FIGURE 8
Boxplots of the distributions of the differences (in Gy) in the dose volume histogram (DVH) extracted values for D2, D50 and D98 of PTV for the different plan comparisons (in red GPLAN vs. APLAN, in green WPLAN vs. APLAN and in blue WPLAN vs. GPLAN).

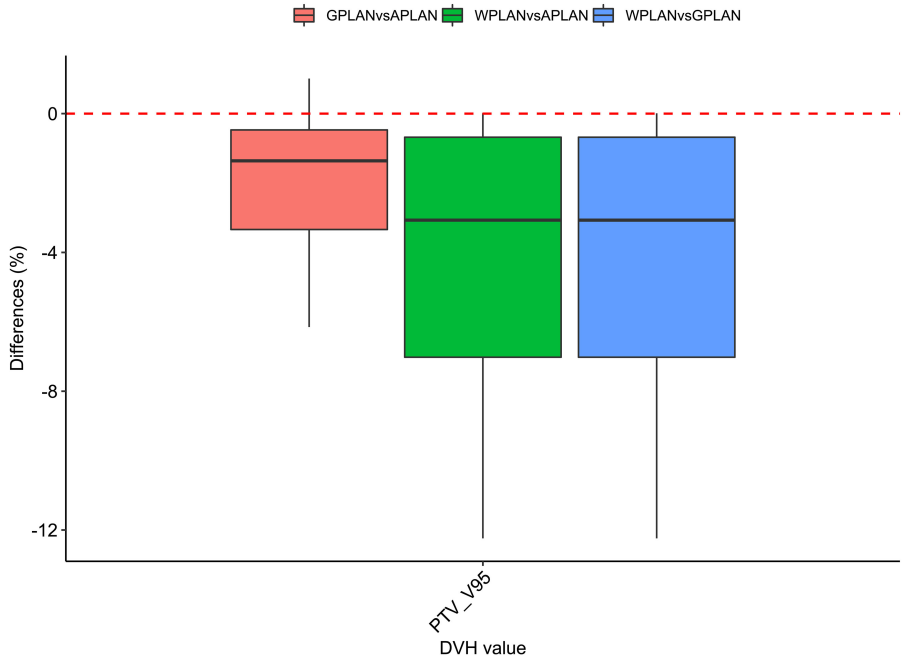

FIGURE 9
Boxplots of the distributions of the percentage differences in the dose volume histogram (DVH) extracted values for V95 of PTV for the different plan comparisons (in red GPLAN vs. APLAN, in green WPLAN vs. APLAN and in blue WPLAN vs. GPLAN).

TABLE 2 Values of the GPR of the 2-D gamma analysis for comparison between variable RED dose distribution and Air RED dose distribution.

RED	GPR
0.1	68.30%
0.2	39.60%
0.3	30.80%
0.4	29.30%
0.5	29.70%
0.6	28.50%
0.7	25.20%
0.8	24.50%
0.9	23.60%
1	23.80%

Dose distribution have been calculated by Monte Carlo using a synthetic phantom (Figure 3).

overwrite it with GIGED. The greater the AGV, the greater the dosimetric error will be.

4.2 Dosimetric analysis

Considering the three trend lines shown in Figure 6, the one with the steepest slope is the one comparing WPLAN and APLAN due to the relevant difference in the REDs used. When compared GPLAN and APLAN, and WPLAN and GPLAN, the slopes are less steep: indeed GIGED is about in the middle between the REDs of air and water. Considering the results obtained in this work in our study concerning the dependence of ERE on the RED of the gap, it can also be understood how, depending primarily on ERE, the difference between GPLAN and APLAN is greater than the difference between GPLAN and WPLAN even though the difference between GIGED and air RED is less than between GIGED and water RED. These differences are also reinforced in Figures 7–9 where the WPLAN vs. APLAN comparison (in green) always shows the highest absolute values. Figure 7 depicts and highlights that the largest differences are found in the high and medium dose regions. For low dose region a minor variance is visible and the results show no differences. Differences of the maximum, mean, and minimum dose have a negative trend in the PTV, as well as the target coverage which decreases as the RED of the GAS volume decreases. At present, we cannot justify why, quite counterintuitively, it would appear that the difference in the very high dose zone (PTV) is smaller between APLAN and GPLAN than between GPLAN and WPLAN, although it must be said that these differences are not statistically significant. Further investigation is needed to unravel this interesting topic.

4.3 Comparison with past studies and future implications

Estabrook et al. (16) recalculated the dose distribution using a daily CBCTs, founding an average reduction in target coverage of 3.3%. This target coverage reduction is comparable to the one found in this work, although they found no correlation between the dose covering the 100% of the PTV and the volume of gas pockets. Jin et al. (14) proposed a retrospective MRgRT analysis on 5 cases of pancreatic cancer patients in which the treatment plans of each fraction are recalculated using gas volume contours on the MRs and overwritten with air density. In this paper, the results obtained describe the variation of dosimetric parameters based on intra-fraction variations in the volume and position of the gas pockets. As

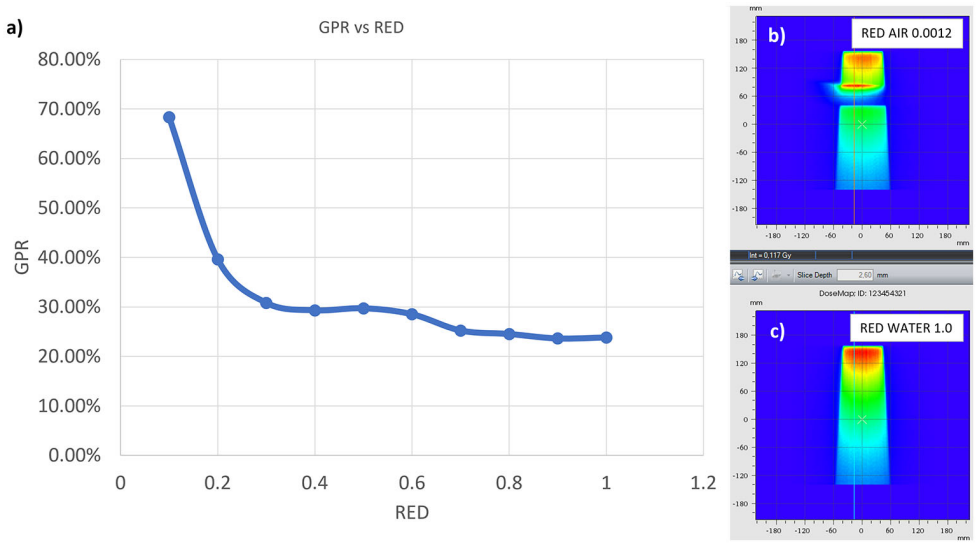

FIGURE 10
GPR trend as a function of the RED of the interface in the synthetic phantom **(A)**. In **(B, C)** the axial projection of the dose distribution in the phantom generated by a 10x10 cm^2 field in the presence of an air gap **(B)** and with the gap filled with water **(C)**.

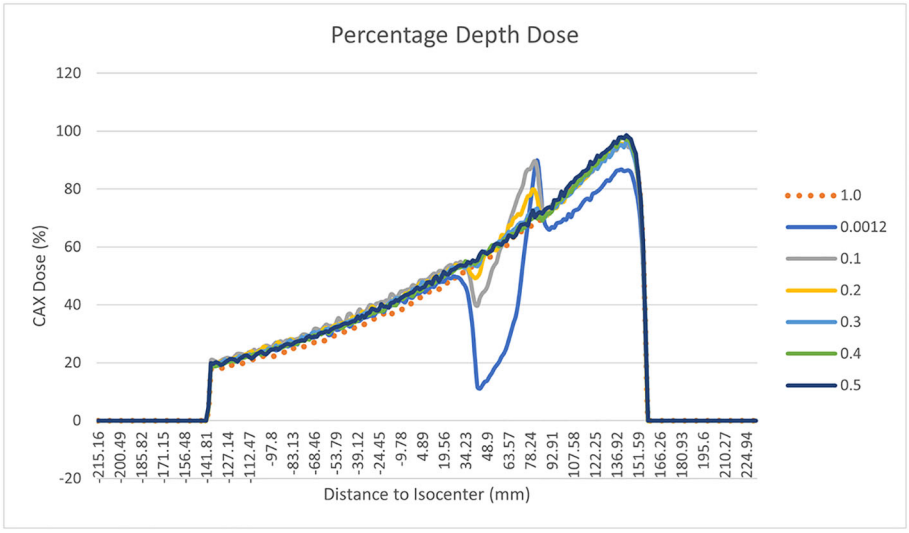

FIGURE 11
Percentage Depth Dose trend measured on the central field axis and normalised to the maximum dose for different RED of the gap of the synthetic phantom. The various curves with different colours relate to the different RED values of the gap. In particular the orange dotted line is related to water's RED value.

far as the PTV is concerned, no significant dosimetric changes were found, with a maximum change of 1 Gy in absolute dose. Jin et al. do not present any data or analysis to evaluate the dosimetric impact as a function of the volume variations of the gas pockets. The work carried out by Su et al. within the framework of the SMART protocol (23), reports the results obtained in a dosimetric study where air pockets were recontoured during adaptive MRgRT of 30 patients undergoing SBRT on pancreas in 5 fractions. Homogeneity index (HI), Conformity Index (CI) and Conformity Number (15) are compared for the resulting plans that benefited from the recontouring of gas pockets with the corresponding correction of the electron densities and those that were calculated leaving the CT uncorrected. The reported differences, in terms of D98, D95, D50 and D2 for both PTV and GTV, are not significant. Also in the study by Su et al., no correlations between gas pockets and dosimetric variation has been found. This is due to the small gas volume variation (order of a few cc) that do not allow a direct comparison with our study. This study has some limitations that have to be considered. The number of patients enrolled in this study could be increased even if it a well representative dataset for such analysis, also in comparison within the published literature. Afterwards, the results obtained in this study are related to the calibration curve of the simulation CT of our center: it could be interesting to extend the analysis to other centers. Obviously, with the advent of synthetic CT (24, 25), the considerations and results obtained may be overcome as this technology will allow an automatic, fast and accurate electronic densities correction based on to the daily anatomy although no algorithms sophisticated enough to generate synthetic CTs from MR scans that accurately reproduce the position and volume of both abdominal and pelvic gas pockets can be found in the state of the art. In conclusion this study, as far as our knowledge, is the first that provide a quantitative parameter for correlation between gas pocket s' volume and its dosimetric effect. No difference in terms of HU for the gas contained in the various GI organs was found and the average HU value is -620 which corresponds to a RED of 0.38 (GIGED), according to our center's simulation CT calibration curve. The dosimetric results showed that correlations are found between the reduction of the gamma passing rate and the value of the measured AGV. Therefore, AGV is a useful parameter to evaluate the effect of gas pocket on the clinical dose distribution in MRgRT GI treatments. In particular, we found that, using the gamma passing rate metric, a difference of 139 cc of AGV is sufficient to create a significant difference in dose. This value could be used as a threshold for deciding whether or not to recontour gas volumes in the abdomen during an online adaptive workflow.

Data availability statement

The raw data supporting the conclusions of this article will be made available by the authors, without undue reservation.

Ethics statement

Ethical approval was not required for the study involving humans in accordance with the local legislation and institutional requirements. Informed consent was obtained from all individual participants included in the study.

Author contributions

MN: Conceptualization, Data curation, Investigation, Methodology, Writing – original draft, Formal Analysis, Project

administration. GM: Validation, Visualization, Writing – review & editing. MG: Data curation, Formal Analysis, Methodology, Validation, Writing – review & editing. LB: Supervision, Validation, Visualization, Writing – review & editing. GC: Supervision, Validation, Visualization, Writing – review & editing. AR: Supervision, Validation, Visualization, Writing – review & editing. GP: Supervision, Validation, Visualization, Writing – review & editing. AB: Data curation, Formal Analysis, Investigation, Writing – review & editing. GT: Data curation, Supervision, Validation, Visualization, Writing – review & editing. CV: Data curation, Supervision, Validation, Visualization, Writing – review & editing. AC: Supervision, Validation, Visualization, Writing – review & editing. RM: Supervision, Validation, Visualization, Writing – review & editing. MAG: Supervision, Validation, Visualization, Writing – review & editing. LI: Supervision, Validation, Visualization, Writing – review & editing. LP: Conceptualization, Funding acquisition, Methodology, Project administration, Resources, Supervision, Validation, Visualization, Writing – review & editing.

Funding

The author(s) declare that no financial support was received for the research, authorship, and/or publication of this article.

Conflict of interest

The authors declare that the research was conducted in the absence of any commercial or financial relationships that could be construed as a potential conflict of interest.

Publisher's note

References

1. Kerkmeijer LGW, Valentini V, Fuller CD(, Slotman BJ. Editorial: online adaptive MR-guided radiotherapy. *Front Oncol* (2021) 11. doi: 10.3389/fonc.2021.748685

2. Kerkmeijer LGW, Kishan AU, Tree AC. Magnetic resonance imaging-guided adaptive radiotherapy for urological cancers: what urologists should know. *Eur Urol* (2022) 82(2):149–51. doi: 10.1016/j.eururo.2021.12.019

3. Boldrini L, Corradini S, Gani C, Henke L, Hosni A, Romano A, et al. MR-guided radiotherapy for liver Malignancies. *Front Oncol* (2021) 11:616027. doi: 10.3389/fonc.2021.616027

4. Witt JS, Rosenberg SA, Bassetti MF. MRI-guided adaptive radiotherapy for liver tumours: visualising the future. *Lancet Oncol* (2020) 21(2):e74–82. doi: 10.1016/S1470-2045(20)30034-6

5. Boldrini L, Cusumano D, Cellini F, Azario L, Mattiucci GC, Valentini V. Online adaptive magnetic resonance guided radiotherapy for pancreatic cancer: state of the art, pearls and pitfalls. *Radiat Oncol Lond Engl* (2019) 14(1):71. doi: 10.1186/s13014-019-1275-3

6. McDermott LN, Wendling M, Sonke JJ, van Herk M, Mijnheer BJ. Anatomy changes in radiotherapy detected using portal imaging. *Radiother Oncol* (2006) 79 (2):211–7. doi: 10.1016/j.radonc.2006.04.003

7. Shortall J, Vasquez Osorio E, Chuter R, Green A, McWilliam A, Kirkby K, et al. Characterizing local dose perturbations due to gas cavities in magnetic resonance-guided radiotherapy. *Med Phys* (2020) 47(6):2484–94. doi: 10.1002/mp.14120

8. Pham J, Cao M, Yoon SM, Gao Y, Kishan AU, Yang Y. Dosimetric effects of air cavities for MRI-guided online Adaptive Radiation Therapy (MRgART) of prostate bed after radical prostatectomy. *J Clin Med* (2022) 11(2):364. doi: 10.3390/jcm11020364

9. Godoy Scripes P, Subashi E, Burleson S, Liang J, Romesser P, Crane C, et al. Impact of varying air cavity on planning dosimetry for rectum patients treated on a 1.5 T hybrid MR-linac system. *J Appl Clin Med Phys* (2020) 21(7):144–52. doi: 10.1002/acm2.12903

10. Uilkema S, van der Heide U, Sonke JJ, Moreau M, van Triest B, Nijkamp J. A 1.5 T transverse magnetic field in radiotherapy of rectal cancer: Impact on the dose distribution. *Med Phys* (2015) 42(12):7182–9. doi: 10.1118/1.4936097

11. Cusumano D, Teodoli S, Greco F, Fidanzio A, Boldrini L, Massaccesi M, et al. Experimental evaluation of the impact of low tesla transverse magnetic field on dose distribution in presence of tissue interfaces. *Phys Med PM Int J Devoted Appl Phys Med Biol Off J Ital Assoc BioMed Phys AIFB* (2018) 53:80–5. doi: 10.1016/j.ejmp.2018.08.007

12. Shortall J, Vasquez Osorio E, Aitkenhead A, Berresford J, Agnew J, Budgell G, et al. Experimental verification the electron return effect around spherical air cavities for the MR-Linac using Monte Carlo calculation. *Med Phys Jun* (2020) 47(6):2506–15. doi: 10.1002/mp.14123

13. Shortall J, Osorio EV, Cree A, Song Y, Dubec M, Chuter R, et al. Inter- and intra-fractional stability of rectal gas in pelvic cancer patients during MRIgRT. *Med Phys* (2021) 48(1):414–26. doi: 10.1002/mp.14586

14. Jin H, Kim DY, Park JM, Kang HC, Chie EK, An HJ. Dosimetric effects of air pocket during magnetic resonance-guided adaptive radiation therapy for pancreatic cancer. *Prog Med Phys* (2019) 30(4):104–11. doi: 10.14316/pmp.2019.30.4.104

15. Su C, Okamoto H, Nishioka S, Sakasai T, Fujiyama D, Miura Y, et al. Dosimetric effect of the intestinal gas of online adaptive stereotactic body radiotherapy on target and critical organs without online electron density correction for pancreatic cancer. *Br J Radiol* (2021) 94(1119):20200239. doi: 10.1259/bjr.20200239

16. Estabrook NC, Corn JB, Ewing MM, Cardenes HR, Das IJ. Dosimetric impact of gastrointestinal air column in radiation treatment of pancreatic cancer. *Br J Radiol* (2017) 91:20170512. doi: 10.1259/bjr.20170512

17. Nardini M, Placidi L. Chapter 6 - Robust online adaptive planning: Toward a uniform MR-LINAC treatment planning technique. In: Ozyar E, Onal C, Hackett SL, editors. *Advances in Magnetic Resonance Technology and Applications*. Cambridge, Massachusetts: Academic Press (2022). p. 101–22. Available at: https://www.sciencedirect.com/science/article/pii/B978032391689900025X. MR Linac Radiotherapy; vol. 8.

18. Placidi L, Nardini M, Cusumano D, Boldrini L, Chiloiro G, Romano A, et al. VMAT-like plans for magnetic resonance guided radiotherapy: Addressing unmet needs. *Phys Med* (2021) 85:72–8. doi: 10.1016/j.ejmp.2021.05.002

19. Kawrakow I, Fippel M. Investigation of variance reduction techniques for Monte Carlo photon dose calculation using XVMC. *Phys Med Biol* (2000) 45(8):2163–83. doi: 10.1088/0031-9155/45/8/308

20. Wang Y, Mazur TR, Green O, Hu Y, Li H, Rodriguez V, et al. A GPU-accelerated Monte Carlo dose calculation platform and its application toward validating an MRI-guided radiation therapy beam model. *Med Phys* (2016) 43(7):4040–52. doi: 10.1118/1.4953198

21. Miften M, Olch A, Mihailidis D, Moran J, Pawlicki T, Molineu A, et al. Tolerance limits and methodologies for IMRT measurement-based verification QA: Recommendations of AAPM Task Group No. 218. *Med Phys* (2018) 45(4):e53–83. doi: 10.1002/mp.12810

22. Low DA, Dempsey JF. Evaluation of the gamma dose distribution comparison method. *Med Phys* (2003) 30(9):2455–64. doi: 10.1118/1.1598711

23. Parikh PJ, Lee P, Low DA, Kim J, Mittauer KE, Bassetti MF, et al. A multi-institutional phase 2 trial of ablative 5-fraction stereotactic magnetic resonance-guided on-table adaptive radiation therapy for borderline resectable and locally advanced pancreatic cancer. *Int J Radiat Oncol Biol Phys* (2023) 117(4):799–808. doi: 10.1016/j.ijrobp.2023.05.023

24. Cusumano D, Lenkowicz J, Votta C, Boldrini L, Placidi L, Catucci F, et al. A deep learning approach to generate synthetic CT in low field MR-guided adaptive radiotherapy for abdominal and pelvic cases. *Radiother Oncol J Eur Soc Ther Radiol Oncol* (2020) 153:205–12. doi: 10.1016/j.radonc.2020.10.018

25. Lenkowicz J, Votta C, Nardini M, Quaranta F, Catucci F, Boldrini L, et al. A deep learning approach to generate synthetic CT in low field MR-guided radiotherapy for lung cases. *Radiother Oncol J Eur Soc Ther Radiol Oncol* (2022) 176:31–8. doi: 10.1016/j.radonc.2022.08.028

frontiers | Frontiers in Oncology

TYPE Original Research
PUBLISHED 23 November 2023
DOI 10.3389/fonc.2023.1280845

OPEN ACCESS

EDITED BY
Enis Ozyar,
Acıbadem University, Türkiye

REVIEWED BY
Stefano Vagge,
Ente Ospedaliero Ospedali Galliera, Italy
Raees Tonse,
Baptist Hospital of Miami, United States

*CORRESPONDENCE
Matteo Nardini
matteo.nardini@policlinicogemelli.it

RECEIVED 21 August 2023
ACCEPTED 07 November 2023
PUBLISHED 23 November 2023

CITATION
Galetto M, Nardini M, Capotosti A, Meffe G, Cusumano D, Boldrini L, Chiloiro G, Romano A, Votta C, Gambacorta MA, Indovina L and Placidi L (2023) Motion and dosimetric criteria for selecting gating technique for apical lung lesions in magnetic resonance guided radiotherapy. *Front. Oncol.* 13:1280845. doi: 10.3389/fonc.2023.1280845

Motion and dosimetric criteria for selecting gating technique for apical lung lesions in magnetic resonance guided radiotherapy

Matteo Galetto[1,2], Matteo Nardini[2]*, Amedeo Capotosti[2], Guenda Meffe[2], Davide Cusumano[3], Luca Boldrini[2], Giuditta Chiloiro[2], Angela Romano[2], Claudio Votta[2], Maria A. Gambacorta[1,2], Luca Indovina[2] and Lorenzo Placidi[2]

[1]Radiotherapy Department, Università Cattolica del Sacro Cuore, Roma, Italy, [2]Radiotherapy Department, Fondazione Policlinico Universitario A. Gemelli IRCCS, Roma, Italy, [3]Unità Operativa Semplice (UOS), Fisica Medica – Mater Olbia Hospital, Olbia, Italy

Introduction: Patients treatment compliance increases during free-breathing (FB) treatment, taking generally less time and fatigue with respect to deep inspiration breath-hold (DIBH). This study quantifies the gross target volume (GTV) motion on cine-MRI of apical lung lesions undergoing a SBRT in a MR-Linac and supports the patient specific treatment gating pre-selection.

Material and methods: A total of 12 patients were retrospectively enrolled in this study. During simulation and treatment fractions, sagittal 0.35 T cine-MRI allows real-time GTV motion tracking. Cine-MRI has been exported, and an in-house developed MATLAB script performed image segmentation for measuring GTV centroid position on cine-MRI frames. Motion measurements were performed during the deep inspiration phase of DIBH patient and during all the session for FB patient. Treatment plans of FB patients were reoptimized using the same cost function, choosing the 3 mm GTV-PTV margin used for DIBH patients instead of the original 5 mm margin, comparing GTV and OARs DVH for the different TP.

Results: GTV centroid motion is <2.2 mm in the antero-posterior and cranio-caudal direction in DIBH. For FB patients, GTV motion is lower than 1.7 mm, and motion during the treatment was always in agreement with the one measured during the simulation. No differences have been observed in GTV coverage between the TP with 3-mm and 5-mm margins. Using a 3-mm margin, the mean reduction in the chest wall and trachea–bronchus Dmax was 2.5 Gy and 3.0 Gy, respectively, and a reduction of 1.0 Gy, 0.6 Gy, and 2.3% in Dmax, Dmean, and V5Gy, respectively, of the homolateral lung and 1.7 Gy in the contralateral lung Dmax.

Discussions: Cine-MRI allows to select FB lung patients when GTV motion is <2 mm. The use of narrower PTV margins reduces OARs dose and maintains target coverage.

KEYWORDS

MRgRT, gating, target motion, SBRT, lung

1 Introduction

Stereotactic body radiation therapy (SBRT) is currently considered the standard of care for early-stage inoperable non-small cell lung cancer (NSCLC) (1, 2), and there is growing evidence for its applications in the oligometastatic disease setting (3). Due to the high dose per fraction and the sharp dose gradients delivered in SBRT, accurate image guidance is required to ensure an effective and safe treatment delivery. The state-of-the-art in-room image guidance radiotherapy (IGRT) systems (4) generally provide the tumor position verification just before the treatment.

During the treatment delivery, most IGRT systems prevent target misplacement but do not effectively manage intra-fraction motion, unless the treatment system is tracking the tumor. Intra-fraction motion management is therefore still a major challenge in SBRT of lung lesions, also considering that intra-fraction position variability correlates with treatment delivery time (5).

Different motion management strategies have been developed, especially for the determination of ITV (6): such approaches assure target coverage but increase the volume of irradiated healthy tissues. Optimal results can be achieved by double-arc VMAT delivery technique in terms of dose distribution, also reducing treatment delivery time in comparison with non-coplanar IMRT beams (7).

Even though the dose conformality is achievable within the mentioned technologies, intra-fraction motion management may be not efficient, even using surrogate motion system (8). On-board magnetic resonance imaging (MRI) allows the non-invasive continuous and direct monitoring of target and organs at risk (OARs) through the acquisition of 4D-MRI and 2-D cine-MRI during the entire RT course, introducing an unprecedented significant innovation in the field of radiation oncology (9, 10).

The introduction of MRI-Linacs into clinical practice has brought new approaches for the intra- and inter-fraction motion management (11, 12). On-line imaging allows to directly track structures, as target or OARs, on the cine-MRI (13) and to perform active direct beam gating, stopping the radiation beam when a structure moves beyond a user defined tolerance region called boundary. Different strategies can be used in boundary definition (14):

a. Direct gross target volume (GTV) tracking: the boundary can be set as the PTV or an isodose level.
b. Indirect tracking: a surrogate structure that moves integral to the GTV is used for the gating.

This development led to a preference for the use of direct/indirect gating approach instead of ITV-based motion management.

Previous to the delivery, this hybrid system allows a daily plan dose distribution optimization based on the daily anatomy of the patients (15), employing a different approach to the planning to enhance the online treatment adaptation (16, 17), in terms of accuracy and computational time.

Lung treatments can be delivered in FB or using different breathing modality such as the DIBH that can be performed at different respiratory phases (18). However, using an MR-Linac, whichever mode is chosen, direct beam gating can always be performed by tracking the GTV on the cine-MRI. Another peculiarity of MR-Linacs is that it is possible to perform beam gating without the need to use devices like spirometer, fiducials, or abdominal belt to trigger the beam off.

The use of DIBH treatment for lung lesions can reduce the total irradiated lung volume and dose to near OARs with respect to free breathing (FB) treatment (19–21) and can be successfully customized for the different clinical scenarios.

During treatment MRI simulation, the breathing modality is evaluated to identify the most appropriate gating delivery technique, based on both lesion's and patient's factors compliance (i.e., location, dimensions, general conditions, and compliance). However, also the most recent guidelines (22) do not suggest a quantitative method for the selection of the best gating strategy (FB or DIBH) for patient treated on an MR-Linac with cine-MRI-based gating.

Especially for DIBH treatment, patient's compliance is a key point to prevent exhausting treatment sessions with sub-optimal dose delivery (23). As an example, apical lung lesions, especially the most central ones, generally present less motion amplitude in the right–left (RL) direction with respect to cranio-caudal (CC) and antero-posterior (AP) direction and present less motion during the breathing cycle with respect to lower lobe lesions (24–28). However, DIBH treatments turn out to be longer and more demanding for the patient and should therefore be carefully evaluated by the attending physician against other delivery settings (i.e., FB) (29).

The aim of this study is to provide a quantitative method for patient treatment selection between DIBH and FB, based on GTV centroid motion measurements performed on the simulation 0.35 T cine-MRI (30) and then evaluate the GTV to PTV margins reduction in the case of low mobility targets treated in FB (31).

2 Materials and methods

2.1 Patient selection and images dataset

A total of 12 patients with apical lung tumor who underwent MRI-guided SBRT have been retrospectively enrolled in this retrospective single-center study. All treatments were performed on MRIdian hybrid system (ViewRay Inc., Mountain View, CA) that combines a 0.35 T on board MRI scanner with a 6-MV flattening filter free (FFF) Linac system (32).

All patients included in the study underwent a simulation session where different images set were acquired sequentially. First, an MRI simulation session was performed directly inside the MR-Linac where different 3D MRI and cine-MRI were acquired:

a. Two 3D MRI scans were performed with a true fast imaging with steady-state precession (TRUFI) sequence with image resolution of $1.5 \times 1.5 \times 3$ mm^3 and $1.5 \times 1.5 \times 1.5$ mm^3 and an acquisition time of 25 and 172 s, respectively. The former was performed under DIBH, the latter in FB. With the patient still inside the MR-Linac, a radiation oncologist had

contoured the GTV on MR images to further allow GTV tracking on the subsequent cine-MRI.

b. RTT sets the TDS tracking algorithm in order to have real-time GTV tracking on the cine-MRI, and then, two sagittal 2D cine TrueFISP sequence (true fast imaging with steady state precession) were recorded with a spatial resolution of 0.35×0.5 cm^2 and an acquisition frequency of 4 frames/s:
   i. a cine-MRI with at least 20 s of FB
   ii. a cine-MRI with several DIBH.

During the DIBH cine-MRI, a multidisciplinary team, composed of a radiation oncologist, a physicist, and an RTT, had verified the clinical/dosimetric suitability and the patient's compliance and had define the treatment gating techniques. However, the choice between the two different gating strategies (FB and DIBH) was performed without a quantitative analysis on the GTV motion.

Next to the MRI simulation session, a CT simulation session was carried out (GE, Optima CT580 W, HiSpeed Dx/I Spiral): 1.25 mm slice thickness, without contrast agent, acquired in the same MRI simulation position, and with the same positioning system. The CT image was acquired in DIBH or FB, based on the information obtained during the MRI simulation. CT images are needed only for the creation of the electronic density map of the patient. CT image was then deformably fused to the MRI images to perform the nominal dose distribution that will be the reference dose distribution during the first treatment fraction. In case of a daily anatomical variation, the nominal dose distribution is online re-optimized to achieve optimal target coverage and OARs sparing.

The acquisition in DIBH is carried out without the aid of dedicated breath hold systems (i.e., RPM, surface surrogate, …); in fact, thanks to the possibility of performing cine-MRI, the TDS can directly track the target on the cine images in real time and perform the beam gating.

Six (50%) out of the 12 selected patients were treated in FB and six patients in DIBH gating delivery technique. All patients' fractionation schemes are listed in Table 1.

TABLE 1 Numbers of fractions for the FB and DIBH patients and dose prescribed to the isodose level.

Patient ID	Gating	Fractions	Prescription
1	FB	5	50 Gy@80%
2	FB	5	50 Gy@80%
3	FB	3	42 Gy@80%
4	FB	5	50 Gy@80%
5	FB	5	50 Gy@80%
6	FB	5	40 Gy@80%
7	DIBH	8	40 Gy@50%
8	DIBH	5	40 Gy@80%
9	DIBH	8	56 Gy@50%
10	DIBH	5	50 Gy@80%
11	DIBH	5	50 Gy@80%
12	DIBH	5	50 Gy@80%

Intensity-modulated radiation therapy (IMRT) step-and-shoot treatment plans were then calculated using the MRIdian treatment planning system (TPS). Dose calculation was carried out with the Monte Carlo algorithm on the MRIdian TPS (2,500,000 histories) using a calculation grid of 0.2 cm × 0.2 cm × 0.2 cm.

When optimizing the treatment plan, we pay special attention to the total treatment time, which we always keep below 13 min by adjusting the optimization parameters. For FB treatments, this is the actual treatment time. For DIBH treatments, we need to add the gating time to this. The gating time is closely linked to the patient's compliance and therefore varies from case to case.

In the clinical practice, PTV was created through an isotropic GTV expansion with a 0.3-cm margin for all DIBH treatments and 0.5 cm expansion for all FB treatments. GTV was set as direct gating structure, and the gating boundary was set equal to PTV or to the 95% isodose level. The TDS had been set in order to stop the dose delivery when more than 5% of GTV was outside the boundary for both FB and DIBH treatments, according to internal department guidelines. The mentioned values have been user defined and reflect the clinical experience of our center since 2017; however, they had been borrowed from clinical practice on conventional linac. The absence of international guidelines for MRgRT treatments has resulted in many practices common in treatments with traditional linacs being carried over to MR-Linacs. The 3-mm margin used for DIBH treatments is considered to be the lowest possible due to other limitations like image and dose grid resolution.

2.2 Image segmentation

ViewRay tracking algorithm overwrites over the grayscale image of the cine-MRI the gating boundary in yellow contour and the outline of the structure to be tracked (in this case GTV) in red (Figure 1). GTV contour was tracked for beam gating on all patients (both DIBH and FB) analyzed in this study. Positional data of the tracked structures over the cine-MRI could not be exported from the TPS, but it was possible to export the cine-MRI video in mp4 format. Employing an in-house developed MATLAB® R2019a (The Math-Works, Inc., Natick, MA) script, it was possible to identify the GTV contour and measure the centroid position. In the mp4 video, the only two colors over the grayscale of the MRI were the yellow of the gating boundary and the red of the GTV. All the frames of the mp4 video were exported as single RGB images where it was possible to find a threshold in the values of the RGB channels to select only the red GTV contour or the yellow outline of the gating boundary. In this way, it was therefore possible to select only the GTV structure to measure the position of the GTV centroid on every cine-MRI frames.

2.3 Motion analysis

The target's motion was evaluated by measuring the standard deviation of the GTV centroid position (Figure 1). The motion was measured in CC and AP directions, which were the only two directions visible on the sagittal cine-MRI (Figure 1). However, it

10.3389/fonc.2023.1280845

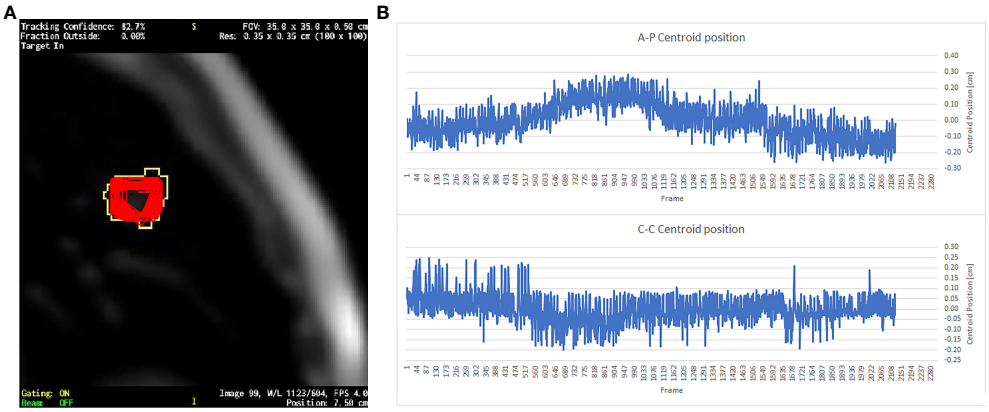

FIGURE 1
(A) A single frame of a sagittal cine-MRI where the red contours represent the superposition of the GTV contours exported from all the 2,124 cine frames; yellow contour is the gating boundary. **(B)** The GTV centroid relative position respect to its mean value in the AP direction and CC direction.

can be assumed that the movement in the third direction of RL is of the same order of magnitude as the others (24, 25).

Motion analyses were performed on the simulation cine-MRI and over all the cine-MRI recorded during the treatment fractions for all the patients.

Up to four tracking points can be manually placed on the MRI images during cine-MRI acquisition, which the clinical algorithm can track together with the contour of the GTV. Coordinates of such tracking points on all the cine frames can then be exported from the TPS. These values can be used to compare the values obtained by in-house tracking algorithm, in order to evaluate its accuracy. As a case test, the five fractions of FB patient no. 6 were selected, placing manually a tracking point at the center of the GTV as a benchmark value to be compared with the centroid position obtained by the homemade algorithm. This was done only on a single patient because this is a retrospective study and tracking points were placed at the time of the treatment only on this patient.

Different measurements of GTV motion were performed on DIBH patients:

a. Simulation cine-MRI GTV motion measurements:
    i. in deep inspiration phase (DIP)
    ii. in free breathing phase (FBP)
b. Treatment cine-MRI GTV motion measurements:
    i. in DIP

At least six complete deep inspirations cycle were available for each treatment cine in DIBH patients.

For FB patients, GTV motion was measured on all frames of each cine separately:

a. in simulation cine-MRI
b. in treatment fractions cine-MRI
c. mean GTV motion measured for each patient

Different comparisons between the measured GTV motion were considered in this study:

a. DIBH patients:
    i. DIP vs. FBP GTV motion
    ii. DIP GTV motion simulation vs. first fraction vs. last fraction
b. FB patients:
    i. simulation vs. treatment motion
    ii. mean GTV motion vs. DIP GTV motion

Homolateral lung and GTV volume had been also considered, together with the movement of the hepatic dome, to further evaluate possible correlation with GTV CC motion on FB patients using the Pearson correlation coefficient.

2.4 Dosimetric assessment of margin reduction

The dosimetric effect of reducing the GTV to PTV margin was evaluated on FB patients, comparing dose–volume constraints of the nearest OARs in treatment plans optimized with different GTV to PTV margins. In particular, two different margins were evaluated:

a. standard margin (SM): GTV to PTV equal to 5 mm, which is the current treatment margin used for FB patients
b. magnetic resonance image guided margin (MRIgM): GTV to PTV equal to 3 mm, which is the current treatment margin used for DIBH patients.

Treatment plans with the described margins were generated for the different margins using the same cost function. Maximum dose (Dmax) of the contralateral lung, chest wall, and trachea–bronchus structures were compared, together with mean dose (Dmean) and V5Gy of both lungs and V20Gy of the homolateral lung. PTV and GTV coverage were also considered in the evaluation of margin reduction comparing V100% and V80% of the prescribed dose in both structures for the different margins.

3 Results

A total of 77 cine-MRI had been exported, for a total of more than 13 h of recorded cine-MRI and more than 190,000 frames.

GTV centroid standard deviations for all the cine-MRI measured for FB patients are shown in Table 2, for both directions of motion visible on the cine-MRI. Observed motions for FB patients range from 0.04 cm to 0.17 cm in AP and CC directions, while mean motion during all the treatment goes from 0.07 cm to 0.12 cm in the AP direction and from 0.06 cm to 0.12 cm in the CC direction for all the FB patients.

In all fractions of patient no. 6, where a tracking point was manually placed at the center of the GTV, the standard deviation of the motion of the tracking point, averaged over all the fractions, is 0.07 cm in AP direction and 0.08 cm in CC, in agreement with the ones measured with the in-house script.

Figure 2 reports a box plot of DIBH patients' motion, analyzed both during the DIP, where GTV centroid motion ranges from 0.04 cm to 0.13 cm in both directions during the simulation and from 0.04 cm to 0.22 cm during the treatment fractions. In the FBP acquired during the simulation, the motion is between 0.14 cm and 0.98 cm in both directions. In the box plot, the horizontal lines represent the median and the 25th and 75th percentile, while the whiskers represent the minimum and maximum value, excluding the outliers represented as points outside the whiskers.

FB patients' GTV motions recorded in simulation cine-MRI are shown in Figure 3 together with the GTV motion measured on all the FB cine-MRI and the GTV motion evaluated during the DIP in DIBH patients.

Possible correlations between the amplitude of GTV CC motion and the GTV volume, the ratio between GTV and lung volumes, and the hepatic dome motion were investigated; Table 3 shows the GTV motions versus the volume of GTV and homolateral lung contours and the maximum amplitude of hepatic dome motion in CC direction. In Table 3, the ratio between the GTV volume and the lung volume is also presented.

The measured Pearson correlation coefficient between the GTV CC motion and the GTV volume, the ratio between GTV and lung volume, and the hepatic dome motion are, respectively, −0.25, −0.24, and −0.18.

Dosimetric differences between the treatment plans generated with SM and MRIgM can be found in Table 4 (MRIgM-SM).

The average difference over all patients is reported in the last column of Table 4. A mean Dmax reduction of 2.5 Gy and 3.0 Gy is observed in the chest wall and trachea–bronchus, respectively, with reductions of more than 5 Gy on a single patient when narrower margins are used.

Dmean and V5Gy decrease in both lungs using MRIgM together with V20Gy of the homolateral lung.

As expected, the 80% isodose covers the whole volume of the GTV using both treatment margins, while there is an increase in PTV V80% and V100% of treatment plans with MRIgM. A mean reduction of 1.88% in GTV V100% is observed when using MRIgM as expected if the treatment plan is being delivered to a smaller volume.

4 Discussion

The movement of the GTV as a result of the respiratory cycle is not homogeneous in the different parts of the lung, as has already been described in the literature (26–28). This study had investigated the possibility of treating patients with a FB technique to increase patient's compliance and reduce treatment time respect to DIBH treatments in the case of upper lobe lesions. Sagittal cine-MRI were used to measure GTV centroid motion in AP and CC directions.

TABLE 2 GTV motion defined as standard deviation of the centroid position, measured during the simulation (SIM) and the mean, minimum, and maximum motion measured during the treatment fractions for FB patients and DIP of DIBH patients in the two directions visible on the cine-MRI.

Patient	AP [cm]			CC [cm]		
	SIM	Mean SD	Min–Max SD	SIM	Mean SD	Min–Max SD
1	0.06	0.09	0.06–0.11	0.11	0.09	0.07–0.12
2	0.15	0.10	0.08–0.15	0.10	0.10	0.07–0.14
3	0.13	0.12	0.07–0.17	0.06	0.06	0.04–0.08
4	0.06	0.07	0.06–0.08	0.08	0.06	0.06–0.08
5	0.10	0.09	0.05–0.12	0.17	0.12	0.05–0.17
6	0.10	0.08	0.04–0.11	0.11	0.08	0.05–0.11
7	0.07	0.08	0.04–0.13	0.04	0.11	0.04–0.20
8	0.07	0.09	0.06–0.12	0.07	0.08	0.04–0.12
9	0.09	0.08	0.04–0.12	0.13	0.09	0.06–0.13
10	0.06	0.09	0.04–0.11	0.05	0.11	0.05–0.22
11	0.08	0.11	0.08–0.17	0.06	0.14	0.06–0.21
12	0.15	0.13	0.07–0.18	0.12	0.12	0.09–0.17

10.3389/fonc.2023.1280845

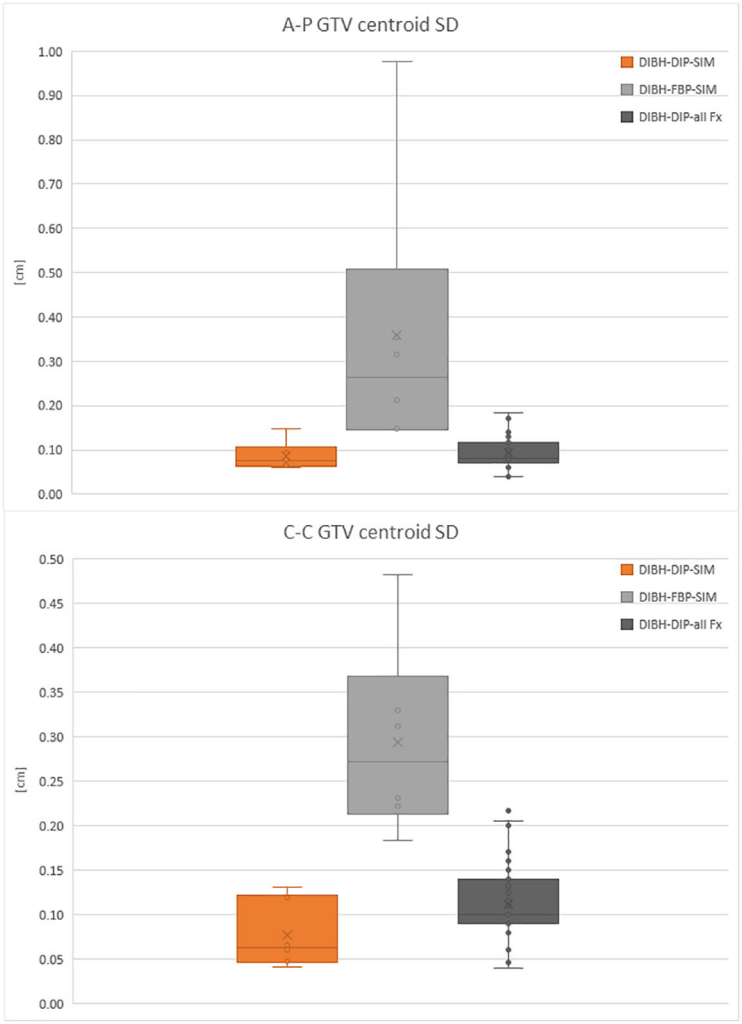

FIGURE 2
Box plot of the GTV centroid SD in antero-posterior (A-P) direction and cranio-caudal (C-C) direction for DIBH patients in the DIP.

The motion measured during DIP of DIBH patients was comparable with the one observed by Van Sornsen de Koste et al. (30) with a similar method based on GTV centroid tracking on cine-MRI. The Motions measured in other works are difficult to compare because of different lesion positions inside the lungs or different gating and imaging techniques, but overall motion appeared to be comparable with the one measured by Barnes et al. (19) and Britton et al. (25), considering only upper lung lesions data of these works.

No correlations were found between GTV CC motion and hepatic dome motion, GTV volume, and the ratio between GTV and lung motion.

Analysis of GTV motion performed on both FB and DIBH patients had shown that the GTV motion observed during simulation was representative of the motion that will be present throughout the treatment, for FB patients. Indeed, based on the collected data, the motion measured during simulation was always in agreement with the one observed during treatment fractions (Figure 3).

This result supports the choice to perform treatment in FB in those patients who present during the MRI simulation a motion amplitude lower than 2 mm. When compared to DIBH patients, the motion of the GTV during treatment of FB patients, which have a GTV motion smaller than 2 mm in simulation, turned out to be similar than that observed on DIBH patients during the DIP (as shown in Figure 3).

This further justifies the choice of the GTV to PTV margin of 3 mm, keeping in mind that the volume of the GTV on the MRI acquired in FB already turns out to be an average of the position of the GTV over the 172 s of image acquisition time (33). This point also appears in the simulation CT where the structures can be also contoured for the treatment planning.

It was also possible to measure GTV motion manually placing tracking points on the simulation and treatment images, thanks to a dedicated functionality of the ViewRay TPS. This procedure had been performed on a patient treated in FB: a tracking point was placed in the center of the GTV to obtain an additional measure of GTV motion in order to validate the in-house script used for image

10.3389/fonc.2023.1280845

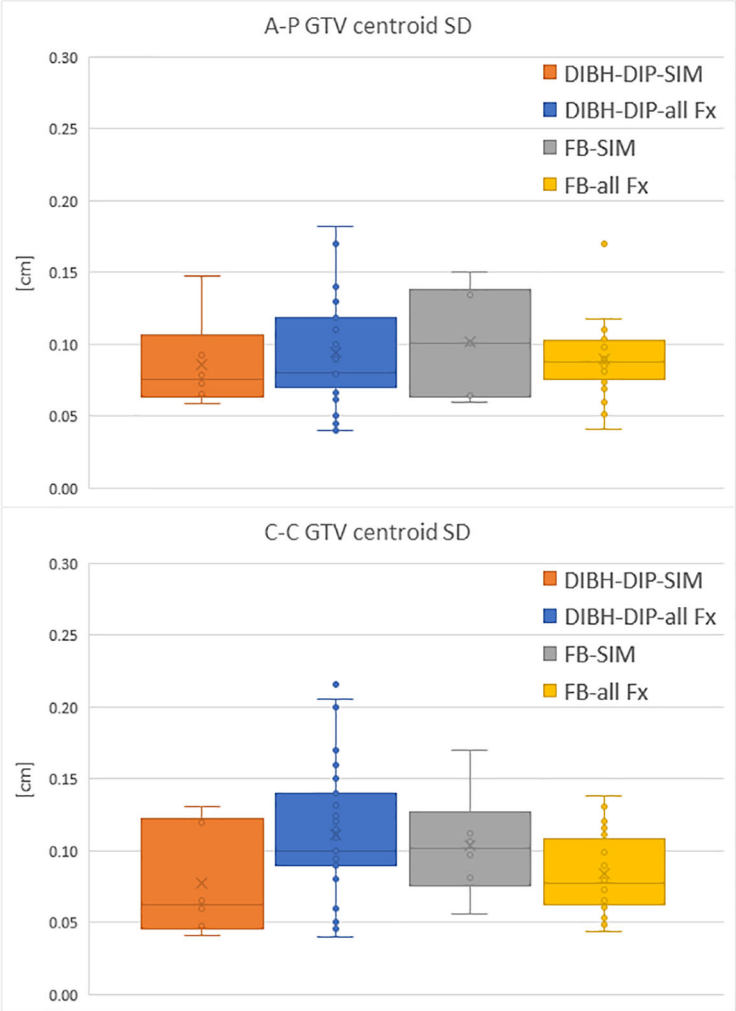

FIGURE 3
Comparison of the GTV centroid SD in A-P direction and C-C direction between DIP of DIBH patients and motion measured on FB patients. Motion is evaluated both during the simulation (SIM) and the treatment fractions (all Fx).

segmentation and motion tracking. The standard deviation of the position of the tracking points turned out to be in agreement with the motion of the GTV analyzed using our technique (0.07 cm in AP direction and 0.08 cm in CC).

When GTV motion is >2 mm in at least one of the two directions during the MRI FB simulation, the use of DIBH gating technique leads to a considerable reduction in GTV motion as observed in Figure 2 for the patient treated in DIBH, which then justifies the use of a more demanding active gating technique for the patient and an increased treatment time.

The main advantages of FB treatments are a reduction in treatment time and less patient fatigue from holding their breath, and a reduction

TABLE 3 Hepatic dome motion compared with GTV and lung properties.

Patient	GTV motion [cm]	V lung [cc]	V GTV [cc]	V GTV/V lung [$\times 10^{-4}$]	Hepatic dome motion [cm]
1	0.09	1,934.39	1.92	9.93	1.68
2	0.10	1,447.68	0.47	3.25	1.36
3	0.06	2,301.69	1.86	8.08	1.28
4	0.06	2,395.99	8.95	37.35	2.00
5	0.12	2,764.78	0.42	1.52	1.60
6	0.08	2,132.50	36.49	171.11	2.60

TABLE 4 DVH differences between treatment plans generated with magnetic resonance image guided margin (MRIgM) and standard margin (SM).

Structure	DVH index	Patient						
		1	2	3	4	5	6	mean
PTV	V80%	1.00%	0.00%	5.70%	5.54%	0.09%	3.98%	2.72%
	V100%	5.01%	9.11%	12.97%	15.58%	6.88%	3.37%	8.82%
GTV	V80%	0.00%	0.00%	0.00%	0.03%	0.00%	−0.16%	−0.02%
	V100% [%]	−14.17%	−13.61%	4.98%	20.58%	−6.20%	−2.84%	−1.88%
	V100% [cc]	−0.27	−0.07	−0.26	−1.27	−0.06	−5.17	−1.18
Homolateral lung—GTV	V20Gy	−1.83%	−1.67%	−0.83%	−1.66%	−0.64%	−0.22%	−1.14%
	D_{mean} (Gy)	−0.91	−0.78	−0.35	−0.71	−0.57	−0.01	−0.56
	V5Gy	−3.80%	−3.34%	−1.74%	−2.25%	−2.74%	−0.32%	−2.37%
Contralateral lung	D_{max} (Gy)	−0.65	−1.27	−0.36	−2.92	−4.14	−1.02	−1.73
	D_{mean} (Gy)	−0.18	−0.01	−0.13	−0.14	−0.34	−0.29	−0.18
	V5Gy	−0.03%	−0.85%	−0.19%	−1.37%	−1.52%	−2.44%	−1.07%
Chest wall	D_{max} (Gy)	−5.10	−3.73	−0.70	−1.82	−3.39	−0.56	−2.55
Trachea and bronchial tree	D_{max} (Gy)	−6.85	−2.57	−1.85	−0.03	−5.82	−0.88	−3.00

in the time spent in an uncomfortable position in the MR-Linac bore (arms raised above the head throughout the treatment).

Finally, the possibility to perform simulation cine-MRI and gating during treatment on this hybrid system safely allows to perform a margin reduction, since the GTV segmentation on the simulation and treatment cine-MRI is performed by the same algorithm, which also feeds the treatment gating. Another well-known advantage of gating treatment is the dose reduction in the surrounding healthy tissue, since no dose would be delivered if the GTV motion resulted greater than the boundary during treatment. On the other hand, for linacs without integrated MRI, simulation cine-MRI can always be performed if the facility is equipped with a dedicated MRI. Therefore, cine-MRI could be clinically used to assess lesion motion; however, the GTV segmentation software on the cine-MRI could be different from that used for gating, potentially introducing an additional source of error. In order to better explore such workflow, further studies are required.

The reduction in treatment margins in the planning stage leads to a reduction in OARs dose. In particular, in the case of OARs located near or even inside the PTV, the reduction in GTV to PTV margins obviously increases the distance for the dose fall-off outside the target, increasing PTV coverage and decreasing the dose to OARs. A reduction in the GTV V100% was observed in treatment plans with MRIgM; however, it was still clinically acceptable. Computing the treatment plans with MRIgM, the same cost function had been employed to exclude differences due to the optimizer; however, a finer optimization could lead to treatment plans with the same GTV V100%.

The impact of this work on SABR of the lung is expressed in the fact that we can identify a target movement threshold to determine which patients would benefit from DIBH, a more stressful technique. With a view to margin reduction, this work can be a first step toward realizing personalized treatment margins for FB patients as well.

A limitation of this study is the lack of information about the motion in the right-left (RL) direction; however, the motion in this direction is lower or of the same amplitude of the one observed on AP and CC directions [16,17]. The ongoing release of the new MRIdian treatment delivery system will permit recording cine-MRI in the three directions, tracking different regions of interest (both direct and indirect tracking). Therefore, future studies will also evaluate motion in the RL direction.

Further analysis is ongoing to complete an overall 3D GTV lung lesions movement mapping: this would provide a clinical decision tool to select the optimal gating strategy and GTV to PTV margins.

This study suggests a methodology to define MRIgRT SBRT for apical lung lesions. During MRI simulation, a motion of the GTV of <2 mm in all examinable directions support the possibility of FB treatment. Since GTV motion in FB can be compared with treatment in DIBH, the same treatment margins can be used, improving patient compliance, reducing both treatment time and dose to surrounding OARs, without compromising target coverage.

Data availability statement

The original contributions presented in the study are included in the article/supplementary material. Further inquiries can be directed to the corresponding author.

Ethics statement

Ethical approval was not required for the study involving humans in accordance with the local legislation and institutional requirements. Written informed consent to participate in this study was not required from the participants or the participants' legal guardians/next of kin in accordance with the national legislation and the institutional requirements.

Author contributions

MG: Conceptualization, Data curation, Formal Analysis, Investigation, Methodology, Software, Writing – original draft, Writing – review & editing. MN: Conceptualization, Investigation, Supervision, Visualization, Writing – review & editing. AC: Supervision, Validation, Visualization, Writing – review & editing. GM: Supervision, Validation, Visualization, Writing – review & editing. DC: Validation, Visualization, Writing – review & editing. LB: Supervision, Validation, Visualization, Writing – review & editing. GC: Supervision, Validation, Visualization, Writing – review & editing. AR: Supervision, Validation, Visualization, Writing – review & editing. CV: Conceptualization, Data curation, Supervision, Validation, Visualization, Writing – review & editing. MAG: Funding acquisition, Visualization, Writing – review & editing. LI: Funding acquisition, Visualization, Writing – review & editing. LP: Conceptualization, Investigation, Methodology, Project administration, Supervision, Validation, Visualization, Writing – review & editing.

Funding

The author(s) declare that no financial support was received for the research, authorship, and/or publication of this article.

Conflict of interest

The authors declare that the research was conducted in the absence of any commercial or financial relationships that could be construed as a potential conflict of interest.

Publisher's note

All claims expressed in this article are solely those of the authors and do not necessarily represent those of their affiliated organizations, or those of the publisher, the editors and the reviewers. Any product that may be evaluated in this article, or claim that may be made by its manufacturer, is not guaranteed or endorsed by the publisher.

References

1. Grills IS, Hope AJ, Guckenberger M, Kestin LL, Werner-Wasik M, Yan D, et al. A collaborative analysis of stereotactic lung radiotherapy outcomes for early-stage non-small-cell lung cancer using daily online cone-beam computed tomography image-guided radiotherapy. *J Thorac Oncol* (2012) 7:1382–93. doi: 10.1097/JTO.0b013e318260e00d

2. Baumann P, Nyman J, Hoyer M, Wennberg B, Gagliardi G, Lax I, et al. Outcome in a prospective phase II trial of medically inoperable stage I non-small-cell lung cancer patients treated with stereotactic body radiotherapy. *J Clin Oncol* (2009) 27:3290–6. doi: 10.1200/JCO.2008.21.5681

3. Milano MT, Philip A, Okunieff P. Analysis of patients with oligometastases undergoing two or more curative-intent stereotactic radiotherapy courses. *Int J Radiat Oncol Biol Phys* (2009) 73:832–7. doi: 10.1016/j.ijrobp.2008.04.073

4. Dieterich S, Green O, Booth J. SBRT targets that move with respiration. *Physica Med* (2018) 56:19–24. doi: 10.1016/j.ejmp.2018.10.021

5. Purdie TG, Bissonnette JP, Franks K, Bezjak A, Payne D, Sie F, et al. Cone-beam computed tomography for on-line image guidance of lung stereotactic radiotherapy: localization, verification, and intrafraction tumor position. *Int J Radiat Oncol Biol Phys* (2007) 68:243–52. doi: 10.1016/j.ijrobp.2006.12.022

6. Korreman SS. Image-guided radiotherapy and motion management in lung cancer. *Br J Radiol* (2015) 88. doi: 10.1259/bjr.20150100

7. Xhaferllari I, El-Sherif O, Gaede S. Comprehensive dosimetric planning comparison for early-stage, non-small cell lung cancer with SABR: Fixed-beam IMRT versus VMAT versus TomoTherapy. *J Appl Clin Med Phys* (2016) 17:329–40. doi: 10.1120/jacmp.v17i5.6291

8. Brandner ED, Chetty IJ, Giaddui TG, Xiao Y, Huq MS. Motion management strategies and technical issues associated with stereotactic body radiotherapy of thoracic and upper abdominal tumors: A review from NRG oncology. *Med Phys* (2017) 44:2595–612. doi: 10.1002/mp.12227

9. Corradini S, Alongi F, Andratschke N, Belka C, Boldrini L, Cellini F, et al. MR-guidance in clinical reality: Current treatment challenges and future perspectives. *Radiat Oncol* (2019) 14:1–22. doi: 10.1186/s13014-019-1308-y

10. Ménard C, van der Heide UA. Introduction: magnetic resonance imaging comes of age in radiation oncology. *Semin Radiat Oncol* (2014) 24:149–50. doi: 10.1016/j.semradonc.2014.02.001

11. Cusumano D, Dhont J, Boldrini L, Chiloiro G, Teodoli S, Massaccesi M, et al. Predicting tumour motion during the whole radiotherapy treatment: a systematic approach for thoracic and abdominal lesions based on real time MR. *Radiother Oncol* (2018) 129:456–62. doi: 10.1016/j.radonc.2018.07.025

12. Thomas DH, Santhanam A, Kishan A, Cao M, Lamb J, Min Y, et al. Initial clinical observations of intra-and interfractional motion variation in MR-guided lung SBRT. *British J Radiol* (2018) 91. doi: 10.1259/bjr.20170522

13. Dhont J, Vandemeulebroucke J, Cusumano D, Boldrini L, Cellini F, Valentini V, et al. Multi-object tracking in MRI-guided radiotherapy using the tracking-learning-detection framework. *Radiother Oncol* (2019) 138:25–9. doi: 10.1016/j.radonc.2019.05.008

14. Votta C, Cusumano D, Boldrini L, Dinapoli N, Placidi L, Turco G, et al. Delivery of online adaptive magnetic resonance guided radiotherapy based on isodose boundaries. *Phys Imaging Radiat Oncol* (2021) 18:78–81. doi: 10.1016/j.phro.2021.05.005

15. Placidi L, Romano A, Chiloiro G, Cusumano D, Boldrini L, Cellini F, et al. On-line adaptive MR guided radiotherapy for locally advanced pancreatic cancer: Clinical and dosimetric considerations. *Tech Innov Patient Support Radiat Oncol* (2020) 15:15–21. doi: 10.1016/j.tipsro.2020.06.001

16. Placidi L, Nardini M, Cusumano D, Boldrini L, Chiloiro G, Romano A, et al. VMAT-like plans for magnetic resonance guided radiotherapy: Addressing unmet needs. *Physica Med* (2021) 85:72–8. doi: 10.1016/j.ejmp.2021.05.002

17. Nardini M, Placidi L. Robust online adaptive planning: Toward a uniform MR-LINAC treatment planning technique. *Advances in Magnetic Resonance Technology and Applications* (2022) 8:101–22. doi: 10.1016/B978-0-323-91689-9.00025-X

18. Botticella A, Levy A, Auzac G, Chabert I, Berthold C, Le Pechoux C. Tumour motion management in lung cancer: A narrative review. *Transl Lung Cancer Res* (2021) 10:2011–7. doi: 10.21037/tlcr-20-856

19. Barnes EA, Murray BR, Robinson DM, Underwood LJ, Hanson J, Roa WHY. Dosimetric evaluation of lung tumor immobilization using breath hold at deep inspiration. *Int J Radiat Oncol Biol Phys* (2001) 50(4):1091–8. doi: 10.1016/s0360-3016(01)01592-9

20. Kim DJW, Murray BR, Halperin R, Roa WHY. Held-breath self-gating technique for radiotherapy of non-small-cell lung cancer: a feasibility study. *Int J Radiat Oncol Biol Phys* (2001) 49(1):43–9. doi: 10.1016/s0360-3016(00)01372-9

21. Fjellanger K, Rossi L, Heijmen BJM, Pettersen HES, Sandvik IM, Breedveld S, et al. Patient selection, inter-fraction plan robustness and reduction of toxicity risk with deep inspiration breath hold in intensity-modulated radiotherapy of locally advanced non-small cell lung cancer. *Front Oncol* (2022) 12:966134. doi: 10.3389/fonc.2022.966134

22. Aznar MC, carrasco de fez P, Corradini S, Mast M, McNair H, Meattini I, et al. ESTRO-ACROP guideline: Recommendations on implementation of breath-hold techniques in radiotherapy. *Radiother Oncol* (2023) 185. doi: 10.1016/j.radonc.2023.109734

23. Placidi L, Cusumano D, Boldrini L, Votta C, Pollutri V, Antonelli MV, et al. Quantitative analysis of MRI-guided radiotherapy treatment process time for tumor real-time gating efficiency. *J Appl Clin Med Phys* (2020) 21:70–9. doi: 10.1002/acm2.13030

24. Seppenwoolde Y, Shirato H, Kitamura K, Shimizu S, Van Herk M, Lebesque JV, et al. Precise and real-time measurement of 3D tumor motion in lung due to breathing and heartbeat, measured during radiotherapy. *Int J Radiat Oncol Biol Phys* (2002) 53(4):822–34. doi: 10.1016/s0360-3016(02)02803-1

25. Britton KR, Starkschall G, Tucker SL, Pan T, Nelson C, Chang JY, et al. Assessment of gross tumor volume regression and motion changes during radiotherapy for non-small-cell lung cancer as measured by four-dimensional computed tomography. *Int J Radiat Oncol Biol Phys* (2007) 68:1036–46. doi: 10.1016/j.ijrobp.2007.01.021

26. Rabe M, Thieke C, Düsberg M, Neppl S, Gerum S, Reiner M, et al. Real-time 4DMRI-based internal target volume definition for moving lung tumors. *Med Phys* (2020) 47:1431–42. doi: 10.1002/mp.14023

27. Redmond KJ, Song DY, Fox JL, Zhou J, Rosenzweig CN, Ford E. Respiratory motion changes of lung tumors over the course of radiation therapy based on respiration-correlated four-dimensional computed tomography scans. *Int J Radiat Oncol Biol Phys* (2009) 75:1605–12. doi: 10.1016/j.ijrobp.2009.05.024

28. Yu ZH, Lin SH, Balter P, Zhang L, Dong L. A comparison of tumor motion characteristics between early stage and locally advanced stage lung cancers. *Radiother Oncol* (2012) 104:33–8. doi: 10.1016/j.radonc.2012.04.010

29. Keall PJ, Mageras GS, Balter JM, Emery RS, Forster KM, Jiang SB, et al. The management of respiratory motion in radiation oncology report of AAPM Task Group 76. *Med Phys* (2006) 33:3874–900. doi: 10.1118/1.2349696

30. van Sörnsen de Koste JR, Palacios MA, Bruynzeel AME, Slotman BJ, Senan S, Lagerwaard FJ. MR-guided gated stereotactic radiation therapy delivery for lung, adrenal, and pancreatic tumors: A geometric analysis. *Int J Radiat Oncol Biol Phys* (2018) 102:858–66. doi: 10.1016/j.ijrobp.2018.05.048

31. Masuda H, Kawahara D, Saito A, Kimura T, Ozawa S, Nakashima T, et al. Reduction of margin to compensate the respiratory tumor motion by the analysis of dosimetric internal target volume in lung SBRT with nonuniform volume prescription method. *Med Phys* (2021) 48:3200–7. doi: 10.1002/mp.14871

32. Mutic S, Dempsey JF. The viewRay system: magnetic resonance-guided and controlled radiotherapy. *Semin Radiat Oncol* (2014) 24:196–9. doi: 10.1016/j.semradonc.2014.02.008

33. Wolthaus JWH, Sonke JJ, van Herk M, Belderbos JSA, Rossi MMG, Lebesque JV, et al. Comparison of different strategies to use four-dimensional computed tomography in treatment planning for lung cancer patients. *Int J Radiat Oncol Biol Phys* (2008) 70:1229–38. doi: 10.1016/j.ijrobp.2007.11.042

frontiers | Frontiers in Oncology

TYPE Original Research
PUBLISHED 24 November 2023
DOI 10.3389/fonc.2023.1289919

OPEN ACCESS

EDITED BY
Nadia Gisella Di Muzio,
Vita-Salute San Raffaele University, Italy

REVIEWED BY
Uma Goyal,
Banner Health, United States
Mora Grisel M.,
University of Lisbon, Portugal
Andrei Fodor,
IRCCS San Raffaele Scientific Institute, Italy

*CORRESPONDENCE
Merav Akiva Ben-David
meravak@assuta.co.il

RECEIVED 06 September 2023
ACCEPTED 30 October 2023
PUBLISHED 24 November 2023

CITATION
Almog G, Pfeffer RM, Zalmanov S, Grinberg V, Lipsky Y, Chernomordikov E, Levin D, Apter S, Arsenault O, Epstein D, Tamimi Q, Hod K, Limon D, Golan T, Ben-Aharon I, Lawrence YR and Ben-David MA (2023) Pancreatic cancer outcome—local treatment with radiation using MRI-LINAC.
Front. Oncol. 13:1289919.
doi: 10.3389/fonc.2023.1289919

Pancreatic cancer outcome—local treatment with radiation using MRI-LINAC

Galit Almog[1], Raphael M. Pfeffer[2,3], Svetlana Zalmanov[2], Vladislav Grinberg[2], Yoav Lipsky[2], Elena Chernomordikov[2], Daphne Levin[2], Sara Apter[2,4], Orit Arsenault[2], Dan Epstein[2], Qusai Tamimi[2], Keren Hod[5], Dror Limon[6], Talia Golan[7], Irit Ben-Aharon[8], Yaacov Richard Lawrence[7] and Merav Akiva Ben-David[2,3]*

[1]Goldman School of Medicine, Ben Gurion University of the Negev, Beer Sheva, Israel, [2]Radiation Oncology Department, Assuta Medical Center, Tel Aviv, Israel, [3]Faculty of Health Sciences, Ben Gurion University of the Negev, Beer Sheva, Israel, [4]School of Medicine, Tel Aviv University, Tel Aviv, Israel, [5]Department of Academy and Research, Assuta Medical Center, Tel Aviv, Israel, [6]Radiation Oncology Department, Rabin Medical Center, Petah-Tikva, Israel, [7]Radiation Oncology Department, Sheba Medical Center, Ramat-Gan, Israel, [8]Oncology Department, Rambam Medical Center, Haifa, Israel

Introduction: Stereotactic MR-guided on-table adaptive radiotherapy (SMART) allows the precise delivery of high-dose radiation to tumors in great proximity to radiation-sensitive organs. The aim of this study is to evaluate the toxicity and clinical outcome in locally advanced or recurrent pancreatic tumors, with or without prior irradiation, treated with SMART.

Methods: Patients were treated for pancreatic cancer (PC) using SMART technology to a prescribed dose of 50 Gy (BED_{10}, 100 Gy) in five fractions, with daily on-table adaptation of treatment plan. Endpoints were acute and late toxicities, local control, local disease-free period, and overall survival.

Results: A total of 54 PC patients were treated between August 2019 and September 2022, with a median follow-up of 8.9 months from SMART. The median age was 70.4 (45.2–86.9) years. A total of 40 patients had upfront inoperable PC (55% were locally advanced and 45% metastatic), and 14 had local recurrence following prior pancreatectomy (six patients also had prior adjuvant RT). Of the patients, 87% received at least one chemotherapy regimen (Oxaliplatin based, 72.2%), and 25.9% received ≥2 regimens. Except from lower CA 19-9 serum level at the time of diagnosis and 6 weeks prior to SMART in previously operated patients, there were no significant differences in baseline parameters between prior pancreatectomy and the inoperable group. On-table adaptive replanning was performed for 100% of the fractions. No patient reported grade ≥2 acute GI toxicity. All previously irradiated patients reported only low-grade toxicities during RT. A total of 48 patients (88.9%) were available for evaluation. Complete local control was achieved in 21.7% (10 patients) for a median of 9 months (2.8–28.8); three had later local progression. Eight patients had regional or marginal recurrence. Six- and 12-month OS were 75.0% and 52.1%, respectively. Apart from mild diarrhea 1–3 months after SMART and

general fatigue, there were no significant differences in toxicity and outcomes between post-pancreatectomy and inoperable groups.

Conclusion: SMART allows safe delivery of an ablative dose of radiotherapy, with minimal treatment-related toxicity, even in previously resected or irradiated patients. In this real-world cohort, local control with complete response was achieved by 20% of the patients. Further studies are needed to evaluate long-term outcome and late toxicity.

KEYWORDS

SMART, MRgRT, pancreatic cancer, re-irradiation, radiation toxicity

1 Introduction

Exocrine pancreatic cancer (PC) is a common and highly lethal malignancy. It is the fourth and seventh leading cause of cancer-related death in the US and worldwide, respectively, with a 5-year overall survival (OS) rate of 12.5% (1) Most pancreatic cancer patients succumb to distant metastatic disease. Patients without evidence of metastases at diagnosis are considered for surgical resection, but most of these tumors are considered inoperable due to tumor involvement of regional blood vessels. Patients with locally inoperable disease often receive chemotherapy in an attempt to shrink the tumor and convert it to resectable, yet only 15%–20% of patients are operable (2) and prognosis is poor even after complete resection, due to frequent metastatic disease and high rates of both systemic and local recurrence (3, 4) Conventional radiotherapy has been studied in these non-resectable patients and has not been found to contribute to long-term local control or survival. On the other hand, dose-escalated radiotherapy delivered in 15–25 fractions to a biologically effective dose (BED) of 98 Gy has been shown to have good local control (local failure 17.6% at 1 year and 32.8% at 2 years) and moderate survival (38% at 2 years) compared to historical control (5).

Stereotactic body radiotherapy (SBRT) is often given as salvage treatment for local inoperable or locally recurrent PC progressing after chemotherapy (6) SBRT delivered to pancreatic cancer without online image guidance is limited to doses of approximately 35 Gy in five fractions due to the risk of toxicity to adjacent critical organs such as the stomach and duodenum. Retrospective studies demonstrated optimistic local control outcomes but no change in OS and provoked some concerns regarding treatment toxicities (7) The use of CT imaging (on-board cone beam CT) in abdominal RT provides limited soft tissue contrast and inability to perform real-time tracking to account for internal organ movement (8). In practice, this translates to subtherapeutic doses of RT in an effort to reduce OAR toxicities (9–11). On the other hand, safely delivering higher doses of radiation may improve long-term local control (LC) and OS. A prospective randomized study showed no benefit from such doses of SBRT following systemic chemotherapy (12).

Stereotactic MR-guided adaptive radiotherapy (SMART) allows delivery of ablative dose to abdomino-pelvic tumors, even when adjacent to OARs. This is possible due to continuous real-time MR-based imaging of internal structures with improved soft tissue visualization compared with CT (8), daily on-table adaptive replanning, and automatic beam delivery cessation based on real-time target position tracking (13, 14). Recent studies have shown that SMART is safe, allows dose escalation with OAR sparing (15), and may improve OS in patients with inoperable PC (16). The development of real-time imaging with MRI allows safe delivery of higher doses of hypofractionated SBRT while ensuring that the dose to the adjacent organs at risk is limited to below what is considered a toxic dose. The recently completed multi-institutional SMART study showed that a dose of 50 Gy in five fractions (BED = >100 Gy_{10} can be delivered with no grade 3 toxicity (17).

While recent studies have shown promising results, research regarding the effectiveness of SMART in PC treatment has mainly focused on primary inoperable cases, leaving little evaluation of cases with local recurrence of PC after surgery or previously irradiated patients (18). This study seeks to evaluate the outcomes and toxicity of SMART in treating primary inoperable, post-surgery locally recurrent, and previously irradiated PC patients. This is the first study, to the best of our knowledge, to assess and compare the effectiveness of SMART in patients with post-operative or recurrent PC.

2 Methods

2.1 Study population

This is a retrospective cohort study enrolling 54 consecutive patients with pancreatic malignancy treated with SMART using MRI-LINAC system (ViewRay Inc. MRIdian ®, Oakwood Village, OH, USA) between August 2019 and September 2022. Patients with inoperable (unresectable/metastatic), medically inoperable (poor performance status, multiple associated morbidities), or recurrent PC following pancreatectomy were included, and patients with either prior pancreas-directed radiation or evidence of distant

metastases were also included in this study. All patients signed informed consent, and the study was approved by the institutional IRB committee (ASMC-0078-22).

2.2 Treatment

Patients underwent MRI simulation using the MRI-LINAC (supine position, both arms above the head, and 400 cc water PO 45 min prior to scanning) followed immediately by CT-based simulation in the same position.

For treatment planning, gross tumor volume (GTV) and OARs (stomach, duodenum, small and large bowel, kidneys, aorta, inferior vena cava, and spinal cord) were contoured on the MR simulation imaging after fusion with pre-treatment imaging (MRI and/or PET-CT). All contours were reviewed by an expert radiologist (SA) prior to planning. Planning target volume (PTV) was generated from GTV with a 3-mm margin. Our planning risk volume (PRV), which was also the optimization structure, was generated by cropping the PTV from OARs with an additional 3 mm to allow for dose fall-off.

The prescription dose was 50 Gy in five fractions (BED_{10}, 100 Gy) delivered on alternate days, with the goal of 95% PRV coverage with 95% of prescribed dose (47.5 Gy). Dose limits for OAR were as follows: for the duodenum, stomach, and small and large bowels, the maximum dose constraint was $V33^{1} \leq 0.5\ cm^3$. The goal for the liver was to achieve a mean dose of <20 Gy while keeping 700 cm^3 under 15 Gy. For the spinal canal, the constraint was a $V25^{2} \leq 0.5\ cm^3$. The constraint for each kidney was mean dose of <12 Gy, with no more than two-thirds of each kidney receiving a dose higher than 14 Gy. If one of these structures exceeded the dose–volume constraint, treatment plan was adapted accordingly to adhere to dose–volume constraints. See Figure 1 for contouring and doses. The treatment was delivered using equally spaced 19–23 fields, with 50–65 segments, and filter-free 6 MV beam energy with 600 mu/minute dose rate. The Monte Carlo calculation algorithm was used (proprietary ViewRay algorithm).

Three patients received concomitant SBRT to celiac lymph nodes to a dose of 35 Gy in five fractions, and five patients received concomitant SBRT to a liver metastasis (50 Gy in five fractions). Patients did not receive chemotherapy during radiation treatment period.

On-board MRI was performed prior to each fraction, and the OARs and the GTV, PTV, and PTV_OPT were re-contoured, to account for inter-fraction movement. The plan was adapted if tumor or OARs doses did not meet the constraints, as we prioritized OAR protection, even at the expense of PTV coverage. During radiation, the tumor was monitored by MRI, and treatment was automatically halted if the target (i.e., GTV) moved out of the boundary range by more than 5%. Breathing instructions were given to the patients during simulation and radiation sessions in order to minimize intra-abdominal organ movements and reduce treatment time.

All patients received oral Ondansetron prior to each radiation session to minimize possible nausea.

2.3 Assessment

Pre-treatment patient data included demographics, prior treatments, symptoms, and baseline tumor measurements to allow post-treatment calculation of Response Evaluation Criteria in Solid Tumors (RECIST) criteria (19) or PET-CT Response Criteria in Solid Tumors (PERCIST) (20). RECIST/PERCIST were used to determine local response alone, independently from disease status in distant sites (which was evaluated separately). Post-treatment assessment of local response was based on matching imaging modalities to minimize errors (i.e., MRI vs. MRI, PET-CT vs. PET-CT, and CT vs. CT).

Throughout and after the RT period, the treating radiation oncologist monitored patients' acute and late (defined as occurring within or after 6 months of therapy completion, respectively) side effects such as gastrointestinal (abdominal pain, nausea, vomiting, diarrhea, constipation, and gastric outlet obstruction) and general side effects (fatigue, loss of appetite, weight loss, and anemia). Additionally, CA 19-9 levels were tracked at baseline and in the following months, and re-induction of chemotherapy was reported.

2.4 Statistical analysis

Associations between patient characteristics and side effects were evaluated by Mann–Whitney test, Spearman correlation, and chi-square test, as appropriate.

A linear mixed model for repeated measure analysis was used to evaluate individual CA 19-9 levels throughout the study follow-up among each group. To avoid multicollinearity, we verified that there are no correlations between independent variables that were included into the model. Disease-free period and overall survival were analyzed using Kaplan–Meier test. The level of significance used for all analyses was two-tailed and set at $p<0.05$. The SPSS statistical package (Version 28, SSPS Inc., Chicago, IL) was used for all statistical analyses.

3 Results

3.1 Patient characteristics

A total of 54 PC patients were treated with radiation using MR-LINAC with median age of 70.4 (45.2–85.9) years. A total of 48 patients (88.9%) had at least 60 days of follow-up at the time of evaluation. All but one patient (98.1%) had a biopsy-proven diagnosis of PC; most (96.2%) patients had pancreatic adenocarcinoma, one patient had adeno-squamous carcinoma, and one patient had cholangiocarcinoma. A total of 40 patients (74.0%) had primary inoperable PC (inoperable group), and 14

1 V33 = volume of tissue or organ that receives a radiation dose of 33 Gy or higher.

2 V25 = volume of tissue or organ that receives a radiation dose of 25 Gy or higher.

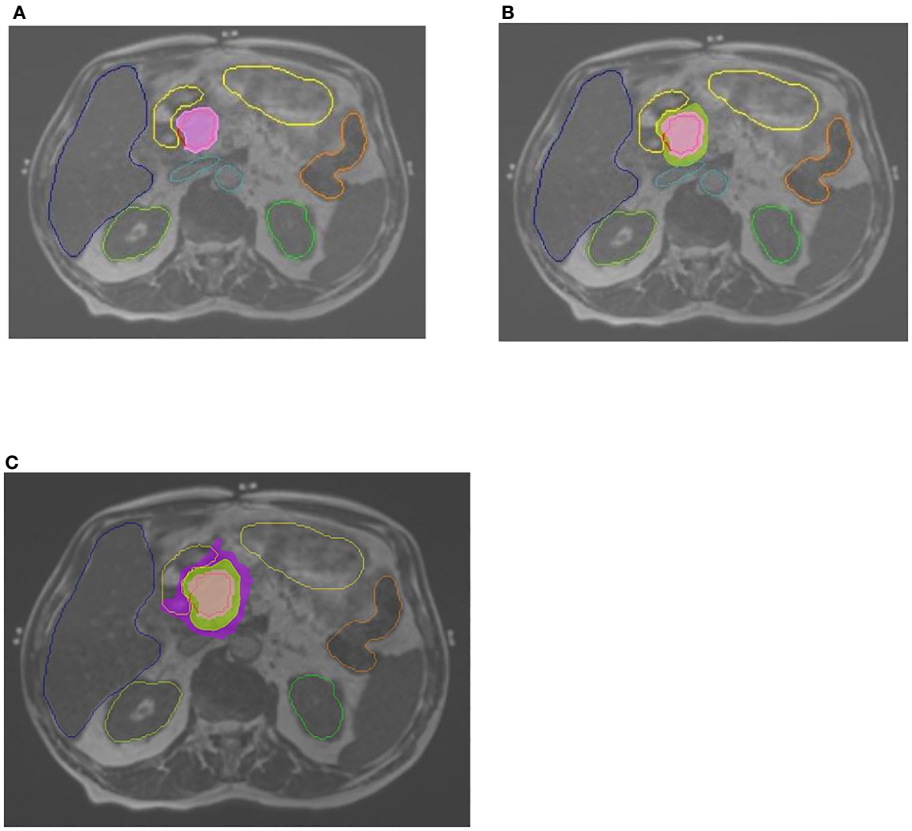

FIGURE 1
Contouring and doses. Abdominal MRI, 0.35T, with contoured OARs: stomach-duodenum, liver, kidneys, large bowel, great vessels. **(A)** GTV contoured in red. Pink color wash–100% dose (of 50 Gy prescribed dose). **(B)** Green color wash—95% dose. **(C)** Purple color wash—50% dose.

patients (25.9%) had local recurrence post Whipple procedure (operated group). One patient had undergone a preventive Whipple procedure 14 years prior to cancer diagnosis and therefore was regarded as inoperable PC. Twenty-one patients (38.9%) had metastatic disease at the time of radiotherapy.

Prior to SMART, 47 patients (87.0%) received chemotherapy, mainly using 5FU+Oxaliplatin-based regimen (n=39, 72.2%), and 14 patients (25.9%) received multiple sequential chemotherapy regimens following SMART. Six patients (11.1%), all previously operated, received RT to the pancreatic region prior to SMART, mostly chemoradiation (n=5, 9.25%) using either Capecitabine or Gemcitabine.

Apart from CA 19-9 serum levels, which were lower among operated patients compared to the inoperable group both at time of diagnosis (n=14, mean of 401, p=0.018 and n=38, mean of 1,877, respectively) and up to 6 weeks prior to RT (n=11, mean of 105, p=0.015 and n=30, mean of 978, respectively), there was no significant difference in demographics and baseline parameters between operated and inoperable groups. See Table 1.

3.2 Treatment characteristics

A total of 53 patients (98.1%) completed SMART to a prescription of 50 Gy in five fractions. On-table adaptive replanning was performed for 100.0% of all (269) fractions; one patient received four fractions due to intolerance for prolonged immobility necessary for accurate radiation delivery. After SMART, 32 patients (69.6%) received additional chemotherapy (26 inoperable patients and 6 recurrence patients).

3.3 Toxicity

None of the patients reported grade ≥2 acute GI toxicity or were hospitalized due to treatment-related side effects.

Prior to SMART, 40 patients (80.0%) reported disease-related symptoms, including abdominal pain (42.6%, n=23), back pain (14.8%, n=8), loss of appetite (27.7%, n=15), weight loss (42.5%, n=23), and fatigue (29.6%, n=16). Two inoperable patients (3.7%) had gastric outlet obstruction prior to SMART, which was resolved during treatments.

Apart from diarrhea at 1–3 months post-SMART and general fatigue, which were reported more frequently by previously resected patients in comparison to the inoperable group (30.0% vs. 10.0%, p=0.03 and 38.5% vs. 10.3%, p=0.033, respectively), no significant differences were found between the groups with respect to the remaining evaluated symptoms. All previously irradiated patients reported only low-grade toxicities during RT (100.0%, n=5, p=0.009).

10.3389/fonc.2023.1289919

TABLE 1 Patient, tumor, and prior therapy characteristics.

	Primary Inoperable Pancreatic Cancer (n = 40)	Local Recurrence Post Whipple Procedure (n = 14)	Total (n = 54)
Median Age (range)	70.3 (46.8-85.7)	64.6 (43.8-78.3)	69 (43.8-85.7)
Sex, n (%)			
Men	26 (65)	10 (71.4)	36 (66.7)
Women	14 (35)	4 (28.6)	18 (33.3)
Comorbidities, n (%)			
IHD	6 (15)	3 (21.4)	9 (16.7)
DM	16 (40)	6 (42.9)	22 (40.7)
BRCA Status, n (%)			
BRCA 1/2	0 (0)	0 (0)	0 (0)
Wild Type	20 (50)	4 (28.6)	24 (44.4)
Unknown	20 (50)	10 (71.4)	30 (55.6)
Smoking Status, n (%)			
Currently	6 (15.8)	3 (23.1)	9 (17.6)
Per History	6 (15.8)	1 (7.7)	7 (13.7)
Non-Smoker	26 (68.4)	9 (69.2)	35 (68.6)
Unknown	2 (5)	1 (7.7)	3 (5.6)
Prior chemotherapy, n (%)			
1 protocol	34 (85)	13 (92.9)	47 (87)
2 protocols	6 (15)	8 (57.1)	14 (25.9)
Oxaliplatin+5FU based	32 (80)	7 (50)	39 (72.2)
Gemcitabine alone	1 (2.5)	4 (28.5)	5 (9.2)
Gemcitabin based	8 (20)	4 (28.5)	12 (22.2)

IHD, Ischemic Heart Disease. DM, Diabetes Mellitus. RT, Radiotherapy. CRT, Chemoradiotherapy. C/G, Capecitabine / Gemcitabine.

3.4 Response and outcomes

A total of 48 patients (88.9%) were available for evaluation; one patient died due to his disease within 10 days following RT, and five patients were lost to follow-up. Median follow-ups from diagnosis were 22.3 and 8.9 months from SMART. As expected, the previously operated group had longer mean follow-up time from diagnosis compared to inoperable patients (40.3 and 20.3 months, respectively, p=0.001), and patients who received prior RT to the pancreas had an additional 8 months of follow-up time from SMART.

The first response and disease status were evaluated after 3.4 months in average. Complete local control was achieved by 21.7% (n=10) of patients for a median of 9 months (2.8–28.8 months); three patients had later local progression. Nine patients (19.6%) achieved partial response, and 21 patients (45.7%) had stable disease at the time of evaluation for a total of 87.0% local control. There was no significant difference between groups in local control, evidence of distant disease (new or known), and regional failure/relapse. None of the patients who underwent prior RT achieved CR; however, they still responded to treatment: one patient achieved partial local response (PR), and three patients had stable local disease (SD). The remaining two patients who had previously undergone RT had either died prior to post-SMART imaging evaluation or had locally progressive disease.

Five patients received concomitant radiation to liver metastases. Two patients were treated using a regular linear accelerator and had multiple new liver lesions upon radiological evaluation post-treatments. The remaining three patients were treated using SMART (45–50 Gy in five fractions); two patients had complete metabolic response in irradiated lesions, while the third patient had disease progression.

Mean CA 19-9 serum levels were consistently lower among previously resected patients and were significantly lower in 50.0% of evaluated time frames. See Table 2 describing treatment outcomes.

OS of 6 and 12 months (from end of SMART) was 75.0% and 52.1%, respectively. Operated patients had an understandably longer mean survival from diagnosis compared to inoperable patients (49.85 and 24 months, respectively); however, there was no significant difference between groups in 6-, 12-, and 18-month OS from end of SMART. See Figure 2 comparing OS between groups. Non-metastatic patients had a 6, 12, and 18 months OS of 55%, 44%, and 28%, respectively. The type of local response to treatment had no significant impact on survival (p=0.935). Patients with previous RT (five patients with more than 60 days follow-up) had 6 months OS of 80%, and one patient remained alive after 12 months.

4 Discussion

In this study, we report our experience on treating pancreatic cancer, either locally advanced or recurrent, with high-dose adaptive MR-guided radiation therapy. We found that SMART is safe, with minimal treatment-related toxicity, even in previously irradiated patients, and that both operated and inoperable patients

can achieve local response, with over 20% rate of complete local response to treatment.

By including patients with metastatic disease, local recurrence post-Whipple, and previously irradiated patients, our study population differed greatly from that of previous studies. To the best of our knowledge, published SMART studies have focused mainly on treating inoperable locally advanced PC in patients without prior RT (15, 21), frequently excluding metastatic disease as well (16, 22, 23), unless the study purpose was to examine re-irradiation specifically (18).

Similar to previously published research with MR-guided SBRT, our prescribed dose to inoperable PC was 50 Gy in five fractions, with special attention to daily on-table adaptation, and 100% of the delivered fractions was adapted. Treatment plan adaptation poses an important aspect in our treatment plan, ensuring that OAR tolerance doses are not exceeded, even at the expense of PTV coverage. Indeed, toxicity was minimal during and after treatment, even in previously resected or irradiated patients. None of the patients experienced grade ≥ 2 toxicities. This is in concordance with other reports with very low toxicity rates. Table 3 contains a summary of selected studies of SMART in PC. For example, in their research, Henke et al. (15), Rudra et al. (16), Hassanzadeh et al. (22), and Chuong et al. (23, 24) treated patients with a comparable prescription dose (BED_{10} over 70 Gy) using SMART and reported aligning results—0.0%, 0.0%, 4.6%, 2.9%, and 8.8% grade ≥ 3 acute toxicities, respectively. In the study by Hassanzadeh et al., some patients received RT using MRIdian Cobalt-60 system, with 4.6% reported associated grade 3 toxicity for all patients with no further information (22). As treatment volumes at the phase II study by Parikh et al. were at the discretion of the treating physician, some patients were treated to adjacent anatomic regions considered to be at high risk for micro-metastatic disease (24). This may contribute to the reported higher rate of grade 3 toxicity, 8.8%. Conventional fractionation (BED_{10} 55.5 Gy) resulted in 15% grade 3 or higher in the study by Rudra et al. (16). These are highly encouraging results, as PC is known for posing a challenge for the treating radiation oncologist due to its proximity to delicate GI structures (25). It should be noted that in our treatment protocol, all patients were prescribed Ondansetron to prevent radiation-related nausea, which might explain the low rate of nausea complaints.

The main endpoints of this study were local control and outcomes. We report that 87.0% of treated patients achieved local control at the time of evaluation, whether in the form of complete local response (CR, 21.7%), partial response (PR, 19.6%), or stable disease (SD, 45.7%), while only 13.0% had local progressive disease (LPD). Due to the frequent use of PET-CT as a physiological imaging modality, we were able to evaluate disease metabolic status using PERCIST criteria (20). Although this allowed for a most accurate evaluation of therapeutic effects, local metabolic response in the form of CR/PR/SD/LPD, and whole-body disease status (26), we find ourselves unable to compare these results to previously published studies, in which "local control" was the main endpoint evaluated by CT scans.

However, as opposed to previously published articles, our research reports 1-year OS of 58.3%, which is considerably lower in comparison to others (15, 17, 18, 22, 23). This could be attributed to the difference in patient selection, as our study population includes metastatic disease or previous local surgical/radiation treatments to the pancreas, suggesting a more advanced disease.

The singularity of this study lies in the comparison of outcomes between previously operated and inoperable patients. We aimed to evaluate differences in outcome and toxicity of SMART between these two groups to better understand the role of patient selection based on disease and treatment history. We found that there were no

TABLE 2 Outcomes Post SMART Treatment.

	Primary Inoperable Pancreatic Cancer	Local Recurrence Post Whipple Procedure	Total	P-Value
Local Response*, n (%)				
Complete Response	8 (22.9)	2 (18.2)	10 (21.7)	NS
Local Recurrence	3 (37.5)	0 (0.0)	3 (30.0)	NS
Partial Response	8 (22.9)	1 (9.1)	9 (19.6)	NS
Stable Disease	14 (40.0)	7 (63.6)	21 (45.7)	NS
Local Progression	5 (14.3)	1 (9.1)	6 (13.0)	NS
Distant Disease, n (%)**				
Prior to SMART	18 (45.0)	3 (21.4)	21 (38.9)	NS
Post SMART	19 (54.3)	5 (45.5)	24 (52.2)	NS
Regional Failure/Relapse	7 (19.4)	1 (9.1)	8 (17.0)	NS
Chemotherapy Re-induction, n (%)	26 (72.2)	6 (60.0)	32 (69.6)	NS
Overall Survival (OS, in months)				
Mean OS	15.1	11.8	14.43	NS
6-months OS from SMART completion	75.0%	83.3%	75.0%	NS
12-months OS from SMART completion	50.0%	58.3%	52.1%	NS
18-months OS from SMART completion	41.6%	41.6%	41.6%	NS

* Local Response was determined based on RECIST & PERCIST criteria

** Distant disease existence was evaluated based on imaging. Post SMART metastatic disease was determined based on the same imaging study used to evaluate local response to treatment. Dx, Diagnosis. SMART, Stereotactic MR-guided Adaptive Radiotherapy. NS, Non-significant, P>0.05.

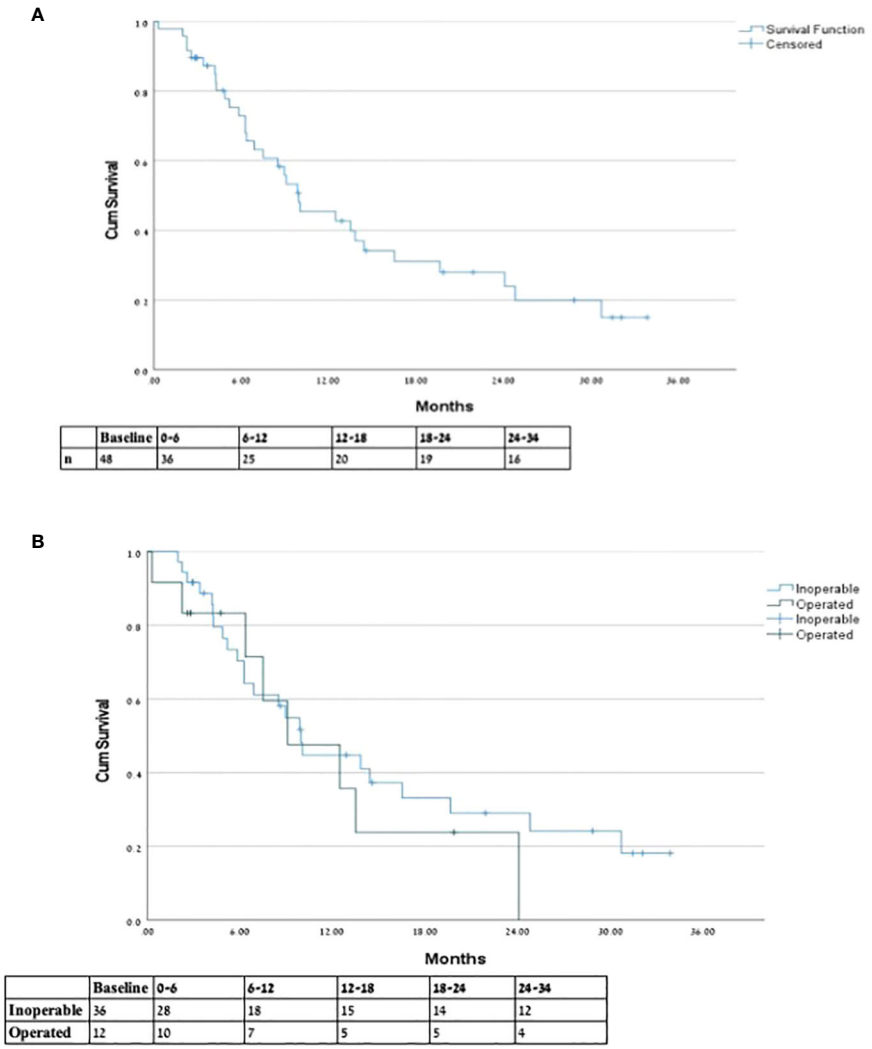

	Baseline	0-6	6-12	12-18	18-24	24-34
n	48	36	25	20	19	16

	Baseline	0-6	6-12	12-18	18-24	24-34
Inoperable	36	28	18	15	14	12
Operated	12	10	7	5	5	4

FIGURE 2
Overall survival from end of SMART. * Overall survival from end of SMART for **(A)** entire cohort and **(B)** inoperable vs. previously operated patients.

significant differences in demographics and response to treatment between the groups, even among patients who have previously undergone RT to the pancreas, suggesting that SMART can potentially benefit patients regardless of previous treatment attempts.

In our study, we found two major areas distinguishing the two groups, the first being CA 19-9 serum levels, which were consistently lower among operated patients in most evaluated time frames, suggesting that inoperable patients had a more advanced disease or that they had a disease less susceptible to treatments. Additionally, we noticed that previously operated patients tended to experience more short-term (although low-grade) toxicities, such as fatigue and diarrhea. While diarrhea could be sporadic or a result of pancreatic endocrine insufficiency, in their review, Chang et al. (27) show that fatigue is more common in previously operated patients in comparison to inoperable patients (73% and 53%, respectively). Thus, it is possible that these findings are essentially disease-related symptoms as opposed to treatment-related toxicities. For example, disease-related fatigue could be supported by longer follow-up time from diagnosis among the operated group, expressing that these patients have been coping with PC diagnosis and systemic treatment for longer time periods. As this is the first research to evaluate the difference in outcomes and toxicities after SMART between operated and inoperable patients, unfortunately and to the best of our knowledge, there is no available literature to compare our results to. Further research is needed to evaluate the difference in SMART-related toxicities in inoperable and previously operated patients regardless of RT-related symptoms.

This study has some limitations. This is a single-center study; however, it is a relatively large series compared to other single-center studies. This is a retrospective study, subject to under-reporting toxicities, although toxicities were documented prospectively. Additionally, our results could benefit from a more extended follow-up to better understand late toxicity and long-term clinical outcomes. Finally, whereas local response was an endpoint for other studies, in this study, physiological imaging modalities (MRI and PET-CT) were used to evaluate local response. This posed a challenge in terms of comparing results, yet we suggest that this

TABLE 3 Summary of selected studies of SMART in pancreatic cancer.

Study	Patient number	Total dose and fractions	BED_{10}	Median follow-up (months)	LC	OS	Acute grade 3+ toxicity (%)
Henke et al. (2018) (15)	5	50 Gy × 5	100	15	6-months 89.1%	1-year 75.0%	0.0%
Rudra et al. (2019) (16)	24+	40–52 Gy × 5	72–106.1	17	2-year 77.0%	2-year 49.0%	0.0%
Placidi et al. (2020) (21)	8	30–40 Gy × 5	48–72	13	25.0%	87.5% at last F/U	0.0%
Hassanzadeh et al. (2021) (22)	44	50 Gy × 5	100	16 (from dx)	1-year 84.3%	1-year 68.2%	4.6%
Chuong et al. (2020) (23)	35	40–50 Gy × 5	100	10.3	1-year 87.8%	1-year 58.9%	2.9%
Chuong et al. (2021) (17)	148	40–50 Gy × 5	100	16 (from dx)	1-year 94.6%	1-year 82.0%	4.1%
Chuong et al. (re-irradiation, 2022) (18)	11[++]**	40 Gy × 6	44.7	14	1-year 88.9%	1-year 70.0%	0.0%
Parikh et al. (2023) (24)	136	50 Gy × 5	100	8.8	1-year 82.9%	1-year 65.0%	8.8%
Current study	54	50 Gy × 5	100	8.9	87.0%*	1-year 52.08%	0.0%

BED, biologically effective dose; LC, local control; OS, overall survival.
[+] Including nine patients with hypofractionated protocol, with median BED_{10} of 82.7.
[++] Including four patients with hypofractionated dose schedule.
* Local control for this study was calculated as the percentage of patients who had either complete local response, partial response, or stable disease at time of first radiological evaluation post-SMART.
** Re-irradiation for multiple malignancies. Out of 11 patients, only 3 patients had PC.

also allowed for a more accurate evaluation of local response, with a potential for standardization thanks to the use of RECIST and PERCIST criteria.

5 Conclusion

SMART is a safe local treatment modality for pancreatic cancer, with minimal treatment-related toxicity, even in previously resected or irradiated patients. Local control with complete response was achieved by 21.7% of patients, regardless of previous surgical history. Further studies are needed to evaluate long-term outcome and late toxicity and to identify significant factors for patient selection.

Data availability statement

The raw data supporting the conclusions of this article will be made available by the authors, without undue reservation.

Ethics statement

The studies involving humans were approved by Assuta Medical Center Helsinki Committee. The studies were conducted in accordance with the local legislation and institutional requirements. Written informed consent for participation was not required from the participants or the participants' legal guardians/next of kin in accordance with the national legislation and institutional requirements.

Author contributions

GA: Writing – original draft, Writing – review & editing. RP: Writing – review & editing. SZ: Writing – review & editing. VG: Writing – review & editing. YLi: Writing – review & editing. EC: Writing – review & editing. DLe: Writing – review & editing. SA: Writing – review & editing. OA: Writing – review & editing. DE: Writing – review & editing. QT: Writing – review & editing. KH: Formal analysis, Writing – review & editing. DLi: Writing – review & editing. TG: Writing – review & editing. IB-A: Writing – review & editing. YRL: Writing – review & editing. MB-D: Conceptualization, Methodology, Project administration, Supervision, Validation, Writing – review & editing.

Funding

The author(s) declare that no financial support was received for the research, authorship, and/or publication of this article.

Conflict of interest

The authors declare that the research was conducted in the absence of any commercial or financial relationships that could be construed as a potential conflict of interest.

The author(s) declared that they were an editorial board member of Frontiers, at the time of submission. This had no impact on the peer review process and the final decision.

Publisher's note

References

1. Cancer of pancreas - cancer stat facts. *SEER*.

2. Spanknebel K, Conlon KC. Advances in the surgical management of pancreatic cancer. *Cancer J* (2001) 7(4):312–23.

3. Willett CG, Czito BG, Bendell JC, Ryan DP. Locally advanced pancreatic cancer. *Vol 23 J Clin Oncol* (2005) 23:4538–44. doi: 10.1200/JCO.2005.23.911

4. Wagner M, Redaelli C, Lietz M, Seiler CA, Friess H, Büchler MW. Curative resection is the single most important factor determining outcome in patients with pancreatic adenocarcinoma. *Br J Surgery* (2004) 91(5):586–94. doi: 10.1002/bjs.4484

5. Reyngold M, O'Reilly EM, Varghese AM, Fiasconaro M, Zinovoy M, Romesser PB, et al. Association of ablative radiation therapy with survival among patients with inoperable pancreatic cancer. *JAMA Oncol* (2021) 7(5):735–8. doi: 10.1001/jamaoncol.2021.0057

6. Yalamanchili A, Thomas TO, Dajani S, Hayes JP. Evolution of radiation therapy in pancreas cancer management toward MRI-guided adaptive radiation therapy. *J Clin Med* (2022) 11:5380. doi: 10.3390/jcm11185380

7. Petrelli F, Comito T, Ghidini A, Torri V, Scorsetti M, Barni S. Stereotactic body radiation therapy for locally advanced pancreatic cancer: A systematic review and pooled analysis of 19 trials. *Int J Radiat Oncol Biol Physics* (2017) 97:313–22. doi: 10.1016/j.ijrobp.2016.10.030

8. Noel CE, Parikh PJ, Spencer CR, Green OL, Hu Y, Mutic S, et al. Comparison of onboard low-field magnetic resonance imaging versus onboard computed tomography for anatomy visualization in radiotherapy. *Acta Oncol (Madr)* (2015) 54(9):1474–82. doi: 10.3109/0284186X.2015.1062541

9. Herman JM, Chang DT, Goodman KA, Dholakia AS, Raman SP, Hacker-Prietz A, et al. Phase 2 multi-institutional trial evaluating gemcitabine and stereotactic body radiotherapy for patients with locally advanced unresectable pancreatic adenocarcinoma. *Cancer*. (2015) 121:1128–37. doi: 10.1002/cncr.29161

10. Hoyer M, Roed H, Sengelov L, Traberg A, Ohlhuis L, Pedersen J, et al. Phase-II study on stereotactic radiotherapy of locally advanced pancreatic carcinoma. *Radiotherapy Oncol* (2005) 76(1):48–53. doi: 10.1016/j.radonc.2004.12.022

11. Mahadevan A, Miksad R, Goldstein M, Sullivan R, Bullock A, Buchbinder E, et al. Induction gemcitabine and stereotactic body radiotherapy for locally advanced nonmetastatic pancreas cancer. *Int J Radiat Oncol Biol Phys* (2011) 81(4):e615-22. doi: 10.1016/j.ijrobp.2011.04.045

12. Katz MHG, Shi Q, Meyers J, Herman JM, Chuong M, Wolpin BM, et al. Efficacy of Preoperative mFOLFIRINOX vs mFOLFIRINOX Plus Hypofractionated Radiotherapy for Borderline Resectable Adenocarcinoma of the Pancreas: The A021501 Phase 2 Randomized Clinical Trial. *JAMA Oncol* (2022) 8(9):1263–70. doi: 10.1001/jamaoncol.2022.6147

13. Boldrini L, Cusumano D, Cellini F, Azario L, Mattiucci GC, Valentini V. Online adaptive magnetic resonance guided radiotherapy for pancreatic cancer: State of the art, pearls and pitfalls. *Radiat Oncol* (2019) 14:71. doi: 10.1186/s13014-019-1275-3

14. Bohoudi O, Bruynzeel AME, Senan S, Cuijpers JP, Slotman BJ, Lagerwaard FJ, et al. Fast and robust online adaptive planning in stereotactic MR-guided adaptive radiation therapy (SMART) for pancreatic cancer. *Radiotherapy Oncol* (2017) 125 (3):439–44. doi: 10.1016/j.radonc.2017.07.028

15. Henke L, Kashani R, Robinson C, Curcuru A, DeWees T, Bradley J, et al. Phase I trial of stereotactic MR-guided online adaptive radiation therapy (SMART) for the treatment of oligometastatic or unresectable primary Malignancies of the abdomen. *Radiotherapy Oncol* (2018) 126(3):519–26. doi: 10.1016/j.radonc.2017.11.032

16. Rudra S, Jiang N, Rosenberg SA, Olsen JR, Roach MC, Wan L, et al. Using adaptive magnetic resonance image-guided radiation therapy for treatment of inoperable pancreatic cancer. *Cancer Med* (2019) 8(5):2123–32. doi: 10.1002/cam4.2100

17. Chuong MD, Kirsch C, Herrera R, Rubens M, Gungor G, Schaff EM, et al. Long-term multi-institutional outcomes of 5-fraction ablative stereotactic MR-guided adaptive radiation therapy (SMART) for inoperable pancreas cancer with median prescribed biologically effective dose of 100 gy10. *Int J Rad Oncol – Biol – Phys (IJROBP)* (2021) 111:S147–8. doi: 10.1016/j.ijrobp.2021.07.330

18. Chuong MD, Bryant JM, Herrera R, McCulloch J, Contreras J, Kotecha R, et al. Dose-escalated magnetic resonance image–guided abdominopelvic reirradiation with continuous intrafraction visualization, soft tissue tracking, and automatic beam gating. *Adv Radiat Oncol* (2022) 7(2):100840. doi: 10.1016/j.adro.2021.100840

19. Eisenhauer EA, Therasse P, Bogaerts J, Schwartz LH, Sargent D, Ford R, et al. New response evaluation criteria in solid tumours: Revised RECIST guideline (version 1.1). *Eur J Cancer* (2009) 45(2):228–47. doi: 10.1016/j.ejca.2008.10.026

20. Wahl RL, Jacene H, Kasamon Y, Lodge MA. From RECIST to PERCIST: Evolving considerations for PET response criteria in solid tumors. *J Nucl Med* (2009) 50:122S–50S. doi: 10.2967/jnumed.108.057307

21. Placidi L, Romano A, Chiloiro G, Cusumano D, Boldrini L, Cellini F, et al. On-line adaptive MR guided radiotherapy for locally advanced pancreatic cancer: Clinical and dosimetric considerations. *Tech Innov Patient Support Radiat Oncol* (2020) 15:15–21. doi: 10.1016/j.tipsro.2020.06.001

22. Hassanzadeh C, Rudra S, Bommireddy A, Hawkins WG, Wang-Gillam A, Fields RC, et al. Ablative five-fraction stereotactic body radiation therapy for inoperable pancreatic cancer using online MR-guided adaptation. *Adv Radiat Oncol* (2021) 6 (1):100506. doi: 10.1016/j.adro.2020.06.010

23. Chuong MD, Bryant J, Mittauer KE, Hall M, Kotecha R, Alvarez D, et al. Ablative 5-fraction stereotactic magnetic resonance–guided radiation therapy with on-table adaptive replanning and elective nodal irradiation for inoperable pancreas cancer. *Pract Radiat Oncol* (2021) 11(2):134–47. doi: 10.1016/j.prro.2020.09.005

24. Parikh PJ, Lee P, Low DA, Kim J, Mittauer KE, Bassetti MF, et al. A multi-institutional phase II trial of ablative 5-fraction stereotactic MR-guided on-table adaptive radiation therapy for borderline resectable and locally advanced pancreatic cancer. *Int J Radiat OncologyBiologyPhysics* (2023) 177:799–808. doi: 10.1016/j.ijrobp.2023.05.023

25. Panje C, Andratschke N, Brunner TB, Niyazi M, Guckenberger M. Stereotactic body radiotherapy for renal cell cancer and pancreatic cancer: literature review and practice recommendations of the DEGRO working group on stereotactic radiotherapy. *Strahlentherapie und Onkologie* (2016) 192:875–85. doi: 10.1007/s00066-016-1053-1

26. Yokose T, Kitago M, Matsusaka Y, Masugi Y, Shinoda M, Yagi H, et al. Usefulness of 18F-fluorodeoxyglucose positron emission tomography/computed tomography for predicting the prognosis and treatment response of neoadjuvant therapy for pancreatic ductal adenocarcinoma. *Cancer Med* (2020) 9(12):4059–68. doi: 10.1002/cam4.3044

27. Chang VT, Sandifer C, Zhong F. GI symptoms in pancreatic cancer. *Clin Colorectal Cancer* (2023) 22:24–33. doi: 10.1016/j.clcc.2022.12.002

frontiers | Frontiers in Oncology

TYPE Original Research
PUBLISHED 15 February 2024
DOI 10.3389/fonc.2024.1308406

OPEN ACCESS

EDITED BY
Enis Ozyar,
Acıbadem University, Türkiye

REVIEWED BY
Sara Lyons Hackett,
University Medical Center Utrecht, Netherlands
Mark Hallman,
Fox Chase Cancer Center, United States

*CORRESPONDENCE
Christoph A. Fink
Christoph.Fink@med.uni-heidelberg.de

†These authors have contributed equally to this work and share senior authorship

RECEIVED 06 October 2023
ACCEPTED 24 January 2024
PUBLISHED 15 February 2024

CITATION
Fink CA, Buchele C, Baumann L, Liermann J, Hoegen P, Ristau J, Regnery S, Sandrini E, König L, Rippke C, Bonekamp D, Schlemmer H-P, Debus J, Koerber SA, Klüter S and Hörner-Rieber J (2024) Dosimetric benefit of online treatment plan adaptation in stereotactic ultrahypofractionated MR-guided radiotherapy for localized prostate cancer. *Front. Oncol.* 14:1308406. doi: 10.3389/fonc.2024.1308406

Dosimetric benefit of online treatment plan adaptation in stereotactic ultrahypofractionated MR-guided radiotherapy for localized prostate cancer

Christoph A. Fink[1,2,3*], Carolin Buchele[1,2,3], Lukas Baumann[4], Jakob Liermann[1,2,3], Philipp Hoegen[1,2,3,5], Jonas Ristau[1,2,3], Sebastian Regnery[1,2,3], Elisabetta Sandrini[1,2,3], Laila König[1,2,3], Carolin Rippke[1,2,3], David Bonekamp[3,6,7], Heinz-Peter Schlemmer[6], Juergen Debus[1,2,3,5,7,8], Stefan A. Koerber[1,2,3,9], Sebastian Klüter[1,2,3†] and Juliane Hörner-Rieber[1,2,3,5†]

[1]Department of Radiation Oncology, Heidelberg University Hospital, Heidelberg, Germany, [2]Heidelberg Institute of Radiation Oncology (HIRO), Heidelberg, Germany, [3]National Center for Tumor Diseases (NCT), Heidelberg, Germany, [4]Institute of Medical Biometry (IMBI), University of Heidelberg, Heidelberg, Germany, [5]Clinical Cooperation Unit Radiation Oncology, German Cancer Research Center (DKFZ), Heidelberg, Germany, [6]Division of Radiology, German Cancer Research Center (DKFZ), Heidelberg, Germany, [7]German Cancer Consortium (DKTK), Partner Side Heidelberg, Heidelberg, Germany, [8]Heidelberg Ion-Beam Therapy Center (HIT), Department of Radiation Oncology, Heidelberg University Hospital, Heidelberg, Germany, [9]Department of Radiation Oncology, Barmherzige Brueder Hospital Regensburg, Regensburg, Germany

Background: Apart from superior soft tissue contrast, MR-guided stereotactic body radiation therapy (SBRT) offers the chance for daily online plan adaptation. This study reports on the comparison of dose parameters before and after online plan adaptation in MR-guided SBRT of localized prostate cancer.

Materials and methods: 32 consecutive patients treated with ultrahypofractionated SBRT for localized prostate cancer within the prospective SMILE trial underwent a planning process for MR-guided radiotherapy with 37.5 Gy applied in 5 fractions. A base plan, derived from MRI simulation at an MRIdian Linac, was registered to daily MRI scans (predicted plan). Following target and OAR recontouring, the plan was reoptimized based on the daily anatomy (adapted plan). CTV and PTV coverage and doses at OAR were compared between predicted and adapted plans using linear mixed regression models.

Results: In 152 out of 160 fractions (95%), an adapted radiation plan was delivered. Mean CTV and PTV coverage increased by 1.4% and 4.5% after adaptation. 18% vs. 95% of the plans had a PTV coverage ≥95% before and after online adaptation, respectively. 78% vs. 100% of the plans had a CTV coverage ≥98% before and after online adaptation, respectively. The $D_{0.2cc}$ for both bladder and rectum were <38.5 Gy in 93% vs. 100% before and after online adaptation. The constraint at the urethra with a dose of <37.5 Gy was achieved in 59% vs. 93% before and after online adaptation.

Conclusion: Online adaptive plan adaptation improves target volume coverage and reduces doses to OAR in MR-guided SBRT of localized prostate cancer. Online plan adaptation could potentially further reduce acute and long-term side effects and improve local failure rates in MR-guided SBRT of localized prostate cancer.

KEYWORDS

stereotactic body radiation therapy, MR-guided radiotherapy, daily adaptive radiotherapy, prostate cancer, dosimetric benefits

Highlights

- MR-guided online plan adaptation improves CTV and PTV Coverage.
- MR-guided online plan adaptation decreases dose at organs at risk.
- MR-guided online plan adaptation improves dose constraint adherence for organs at risk.

Introduction

Radiotherapy for localized prostate cancer has undergone a remarkable evolution over the years, technical advances going along with an increasing emphasis on ultrahypofractionation (1–4). The adoption of high single dose regimens highlights the critical need for precise and accurate dose delivery to the target volume, while simultaneously adhering to strict organ at risk (OAR) constraints. Technical advances in dose optimization and delivery techniques are paving the way toward achieving this balance: The incorporation of MR-guided radiotherapy workflows has introduced a new chapter of precision and adaptability. Due to its superior soft tissue contrast, precise visualization and delineation of the prostate and neighboring anatomy is facilitated (5–7), potentially widening the therapeutic window in pelvic radiotherapy by minimizing the inadvertent irradiation of healthy tissues.

Another advantage of MR-guided radiotherapy is its capability to adapt the treatment plan according to daily anatomical variations observed at and during each session (8). Reoptimization of the daily treatment plan to deliver a base-plan-like dose distribution in each fraction may further improve efficacy and reduce toxicity (8–11). The focus of this study is to evaluate the impact of online plan adaptation on target volume coverage and OAR dose and constraint adherence in ultrahypofractionated MR-guided radiotherapy of localized prostate cancer.

Materials and methods

Treatment planning

We report dosimetry data of the first 32 patients at Heidelberg University Hospital from the prospective SMILE phase II trial (12) (NCT04845503). *SMILE* aims at evaluating the safety and feasibility of ultrahypofractionated radiotherapy with MR-guided radiation therapy in localized prostate cancer. All patients received MR-guided SBRT from 03/2021 to 03/2023 at Heidelberg University Hospital. The detailed treatment planning process was reported previously (12). In short, all patients underwent multiparametric MRI (mpMRI). Subsequently, a True Fast Imaging with Steady State Procession (TRUFI) sequence was utilized for a 0.35T MRI simulation scan at an MRIdian Linear Accelerator for all patients. After the MRI simulation, patients underwent a planning CT without contrast with an identical setup. A base plan was calculated based on the mpMRI and the planning CT.

Dose specifications

Online adaptive MR-guided SBRT was administered as step-and-shoot IMRT using an MRIdian Linear Accelerator system developed by ViewRay, Inc. In cases of low-risk cancers, the clinical target volume comprised solely the prostate, while intermediate-risk cancers included the base of the seminal vesicles in the clinical target volume. The clinical target volume (CTV) was expanded uniformly by 3 mm in all directions to form the planning target volume (PTV). At least 95% of the PTV was required to receive ≥95% of the prescribed dose, with an upper limit of 107% for the maximum dose. The prescribed dose of 37.5 Gy was delivered over 5 fractions administered on alternate days. 5 patients received a simultaneous integrated boost of 40 Gy to the dominant intraprostatic lesion. A planning organ at risk volume (PRV) was created around the urethra by adding a 2 mm margin, with a dose constraint of $D_{0.2cc}$ ≤37.5 Gy. For both bladder and rectum, a $D_{0.2cc}$ ≤38.5 Gy was prescribed according to the protocol. No fiducial markers, rectal spacer gels, or other rectal devices were employed.

Treatment

Patients were instructed to have an empty bowel before receiving radiation therapy. Additionally, patients were asked to consume 500 ml of water 30 minutes prior to the start of therapy to ensure an adequate bladder volume. Following the patient's treatment setup, an MRI scan was conducted at the MRIdian Linear Accelerator and examined to confirm an empty rectum and satisfactory bladder filling. In a first step of adjustment, the daily MRI was matched with the base plan by translational repositioning. Subsequently, this MRI scan was registered to the MRI of the base plan based on the CTV contours. OAR contours from the planning MRI scan were deformably transferred to the daily MRI, while CTV and PTV contours were transferred rigidly. In all cases, CTV contours were adjusted by the treating physician. OARs were modified within an area around the PTV expanded by 1 cm in the cranio-caudal direction and 3 cm in all other directions on the daily MRI (13). After recontouring, the base plan was applied onto the anatomy of the day (= predicted plan). In case of any violations of either OAR dose constraints or the PTV coverage, the plan was reoptimized based on the current anatomy (= adapted plan). After reoptimization, a second MRI scan was performed to account for anatomical changes during reoptimization. In case of satisfactory anatomic alignment, the adapted plan was approved by the treating physician. On-table quality assurance was conducted using a vendor-supplied secondary dose calculation as well as an in-house software developed for evaluating target volume extension, contour accuracy and fluence modulation (14).

Statistical analysis

The predicted and adapted treatment plans of 32 consecutive patients were analyzed to assess the coverage of CTV and PTV, as well as the radiation doses received by the rectum, urethra, and bladder as OAR. Predicted and adapted plans were analyzed based on dose volume histogram analysis considering dose constraints for OAR and target volumes as well as absolute percentages for CTV and PTV coverage. Linear mixed regression models were used to analyze dose and target coverage as continuous variables. The plan (predicted vs. adapted) was included as a fixed factor. Random intercepts for patients and days (nested within patients) were specified to account for the repeated measures. However, in many cases the estimated variance of the day-specific random intercepts was 0 and thus the random effect was removed from the respective model. 95% profile-likelihood confidence intervals (CIs) were computed for the plan differences.

When model residuals were non-normal or outliers were present, the robust variance-covariance matrix CR2 was used (15, 16). The analysis was done in R 4.3.0 using the packages lmerTest (17) and clubSandwich (18).

Results

A total of 160 treatment sessions, consisting of five fractions per patient, were administered. Among these, plan adaptations were carried out for 152 fractions (95%). The median duration for the recontouring and the plan reoptimization was 39 minutes (range 22 – 78 minutes).

Target volumes

Although PTV size varied from first to last adapted fraction by a median of -1.7% (range -11.2 – 11.1%), online plan reoptimization did not cause a substantial change in PTV size with a median change of 0.4% (range 0.2 – 1.3%).

Online plan adaptation yielded a 4.5% increase in mean PTV coverage (95% CI: 3.0; 6.0, $p < 0.001$). Regarding treatment goals, online plan adaptation enabled a PTV coverage ≥95% in 95% of the plans compared to 18% before adaptation (predicted plans), respectively (see Figure 1A). Regarding outliers, the patient who most profited from online plan adaptation regarding PTV coverage had a mean (median) increase of the PTV coverage of 18.9% (14.4%), whereas two patients had a slight decrease in mean (median) PTV coverage up to 1.8% (1.8%) due to OAR constraints.

The mean CTV coverage after online adaptation was 1.4% higher (95% CI: 0.5; 2.3, $p = 0.004$) in the adapted plans than in the predicted plans. 78% of the predicted plans had a CTV coverage ≥98%, while adaptation allowed for a CTV coverage ≥98% in all plans (see Figure 1B).

The mean $D_{95\%}$ increased by 0.96 Gy (95% CI: 0.49; 1.43, $p < 0.001$) from predicted to adapted plans. Adaptation yielded a $D_{95\%}$ of ≥35.625 Gy (95% of 37.5 Gy), in 95% of the plans compared to 18% in a non-adapted scenario, respectively. The mean $D_{50\%}$ was higher by 0.08 Gy (95% CI: 0.031; 0.133, $p = 0.002$) in the adapted plans than in the predicted plans. Adaptation further increased the $D_{50\%}$ of ≥37.5 Gy to 65% compared to 55% without adaptation, respectively.

Organs at risk

Adaptation enabled adherence to the $D_{0.2cc}$ for both bladder and rectum in all cases compared to 93% without adaptation (Figures 2A, B). Furthermore, adaptation allowed for the PRV of the urethra to meet the constraint of <37.5 Gy in 93% of the fractions compared to only 59% without adaptation (Figure 2C).

Discussion

This study aimed at quantifying the effect of MR-guided online plan adaptation on relevant dose specifics in patients treated with SBRT of localized prostate cancer. In this study, online adaptation was performed by the treating physician and medical physicist in 95% of fractions. Mean PTV and CTV coverage were higher and inadvertent OAR doses lower after online plan adaptation.

In alignment with recently reported changes in prostate volume over the course of SBRT (19), PTV size varied between the first and last adapted fractions with some patients experiencing a prostate swelling while others demonstrated prostate shrinkage. However, there was no substantial change in PTV size observed through online plan adaptation.

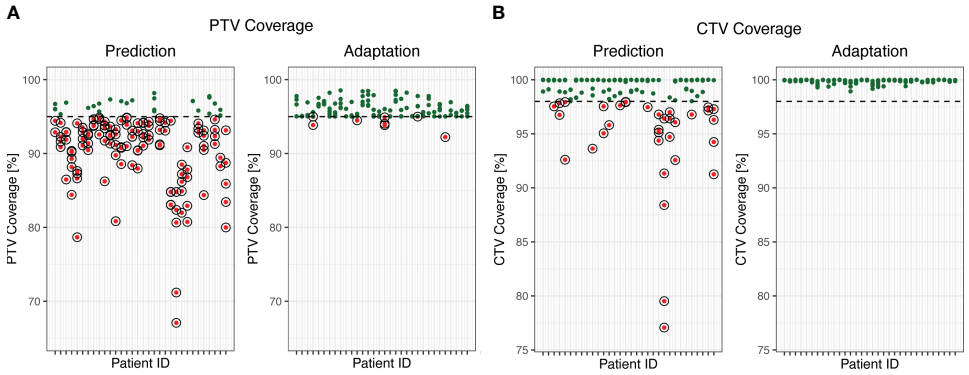

FIGURE 1
PTV **(A)** and CTV **(B)** coverage before and after online adaptation. Dots represent single fractions. Green dots meet the prespecified treatment goals. Red circled dots do not meet the prespecified treatment goals. The dashed line marks the 95% threshold **(A)** and the 98% threshold **(B)**.

When discussing the clinical significance of the observed effect of online adaptation, it is crucial not only to focus on the mean value deviation but also on individual patient's single-fraction data. Kishan et al. demonstrated in their analysis of individual patient data involving over 2000 patients treated with low- and intermediate-risk prostate cancer that with a biochemical recurrence-free survival rate exceeding 90%, the cumulative long-term grade 3+ GU and GI toxicity following SBRT for localized prostate cancer is <3% and that acute toxicity acts as a risk factor for the development of late toxicity (20). The MIRAGE trial which randomized patients with localized prostate cancer to either CT- or MR-guided SBRT did not report the use of online plan adaptation techniques. Nevertheless, MIRAGE revealed that a reduction of the PTV margin in the MR-guided SBRT arm can reduce grade 2+ toxicity, with pending data on its oncological equivalence (21). However, it should be noted that some degree of grade 2+ toxicity is expected regardless of PTV margins due to the inclusion of the urethra in the CTV. In short, the majority of patients do not experience grade 2+ toxicity or local failure. Nonetheless, for those at risk, an optimized radiation plan may mitigate the risk of toxicity or local recurrence.

In line with previous dosimetric comparisons of MR-guided SBRT in localized prostate cancer (22), in this study, almost 80% of

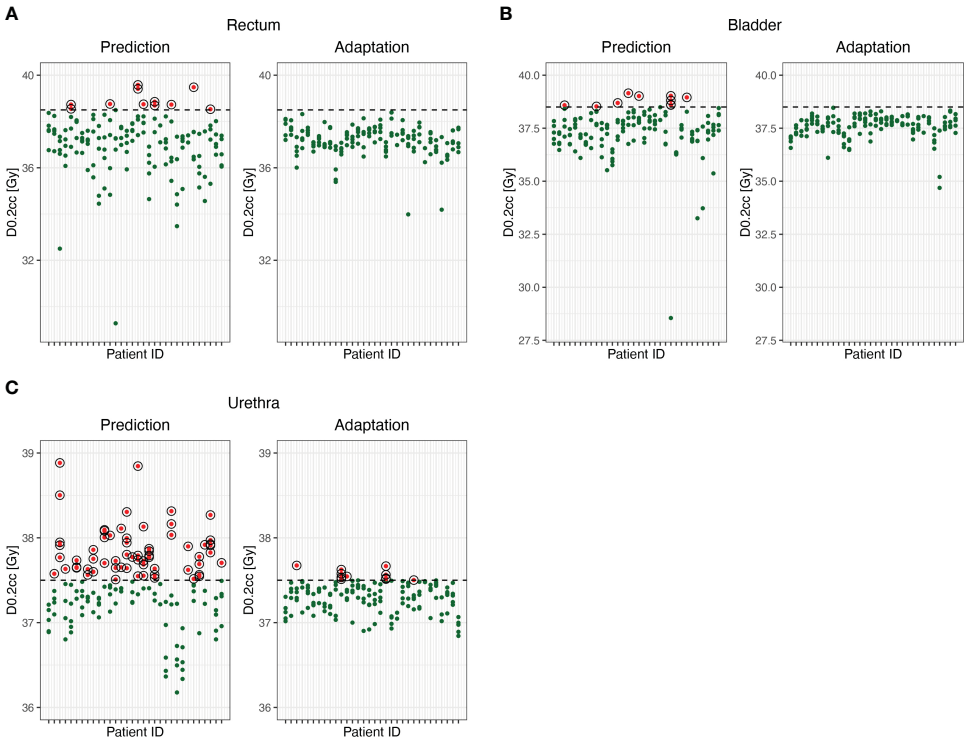

FIGURE 2
$D_{0.2cc}$ of rectum **(A)**, bladder **(B)** and urethral PRV **(C)** before and after online adaptation. Dots represent single fractions. Green dots meet the prespecified treatment goals. Red circled dots do not meet the prespecified treatment goals.

radiation plans had a CTV coverage over 98%, with nearly all plans adhering to OAR constraints before online plan adaptation, consequently resulting in a relatively low risk of toxicity. For the small fraction of cases not meeting target volume goals or OAR constraints, online adaptation could potentially affect toxicity, quality of life and failure free survival. In a recent analysis with 26 patients with localized prostate cancer, Dassen et al. compared radiation plans with separate adaptation strategies for position, rotation and shape in MR-guided online adaptive SBRT, concluding that a PTV margin reduction is probably safe in patients with inclusion of (parts of) the seminal vesicles, but not in cases of prostate-only irradiation (23). The presented dataset, illustrating the 10^{th} to 90^{th} percentile range of target volume coverage and OAR overlap, suggests variations among the plans in a similar range as presented in our study: Some radiation plans easily achieve target volume goals and OAR constraints, while others (at the lower end of the trajectories and below) may especially benefit from adaptation. Alongside individual patient risk factors such as prior cystoscopy, TUR-P, or a history of inflammatory bowel disease, there may also be planning-related risk factors, where online adaptation with plan reoptimization could play a role in minimizing the rate of low-grade toxicity and potentially eliminating high-grade toxicity (24).

Our data show that online plan adaptation may help replicating a dose distribution similar to the base plan. It further improves largely acceptable dose distributions which is of particular interest where further precision is key, i.e. with the adoption of a boost to the dominant intraprostatic lesion (2), when sparing the urethra without compromising oncological efficacy or in re-irradiation scenarios (25). Currently, it remains unclear which patients might derive the greatest advantage from online plan adaptation. For an adequate and efficient utilization of MR-guided radiotherapy in localized prostate cancer, research on both patient selection criteria and strategies to enhance workflow efficiency are warranted. Nachbar et al. have successfully trained and validated a fast, accurate deep learning model for automated MRI segmentation (26). Additionally, efforts are underway to incorporate entirely autonomous workflows, encompassing automatic OAR contouring, target delineation, and automatic planning, within the clinical setting (27). This progress could alleviate the challenges of patient selection by streamlining the workflow in MR-guided radiation therapy, especially when treatment times become more comparable to non-adaptive radiotherapy.

Limitations of our study include the small sample size and the missing estimation of the accuracy of image fusion or geometric congruence of the target volumes or OAR among the predicted and adapted plans. Dosimetric benefits may also result from enhanced alignment, which is supported by the absence of PTV size changes in median in this study. Nevertheless, PTV sizes do not truly reflect the deformation of the prostate and neither the displacement and deformation of surrounding OARs (e.g. rectum), which were often the reason for adaptation. Of note, the dosimetric benefits presented in this work are caused by daily plan adaptation after matching the current MRI with the planning MRI and hence do not result from superior alignment. This is in contrast to the MIRAGE trial, where no online plan adaptation was performed and superior toxicity results may primarily attributed to superior alignment and the possibility of gated dose delivery when compared to conventional IGRT techniques (21). A further limitation is the lack of post-adaptation MRI scan analysis for assessing potential changes in adapted plan quality due to organ motion during the replanning process. An MRI scan prior to dose delivery was performed to account for anatomical changes during reoptimization and irradiation was only started in case of satisfactory alignment. To further mitigate anatomical changes, intrafractional gating was applied. The impact of anatomical changes is currently being investigated in a separate study.

Although in CT-guided radiotherapy hyaluronic acid spacer gels have been shown to improve rectal dosimetry and hence gastrointestinal toxicity (28), this effect has not been demonstrated, to our knowledge, in MR-guided radiotherapy. Due to the occurrence of rectal fistulas after rectal spacer placement in previous trials (29), their utilization at our center has been omitted in favor of a non-interventional workflow. Nevertheless, dosimetric benefits of MR-guided online-adaptation to the rectum may be reduced by rectal spacers.

Real-time tracking of the prostate via surrogate fiducial markers may permit a similar reduction in PTV margins (30). However, fiducial marker implantation is an invasive procedure accompanied by a slightly increased risk for infection or even fiducial migration in rare cases which might lead to impaired tracking (31). Furthermore, the application of radiopaque fiducials enables rigid-registration and therefore does provide limited information on organ deformation, seminal vesicle location, or bladder and rectal distension. A deviation in the shape of the prostate may not be effectively corrected by standard IGRT applications with or without the use of fiducials. This again underlines the need for deformable image registration and adaptive planning in prostate SBRT at least for some patients (32).

In conclusion, this study demonstrates that online plan adaptation improves target volume coverage and reduces doses at OAR in MR-guided SBRT of localized prostate cancer. This could potentially further reduce acute and long-term side effects and improve local failure rates. Future research may focus on identifying subgroups of patients that particularly gain significant clinical benefit from the online adaptation process as well as automatic planning efforts to streamline MR-guided radiotherapy workflows.

Data availability statement

The raw data supporting the conclusions of this article will be made available by the authors, without undue reservation.

Ethics statement

The studies involving humans were approved by ethics committee of the University Hospital Heidelberg. The studies were conducted in accordance with the local legislation and institutional requirements. The participants provided their written informed consent to participate in this study.

Author contributions

CF: Conceptualization, Data curation, Formal analysis, Investigation, Methodology, Visualization, Writing – original draft, Writing – review & editing. CB: Conceptualization, Data curation, Formal analysis, Investigation, Methodology, Software, Visualization, Writing – original draft, Writing – review & editing. LB: Data curation, Formal analysis, Methodology, Software, Validation, Writing – original draft, Writing – review & editing. JL: Data curation, Investigation, Writing – review & editing. PH: Writing – review & editing, Data curation. JR: Data curation, Investigation, Writing – review & editing. SR: Data curation, Investigation, Writing – review & editing. ES: Data curation, Writing – review & editing. LK: Data curation, Writing – review & editing. CR: Data curation, Writing – review & editing. DB: Data curation, Investigation, Methodology, Resources, Writing – review & editing. H-PS: Data curation, Investigation, Methodology, Resources, Writing – review & editing. JD: Conceptualization, Formal analysis, Investigation, Supervision, Writing – review & editing. SAK: Conceptualization, Data curation, Investigation, Supervision, Writing – review & editing. SK: Conceptualization, Data curation, Investigation, Supervision, Writing – review & editing. JH-R: Conceptualization, Data curation, Investigation, Methodology, Supervision, Visualization, Writing – original draft, Writing – review & editing.

Funding

The author(s) declare that no financial support was received for the research, authorship, and/or publication of this article.

Conflict of interest

JH-R received speaker fees from Pfizer Inc. and ViewRay Inc., travel reimbursement from ViewRay Inc., IntraOP Medical and Elekta Instrument AB as well as grants from IntraOP Medical and Varian Medical Systems outside the submitted work. SK has received personal fees and travel reimbursement from Viewray outside the submitted work. JD received grants from View Ray Inc. JD received grants from CRI—The Clinical Research Institute GmbH, Accuray Incorporated, Accuray International Sàrl, RaySearch Laboratories AB, Vision RT limited, Astellas Pharma GmbH, Astra Zeneca GmbH, Solution Akademie GmbH, Ergomed PLC Surrey Research Park, Merck Serono GmbH, Siemens Healthcare GmbH, Quintiles GmbH, Pharmaceutical Research Associates GmbH, Boehringer Ingelheim Pharma GmbH Co, PTW-Freiburg Pychlau GmbH, Nanobiotix A.A. and IntraOP Medical outside the submitted work. DB received speaker fees from Bayer Vital. P.H.H was part of an advisory board for NovoCure GmbH.

The remaining authors declare that the research was conducted in the absence of any commercial or financial relationships that could be construed as a potential conflict of interest.

The author(s) declared that they were an editorial board member of Frontiers, at the time of submission. This had no impact on the peer review process and the final decision.

Publisher's note

References

1. Widmark A, Gunnlaugsson A, Beckman L, Thellenberg-Karlsson C, Hoyer M, Lagerlund M, et al. Ultra-hypofractionated versus conventionally fractionated radiotherapy for prostate cancer: 5-year outcomes of the HYPO-RT-PC randomised, non-inferiority, phase 3 trial. *Lancet* (2019) 394:385–95. doi: 10.1016/S0140-6736(19)31131-6

2. Draulans C, van der Heide UA, Haustermans K, POS FJ, van der Voort Van Zyp J, De Boer H, et al. Primary endpoint analysis of the multicentre phase II hypo-FLAME trial for intermediate and high risk prostate cancer. *Radiother Oncol* (2020) 147:92–8. doi: 10.1016/j.radonc.2020.03.015

3. Tree AC, Ostler P, Van Der Voet H, Chu W, Loblaw A, Ford D, et al. Intensity-modulated radiotherapy versus stereotactic body radiotherapy for prostate cancer (PACE-B): 2-year toxicity results from an open-label, randomised, phase 3, non-inferiority trial. *Lancet Oncol* (2022) 23:1308–20. doi: 10.1016/S1470-2045(22)00517-4

4. Krug D, Imhoff D, Haidenberger A, Hessler N, Schafer J, Huttenlocher S, et al. Robotic stereotactic body radiotherapy for localized prostate cancer: final analysis of the German HYPOSTAT trial. *Strahlenther Onkol* (2023) 199:565–73. doi: 10.1007/s00066-023-02044-2

5. Rasch C, Barillot I, Remeijer P, Touw A, Van Herk M, Lebesque JV. Definition of the prostate in CT and MRI: a multi-observer study. *Int J Radiat Oncol Biol Phys* (1999) 43:57–66. doi: 10.1016/S0360-3016(98)00351-4

6. Pathmanathan AU, Mcnair HA, Schmidt MA, Brand DH, Delacroix L, Eccles CL, et al. Comparison of prostate delineation on multimodality imaging for MR-guided radiotherapy. *Br J Radiol* (2019) 92:20180948. doi: 10.1259/bjr.20180948

7. Pathmanathan AU, Schmidt MA, Brand DH, Kousi E, Van As NJ, Tree AC. Improving fiducial and prostate capsule visualization for radiotherapy planning using MRI. *J Appl Clin Med Phys* (2019) 20:27–36. doi: 10.1002/acm2.12529

8. Corradini S, Alongi F, Andratschke N, Belka C, Boldrini L, Cellini F, et al. MR-guidance in clinical reality: current treatment challenges and future perspectives. *Radiat Oncol* (2019) 14:92. doi: 10.1186/s13014-019-1308-y

9. Regnery S, Buchele C, Weykamp F, Pohl M, Hoegen P, Eichkorn T, et al. Adaptive MR-guided stereotactic radiotherapy is beneficial for ablative treatment of lung tumors in high-risk locations. *Front Oncol* (2021) 11:757031. doi: 10.3389/fonc.2021.757031

10. Weykamp F, Katsigiannopulos E, Piskorski L, Regnery S, Hoegen P, Ristau J, et al. Dosimetric benefit of adaptive magnetic resonance-guided stereotactic body radiotherapy of liver metastases. *Cancers (Basel)* (2022) 14. doi: 10.3390/cancers14246041

11. Hoegen P, Katsigiannopulos E, Buchele C, Regnery S, Weykamp F, Sandrini E, et al. Stereotactic magnetic resonance-guided online adaptive radiotherapy of adrenal metastases combines high ablative doses with optimized sparing of organs at risk. *Clin Transl Radiat Oncol* (2023) 39:100567. doi: 10.1016/j.ctro.2022.100567

12. Ristau J, Horner-Rieber J, Buchele C, Kluter S, Jakel C, Baumann L, et al. Stereotactic MRI-guided radiation therapy for localized prostate cancer (SMILE): a prospective, multicentric phase-II-trial. *Radiat Oncol* (2022) 17:75. doi: 10.1186/s13014-022-02047-w

13. Bohoudi O, Bruynzeel AME, Senan S, Cuijpers JP, Slotman BJ, Lagerwaard FJ, et al. Fast and robust online adaptive planning in stereotactic MR-guided adaptive radiation therapy (SMART) for pancreatic cancer. *Radiother Oncol* (2017) 125:439–44. doi: 10.1016/j.radonc.2017.07.028

14. Rippke C, Schrenk O, Renkamp CK, Buchele C, Horner-Rieber J, Debus J, et al. Quality assurance for on-table adaptive magnetic resonance guided radiation therapy: A software tool to complement secondary dose calculation and failure modes discovered in clinical routine. *J Appl Clin Med Phys* (2022) 23:e13523. doi: 10.1002/acm2.13523

15. McCaffrey DF, Bell RM. Bias reduction in standard errors for linear regression with multi-stage samples. *Qual Control Appl Stat* (2003) 48:677–82.

16. Pustejovsky JE, Tipton E. Small-sample methods for cluster-robust variance estimation and hypothesis testing in fixed effects models. *J Business Econ Stat* (2018) 36:672–83. doi: 10.1080/07350015.2016.1247004

17. Kuznetsova A, Brockhoff PB, Christensen RHB. lmerTest package: tests in linear mixed effects models. *J Stat Softw* (2017) 82:1–26. doi: 10.18637/jss.v082.i13

18. Pustejovsky J. *clubSandwich: Cluster-robust (sandwich) variance estimators with small-sample corrections (R package Version 0.5. 5)*. (2022).

19. Nicosia L, Ravelli P, Rigo M, Giaj-Levra N, Mazzola R, Pastorello E, et al. Prostate volume variation during 1.5T MR-guided adaptive stereotactic body radiotherapy (SBRT) and correlation with treatment toxicity. *Radiother Oncol* (2023) 190:110043. doi: 10.1016/j.radonc.2023.110043

20. Kishan AU, Dang A, Katz AJ, Mantz CA, Collins SP, Aghdam N, et al. Long-term outcomes of stereotactic body radiotherapy for low-risk and intermediate-risk prostate cancer. *JAMA Netw Open* (2019) 2:e188006. doi: 10.1001/jamanetworkopen.2018.8006

21. Kishan AU, Ma TM, Lamb JM, Casado M, Wilhalme H, Low DA, et al. Magnetic resonance imaging-guided vs computed tomography-guided stereotactic body radiotherapy for prostate cancer: the MIRAGE randomized clinical trial. *JAMA Oncol* (2023) 9:365–73. doi: 10.1001/jamaoncol.2022.6558

22. Nicosia L, Sicignano G, Rigo M, Figlia V, Cuccia F, De Simone A, et al. Daily dosimetric variation between image-guided volumetric modulated arc radiotherapy and MR-guided daily adaptive radiotherapy for prostate cancer stereotactic body radiotherapy. *Acta Oncol* (2021) 60:215–21. doi: 10.1080/0284186X.2020.1821090

23. Dassen MG, Janssen T, Kusters M, Pos F, Kerkmeijer LGW, van der Heide UA, et al. Comparing adaptation strategies in MRI-guided online adaptive radiotherapy for prostate cancer: Implications for treatment margins. *Radiother Oncol* (2023) 186:109761. doi: 10.1016/j.radonc.2023.109761

24. Bruynzeel AME, Tetar SU, Oei SS, Senan S, Haasbeek CJA, Spoelstra FOB, et al. A prospective single-arm phase 2 study of stereotactic magnetic resonance guided adaptive radiation therapy for prostate cancer: early toxicity results. *Int J Radiat Oncol Biol Phys* (2019) 105:1086–94. doi: 10.1016/j.ijrobp.2019.08.007

25. Sritharan K, Tree A. MR-guided radiotherapy for prostate cancer: state of the art and future perspectives. *Br J Radiol* (2022) 95:20210800. doi: 10.1259/bjr.20210800

26. Nachbar M, Lo Russo M, Gani C, Boeke S, Wegener D, Paulsen F, et al. Automatic AI-based contouring of prostate MRI for online adaptive radiotherapy. *Z Med Phys* (2023). doi: 10.1016/j.zemedi.2023.05.001

27. Kunzel LA, Nachbar M, Hagmuller M, Gani C, Boeke S, Wegener D, et al. Clinical evaluation of autonomous, unsupervised planning integrated in MR-guided radiotherapy for prostate cancer. *Radiother Oncol* (2022) 168:229–33. doi: 10.1016/j.radonc.2022.01.036

28. Mariados NF, Orio PF 3rd, Schiffman Z, Van TJ, Engelman A, Nurani R, et al. Hyaluronic acid spacer for hypofractionated prostate radiation therapy: A randomized clinical trial. *JAMA Oncol* (2023) 9:511–8. doi: 10.1001/jamaoncol.2022.7592

29. Habl G, Uhl M, Katayama S, Kessel KA, Hatiboglu G, Hadaschik B, et al. Acute toxicity and quality of life in patients with prostate cancer treated with protons or carbon ions in a prospective randomized phase II study–the IPI trial. *Int J Radiat Oncol Biol Phys* (2016) 95:435–43. doi: 10.1016/j.ijrobp.2016.02.025

30. Goddard L, Jeong K, Tang J, Garg M, Tome WA. Reducing PTV margins for prostate SBRT with motion compensation and gating techniques. *J Appl Clin Med Phys* (2023) 24:e13861. doi: 10.1002/acm2.13861

31. O'Neill AG, Jain S, Hounsell AR, O'sullivan JM. Fiducial marker guided prostate radiotherapy: a review. *Br J Radiol* (2016) 89:20160296. doi: 10.1259/bjr.20160296

32. Deegan T, Owen R, Holt T, Fielding A, Biggs J, Parfitt M, et al. Assessment of cone beam CT registration for prostate radiation therapy: fiducial marker and soft tissue methods. *J Med Imaging Radiat Oncol* (2015) 59:91–8. doi: 10.1111/1754-9485.12197

frontiers | Frontiers in Oncology

TYPE Original Research
PUBLISHED 10 May 2024
DOI 10.3389/fonc.2024.1335623

OPEN ACCESS

EDITED BY
Enis Ozyar,
Acıbadem University, Türkiye

REVIEWED BY
Rei Umezawa,
Tohoku University Hospital, Japan
Alessio G. Morganti,
University of Bologna, Italy

*CORRESPONDENCE
Masato Tsuneda
masato.tsune@gmail.com

†These authors have contributed equally to this work and share first authorship

RECEIVED 09 November 2023
ACCEPTED 15 April 2024
PUBLISHED 10 May 2024

CITATION
Kurokawa M, Tsuneda M, Abe K, Ikeda Y, Kanazawa A, Saito M, Kodate A, Harada R, Yokota H, Watanabe M and Uno T (2024) A pilot study on interobserver variability in organ-at-risk contours in magnetic resonance imaging-guided online adaptive radiotherapy for pancreatic cancer. *Front. Oncol.* 14:1335623. doi: 10.3389/fonc.2024.1335623

A pilot study on interobserver variability in organ-at-risk contours in magnetic resonance imaging-guided online adaptive radiotherapy for pancreatic cancer

Marie Kurokawa[1†], Masato Tsuneda[2*†], Kota Abe[2], Yohei Ikeda[3], Aki Kanazawa[3], Makoto Saito[3], Asuka Kodate[3], Rintaro Harada[3], Hajime Yokota[1], Miho Watanabe[1] and Takashi Uno[1]

[1]Diagnostic Radiology and Radiation Oncology, Graduate School of Medicine, Chiba University, Chuo-ku, Chiba, Japan, [2]Department of Radiation Oncology, MR Linac ART Division, Graduate School of Medicine, Chiba University, Chuo-ku, Chiba, Japan, [3]Department of Radiology, Chiba University Hospital, Chuo-ku, Chiba, Japan

Purpose: Differences in the contours created during magnetic resonance imaging-guided online adaptive radiotherapy (MRgOART) affect dose distribution. This study evaluated the interobserver error in delineating the organs at risk (OARs) in patients with pancreatic cancer treated with MRgOART. Moreover, we explored the effectiveness of drugs that could suppress peristalsis in restraining intra-fractional motion by evaluating OAR visualization in multiple patients.

Methods: This study enrolled three patients who underwent MRgOART for pancreatic cancer. The study cohort was classified into three conditions based on the MRI sequence and butylscopolamine administration (Buscopan): 1, T2 imaging without butylscopolamine administration; 2, T2 imaging with butylscopolamine administration; and 3, multi-contrast imaging with butylscopolamine administration. Four blinded observers visualized the OARs (stomach, duodenum, small intestine, and large intestine) on MR images acquired during the initial and final MRgOART sessions. The contour was delineated on a slice area of ±2 cm surrounding the planning target volume. The dice similarity coefficient (DSC) was used to evaluate the contour. Moreover, the OARs were visualized on both MR images acquired before and after the contour delineation process during MRgOART to evaluate whether peristalsis could be suppressed. The DSC was calculated for each OAR.

Results: Interobserver errors in the OARs (stomach, duodenum, small intestine, large intestine) for the three conditions were 0.636, 0.418, 0.676, and 0.806; 0.725, 0.635, 0.762, and 0.821; and 0.841, 0.677, 0.762, and 0.807, respectively. The DSC was higher in all conditions with butylscopolamine administration compared with those without it, except for the stomach in condition 2, as observed in the last session of MR image. The DSCs for OARs (stomach, duodenum, small intestine, large intestine) extracted before and after

contouring were 0.86, 0.78, 0.88, and 0.87; 0.97, 0.94, 0.90, and 0.94; and 0.94, 0.86, 0.89, and 0.91 for conditions 1, 2, and 3, respectively.

Conclusion: Butylscopolamine effectively reduced interobserver error and intrafractional motion during the MRgOART treatment.

KEYWORDS

MRgOART, pancreatic cancer, organs-at-risk, butylscopolamine, contouring, interobserver variability

1 Introduction

In patients with unresectable locally advanced pancreatic cancer, conventional radiation therapy confers a slight survival advantage compared with chemotherapy alone, necessitating the discovery of more effective local approaches (1–3). Dose escalation is essential to achieve local tumor control and improve overall survival. However, dose cannot be escalated due to restrictions on the tolerable dose of healthy organs surrounding the pancreas. Advances in irradiation techniques, such as intensity-modulated radiation therapy, facilitate the administration of high doses while minimizing the dose to the organs at risk (OAR). Treatment of unresectable pancreatic cancer using a general linear accelerator is performed in 15 or 25 fractions, while meeting the dose limit to the surrounding normal organs, using countermeasures against respiratory migration and image-guided technology (4, 5). Recently, magnetic resonance imaging-guided Online Adaptive Radiation Therapy (MRgOART), which fully uses MR image-guided and online adaptive technology for pancreatic cancer, has enabled more effective dose prescription (6–9).

Recommendations for precise delineation of tumors and OARs in abdominal regions with respiratory movements and intestinal peristalsis have been reported (10). Motion artifacts occur due to the movement of internal organs during MRI, reducing visibility. Mostafaei et al. investigated body movements induced by breathing and peristalsis on computed tomography (CT) and MRI scans acquired during free breathing and breath-holding. They concluded that evaluating both respiratory movement and peristalsis is essential (11). Breath-holding and abdominal compression have been reported as countermeasures for respiratory movement (7–9). The pre-treatment images can directly correct the current gastrointestinal position and movement in an online adaptive radiotherapy plan. Some drugs can also inhibit peristalsis (12). No study has investigated whether it is possible to accurately defininig the contours of normal organs on images affected by motion artifacts could be possible.

This study aimed to evaluate interobserver error while delineating OARs in patients with pancreatic cancer treated with MRgOART. Furthermore, we also aimed to demonstrate the utility of drugs that suppress peristalsis by evaluating OAR visualization in multiple patients.

2 Methods

2.1 Patient data and MRI

This study was approved by the Ethics Committee of Chiba University Hospital (HK202304-07). The study enrolled three patients who underwent MRgOART for pancreatic cancer using Elekta Unity MR-linac (Elekta, Stockholm, Sweden). The patient details are presented in Table 1. At our hospital, MRIs are performed using a T2 navigator echo sequence under abdominal compression to measure respiratory movement. Patients 2 and 3 (conditions 2 and 3) who could be treated with butylscopolamine bromide (Buscopan®Injection, Paris, France) were administered the drug to suppress intestinal peristalsis. Butylscopolamine was deemed contraindicated in Patient 1 (condition 1) owing to a history of valvular heart disease. Moreover, our hospital incorporates contour delineation on images captured in multiple sequences into the workflow using the treatment planning support device MIM Maestro (MIM Software, 7.1.5, Cleveland, OH, USA) (condition 3) (9, 13). The imaging sequences provided by the vendor were used for MRI acquisition, except for one sequence, T1-eTHRIVE. Table 2 presents the parameters of the imaging sequence. Figure 1 shows an example of a treatment image captured using the T2 3D Tra Navi sequence and provides an overview of our delineation study.

2.2 Evaluation of contouring

The observers were three radiation oncologists (RO1, RO2, and RO3) and one resident physician (T1); the other observers were blinded to the contours during contour delineation. RO1, RO2, RO3, and T1 had treatment experiences of 14, 15, 13, and 3 years, respectively. In this study, MR images from the initial and final MRgOART sessions were used to delineate the contours of OAR for

TABLE 1 Patient overview.

Patient No.	I	II	III
Condition No.	1	2	3
Age (years)	78	59	51
Sex	F	M	M
Tumor location	Head of the pancreas	Uncinate process of the pancreas	Head of the pancreas
Prior chemotherapy	GEM+nabPTX	GEM+nabPTX→mFOLFIRINOX	GEM+nabPTX→mFOLFIRINOX
KPS at the start of ablative radiotherapy	90	90	100
Imaging sequence	T2 3D Tra Navi	T2 3D Tra Navi	T2 3D Tra Navi with optional imaging
Abdominal compression	+	+	+
Butylscopolamine (20 mg/ampule)	–	+	+

GEM, gemcitabine; nabPTX, nanoparticle albumin-bound paclitaxel; FOLFIRINOX, oxaliplatin, irinotecan, fluorouracil, and leucovorin; KPS, Karnofsky Performance Status.

each condition. Each observer created an outline of the stomach, duodenum, small intestine, and large intestine on this MR image. The range for delineating the contour was an area extending ±2 cm in the craniocaudal direction from the slice coordinates of the planning target volume (PTV). The primary outcome measure was the agreement between observers for each contour. The dice similarity coefficient (DSC) was used to assess interobserver agreement for each contour in each patient (14). DSC has been used broadly in the field of segmentation as a measure of spatial overlap ranging between 0 and 1, where 0 indicates no overlap and 1 indicates exact overlap. The OARs were depicted using the MIM software and exported after anonymization. DSC values were calculated using an in-house program developed in Python and subsequently averaged.

2.3 Peristaltic motion

Two MR images obtained before and after contouring were used to evaluate intestinal peristalsis. In the MRgOART workflow, MR images (pre-treatment MR images) were acquired before the treatment planning. The contouring, optimization, and dose calculation were performed immediately using this image. Since this process was time-consuming, position verification MR images could be acquired immediately before irradiation to assess patient misalignment (15, 16). These two images were compared, and the process proceeded to irradiation if no positional shift was found. The contours to be evaluated were the duodenum, stomach, small intestine, and large intestine, as described above. One observer (RO1) compared the contours using the DSC.

2.4 Evaluation of contouring (distance and area of overlapping)

Figure 2 depicts a conceptual diagram of the distance and area of overlap between the PTV and OARs. We determined the presence or absence of overlap between the PTV and OAR in each slice containing the PTV (range, 0–n). Regarding overlapping region for each observer, the area of overlap was calculated and accumulated, representing the overlap volume. In cases wherein no overlap occurred, the shortest distance between the PTV and each OAR contour was calculated. The average value of the shortest distances for each observer was evaluated.

TABLE 2 Overview of imaging sequences.

Name	T2 3D Tra Navi	b3D VaneXD	T1 3D VaneXD	eTHRIVE*
Scan technique	T2-TSE	B-FFE	T1-FFE	T1-FFE
Scan time	2:21	6:51	6:01	2:29
Voxel size	0.79 × 0.79 × 1.2	0.78 × 0.78 × 1.5	0.78 × 0.78 × 1.5	0.78 × 0.78 × 2.4
Field-of-view	360 × 455	500 × 500	500 × 500	360 × 438
TR/TE	2100/102	3.3/1.31	3.9/1.18	4.6/2.3
ETL	167	94	–	15
FA	90	40	15	10
NEX	2	1	1	5
Fat suppression	–	–	–	+

*These sequences are developed at our facility.
TR/TE, repetition time/echo time; ETL, echo train length; NEX, number of excitations; FA, flip angle.

10.3389/fonc.2024.1335623

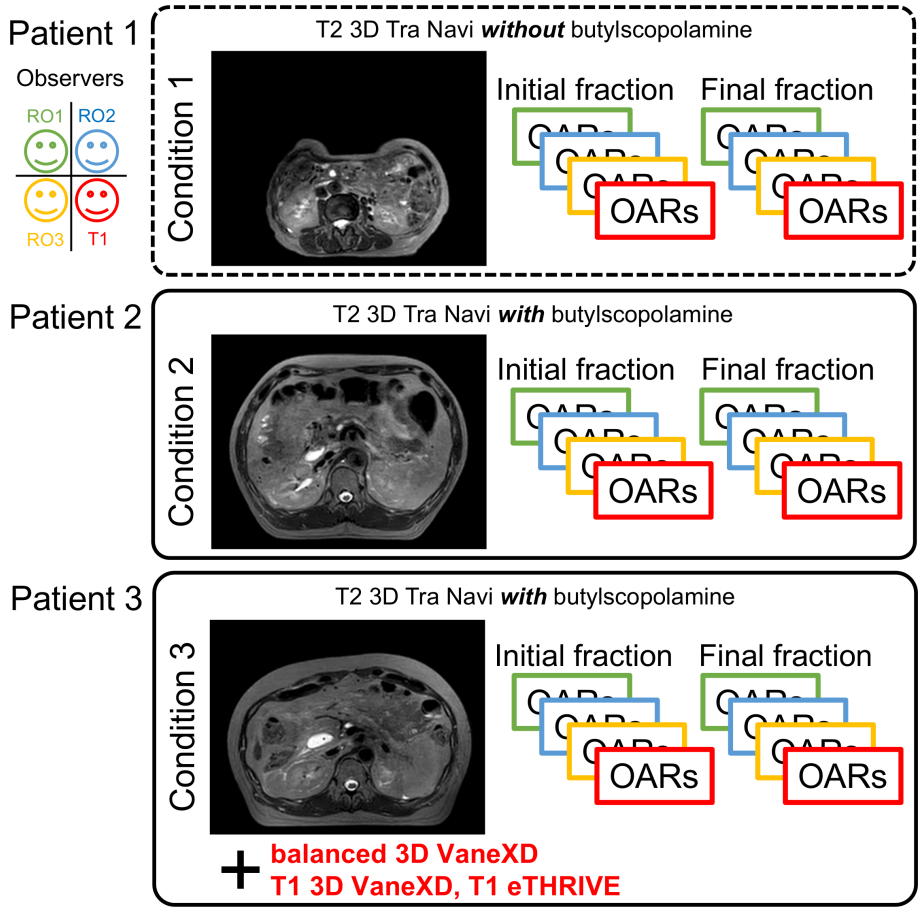

FIGURE 1
Magnetic resonance imaging (T2 3D Tra Navi image) and schematic representation of our delineation study.

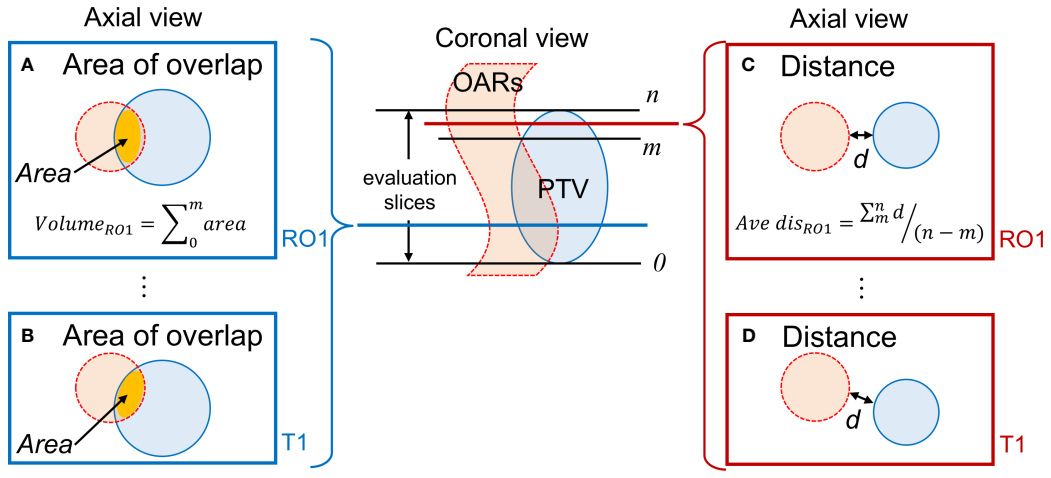

FIGURE 2
Evaluation of the positional relationship between the PTV and OARs. **(A, B)** Calculation of the overlap area for RO1 and T1 when the PTV and OARs overlap; **(C, D)** Determination of the shortest distance *d* for RO1 and T1 when there is no overlap between the PTV and OAR. Evaluation is conducted on slices containing the PTV. PTV, planning target volume; OAR, organ-at-risk.

MR images of two sessions were analyzed. These indicators were calculated using an in-house program developed in Python. In all OARs, the values of overlap volume and averaged shortest distance were calculated for each combination of condition and observers. The values for all observers were averaged. We calculated the standard deviation (SD) and coefficient of variation (CV) as a measure of interobserver error. Larger CVs indicated greater interobserver differences among observers in these indicators.

3 Results

3.1 Treatment time

Treatment was completed within 100 min for the treatment fractions included in our analysis. Figure 3 shows the duration of treatment for each process, including administration time. Subcutaneous, intravenous, and mixed injections of butylscopolamine bromide are denoted by plus, cross, and triangular marks, respectively.

3.2 DSC comparison for each contour

Figure 1 shows T2 Navi images of condition1 without butylscopolamine bromide administration and of conditions 2 and 3 with butylscopolamine bromide administration. The visibility of the image obtained without butylscopolamine bromide administration was poor (Figure 1 upper row). Figure 4 shows the DSC results for each patient. DSC values were higher for all conditions involving butylscopolamine bromide administration compared to condition 1, where butylscopolamine bromide was not administered.

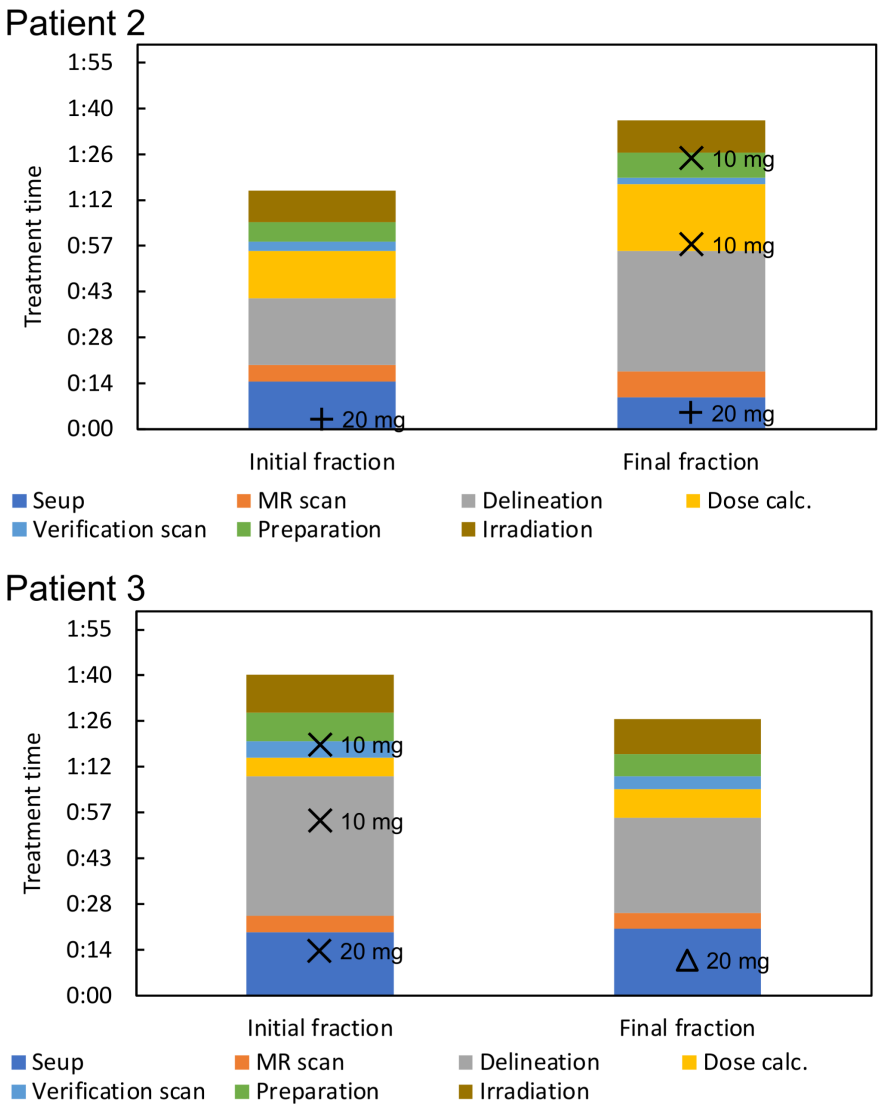

FIGURE 3
Visualization of treatment time and administration time.

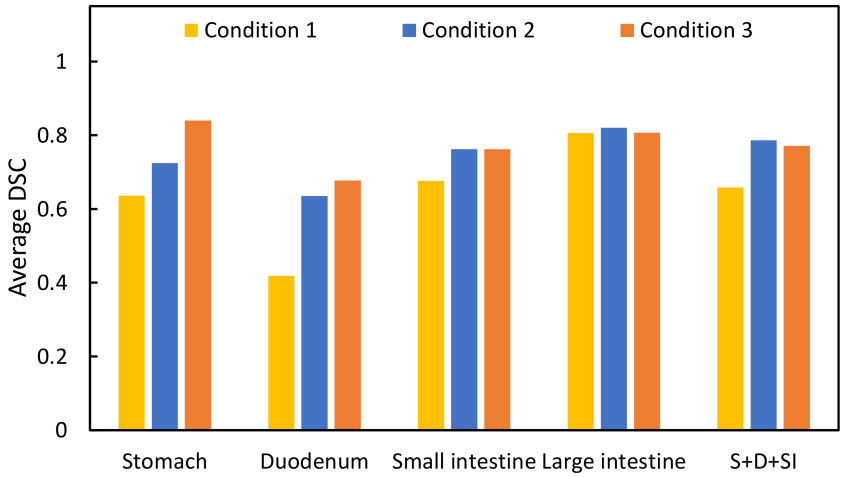

FIGURE 4
Comparison of the DSC values among the three conditions. "S+D+SI" is the outline of the stomach, duodenum, and small intestine.

3.3 Shortest distance and area of overlap between the PTV and OARs

Table 3 summarizes the results of the shortest distance from the PTV to the OARs and CV for each condition, while Table 4 lists the results of the overlap volume between the PTV and OARs and CV for each condition. The overlap volumes of the stomach and large intestine could only be calculated under one condition. Therefore, the volume of these structures was not evaluated (Table 4). Although SD is a measure of dispersion of population, comparing dispersion of multiple ones, it may not be an effective in analysis. In a population wherein the average value is larger, SD is likely to be larger. In such cases, the comparison takes into account the population size by dividing SD by the average value to calculate CV. In some conditions and fractions, administration resulted in lower CV values. However, no trend was found depending on whether butylscopolamine bromide was administered or not. We consider that this is because the anatomical position of OARs differs among patients and positions of OARs change between inter-fractions.

3.4 Peristaltic motion

Figure 5 shows the pre-treatment, and position verification MR images for conditions 1, 2, and 3. The outline created by observer RO1 in the pre-treatment image is depicted in both MR images. It is a solid line on the pre-treatment MR image and a dotted line on the position verification MR image. Furthermore, yellow lines indicate the

TABLE 3 Average values of the shortest distance between the planning target volume and organ-at-risk in each slice.

Average distance [mm]	Condition	Average		Coefficient of variation (↓)	
		Initial fraction	Final fraction	Initial fraction	Final fraction
Stomach	1	19.53 ± 6.67	18.56 ± 8.19	0.34	0.44
	2	N/A	N/A	N/A	N/A
	3	4.55 ± 2.96	5.70 ± 1.91	0.65	0.34
Duodenum	1	12.41 ± 3.02	2.52 ± 1.03	0.24	0.41
	2	13.44 ± 0.98	14.59 ± 5.30	0.07	0.36
	3	N/A	N/A	N/A	N/A
Small intestine	1	9.03 ± 2.77	11.10 ± 5.36	0.31	0.48
	2	26.20 ± 6.65	28.90 ± 3.90	0.25	0.14
	3	12.01 ± 4.00	24.97 ± 4.08	0.33	0.16
Large intestine	1	34.50 ± 7.74	23.24 ± 0.70	0.22	0.03
	2	62.33 ± 3.52	30.53 ± 3.55	0.06	0.12
	3	26.24 ± 1.89	33.48 ± 2.87	0.08	0.08

"N/A" indicates that the OAR does not exist on all evaluated slices and the distance is not calculated.

TABLE 4 Area of overlap between the planning target volume and organ-at-risk.

Area [cc]	Condition	Average		Coefficient of variation (↓)	
		Initial fraction	Final fraction	Initial fraction	Final fraction
Duodenum	1	1.04 ± 0.91	0.77 ± 0.43	0.87	0.56
	2	1.05 ± 0.53	0.66 ± 0.48	0.50	0.72
	3	16.85 ± 2.94	11.34 ± 0.55	0.17	0.05
Small intestine	1	6.12 ± 4.34	0.02 ± 0.03	0.71	1.34
	2	1.66 ± 2.96	N/A	1.78	N/A
	3	1.89 ± 3.05	0.07 ± 0.07	1.62	1.04

"N/A" indicates that the PTV and OAR do not overlap and the volume cannot be calculated.

duodenum, pink lines indicate the small intestine, and light blue lines indicate the large intestine. In the conditions with butylscopolamine, although the movement of gas and water within the intestinal tract was observed, there were no major positional changes. Conversely, positional fluctuations were observed in condition 1. Table 5 shows the results of the DSC. For all OARs, conditions 2 and 3 had higher DSC values than condition 1. Therefore, it can be inferred that butylscopolamine helps suppress peristalsis during the OART workflow.

4 Discussion

In our study, we evaluated three patients with pancreatic cancer who underwent treatment with MRgOART. Normal organ contours were visualized for each observer on MR images acquired during both the initial and final MRgOART sessions. These patients were categorized into three conditions based on the MRI sequence and butylscopolamine administration. We examined the contour delineation accuracy and investigated the conditions suitable for contour delineation. The DSC was used to verify the accuracy of contour delineation among observers and to evaluate peristaltic motion.

Evaluating DSC using the same threshold for multiple organs due to its sensitivity to contour delineation volume is challenging. Therefore, we compared the results for conditions 1, 2, and 3 within the same OAR. The average DSC value was higher in conditions wherein butylscopolamine was administered compared with those wherein it was not used. This suggests that butylscopolamine administration could contribute to the improved accuracy of OARs contour delineation. Thus, using butylscopolamine may be effective in reducing interobserver error.

Regarding the MRgOART workflow, contours are drawn using MRI. There is a concern that artifacts due to respiratory movement or peristalsis may occur during imaging. These movements may reduce the image quality and make identifying lesion challenging. Heerkens et al. evaluated respiratory migration in patients with pancreatic cancer. Respiratory migration of tumor was verified on sagittal and coronal MRI using in-house software. Their results indicated that the body moves by an average of 15 mm in the craniocaudal direction and that the deep expiration (end-expiration position) phase is the most stable (10). In this study, we adopted the T2 navigator echo imaging method, which acquires images in time with deep exhalation, which helps mitigate the effects of respiratory movement. Additionally, abdominal compression suppresses the

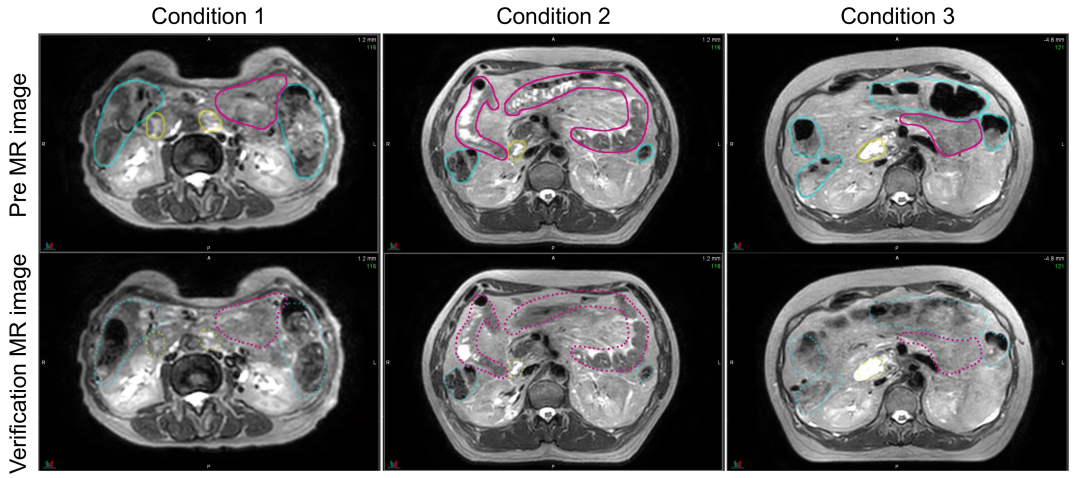

FIGURE 5
Comparison of the pre- and verification MR images for conditions 1, 2, and 3. The contour created in the pre-image is depicted on both MR images. MR, magnetic resonance.

TABLE 5 DSCs for organ-at-risk delineations extracted from pre-treatment and verification magnetic resonance imaging.

		Condition No		
		1	2	3
DSC	Stomach	0.86	0.97	0.94
	Duodenum	0.78	0.94	0.86
	Small intestine	0.88	0.90	0.89
	Large intestine	0.87	0.94	0.91

DSC, dice similarity coefficient.

amount of movement. Mostafaei et al. (11) concluded that peristalsis must also be assessed in addition to respiratory movement. Therefore, we used the DSC in this study to determine whether the contour changed between the pre-treatment and verification MR images to evaluate peristalsis. We found that the DSC was high when butylscopolamine was used.

Wagner et al. reported that butylscopolamine administration before MRI improves the diagnostic accuracy of lesions in the pancreatic head and body during interobserver evaluation (17). In their study, patients received an intramuscular injection of 40 mg of butylscopolamine immediately before undergoing MR imaging. It was reported that repeat imaging after 29 min (mean) did not result in a significant deterioration in image quality. MR imaging of the abdominal region following butylscopolamine administration are of significantly superior quality (18, 19). Additionally, Martí-Bonmatí et al. demonstrated the effectiveness of suppressing peristalsis using medication for MR imaging of pancreatic cancer (12). Our results also could support previous findings; hence we conclude that butylscopolamine contributes to improved contouring accuracy and reduces intra-fractional motion.

The limitations of this study are that it was conducted within a single institution; the number of conditions and observers was small. Due to the small number of cases, discussing the duration of effectiveness of butylscopolamine might be impossible. However, the evaluation of DSC between the pre- and verification-MR images confirmed the suppression of peristaltic movement in the presence of drugs. Our assessment was limited to two specific periods during the MRgOART process –before treatment planning and before irradiation– and we did not extensively evaluate intra-fractional motion. Therefore, we suggest that the following two studies will be needed: 1) an examination of interobserver error with a large number of cases and 2) an evaluation of peristaltic motion during treatment. The number of cases and observers will be increased to assure our result of interobserver error. An analysis of cine 2D MR images (5 frames/second) acquired during irradiation will be required to evaluate the effect of peristaltic suppression.

5 Conclusion

We used DSC to evaluate the interobserver errors in OAR delineation in patients with pancreatic cancer treated with MRgOART at our hospital. Using butylscopolamine resulted in high DSC values in all organs, suggesting that it reduces interobserver error. Furthermore, it helped reduce intra-fractional motion, in addition to improving the accuracy of contour delineation.

Data availability statement

The raw data supporting the conclusions of this article will be made available by the authors, without undue reservation.

Ethics statement

The studies involving humans were approved by Chiba University Clinical Research Center, Chiba University Hospital. The studies were conducted in accordance with the local legislation and institutional requirements. Written informed consent for participation was not required from the participants or the participants' legal guardians/next of kin in accordance with the national legislation and institutional requirements.

Author contributions

MK: Writing – original draft, Conceptualization, Funding acquisition, Project administration, Visualization. MT: Conceptualization, Data curation, Formal analysis, Project administration, Software, Visualization, Writing – original draft. KA: Formal analysis, Software, Writing – review & editing. YI: Resources, Software, Writing – review & editing. AKa: Resources, Writing – review & editing. MS: Resources, Writing – review & editing. AKo: Resources, Writing – review & editing. RH: Writing – review & editing. HY: Writing – review & editing. MW: Writing – review & editing. TU: Writing – review & editing.

Funding

The author(s) declare financial support was received for the research, authorship, and/or publication of this article. This work was supported by JSPS KAKENHI (grant number 21K15822).

Acknowledgments

We borrowed a radiation treatment planning system for this research from Elekta K.K. We thank Mr. Yoshio Iwai of the same company. We thank Editage (www.editage.com) for the English language editing.

Conflict of interest

MT and KA received endowed chairs funded by Elekta K.K.

The remaining authors declare that the research was conducted in the absence of any commercial or financial relationships that could be constructed as a potential conflict of interest.

Publisher's note

References

1. Crane CH. Hypofractionated ablative radiotherapy for locally advanced pancreatic cancer. *J Radiat Res*. (2016) 57 Suppl 1:i53–7. doi: 10.1093/jrr/rrw016

2. Hammel P, Huguet F, van Laethem JL, Goldstein D, Glimelius B, Artru P, et al. Effect of chemoradiotherapy vs chemotherapy on survival in patients with locally advanced pancreatic cancer controlled after 4 months of gemcitabine with or without erlotinib: the LAP07 Randomized Clinical Trial. *JAMA*. (2016) 315:1844–53. doi: 10.1001/jama.2016.4324

3. Loehrer PJ, Feng Y, Cardenes H, Wagner L, Brell JM, Cella D, et al. Gemcitabine alone versus gemcitabine plus radiotherapy in patients with locally advanced pancreatic cancer: an Eastern Cooperative Oncology Group trial. *J Clin Oncol*. (2011) 29:4105–12. doi: 10.1200/JCO.2011.34.8904

4. Reyngold M, Parikh P, Crane CH. Ablative radiation therapy for locally advanced pancreatic cancer: techniques and results. *Radiat Oncol*. (2019) 14:95. doi: 10.1186/s13014-019-1309-x

5. Krishnan S, Chadha AS, Suh Y, Chen HC, Rao A, Das P, et al. Focal radiation therapy dose escalation improves overall survival in locally advanced pancreatic cancer patients receiving induction chemotherapy and consolidative chemoradiation. *Int J Radiat Oncol Biol Phys*. (2016) 94:755–65. doi: 10.1016/j.ijrobp.2015.12.003

6. Bohoudi O, Bruynzeel AME, Senan S, Cuijpers JP, Slotman BJ, Lagerwaard FJ, et al. Fast and robust online adaptive planning in stereotactic MR-guided adaptive radiation therapy (SMART) for pancreatic cancer. *Radiother Oncol*. (2017) 125:439–44. doi: 10.1016/j.radonc.2017.07.028

7. Chuong MD, Bryant J, Mittauer KE, Hall M, Kotecha R, Alvarez D, et al. Ablative 5-fraction stereotactic magnetic resonance-guided radiation therapy with on-table adaptive replanning and elective nodal irradiation for inoperable pancreas cancer. *Pract Radiat Oncol*. (2021) 11:134–47. doi: 10.1016/j.prro.2020.09.005

8. Hassanzadeh C, Rudra S, Bommireddy A, Hawkins WG, Wang-Gillam A, Fields RC, et al. Ablative five-fraction stereotactic body radiation therapy for inoperable pancreatic cancer using online MR-guided adaptation. *Adv Radiat Oncol*. (2021) 6:100506. doi: 10.1016/j.adro.2020.06.010

9. Tyagi N, Liang J, Burleson S, Subashi E, Godoy Scripes P, Tringale KR, et al. Feasibility of ablative stereotactic body radiation therapy of pancreas cancer patients on a 1.5 Tesla magnetic resonance-linac system using abdominal compression. *Phys Imaging Radiat Oncol*. (2021) 19:53–9. doi: 10.1016/j.phro.2021.07.006

10. Heerkens HD, Hall WA, Li XA, Knechtges P, Dalah E, Paulson ES, et al. Recommendations for MRI-based contouring of gross tumor volume and organs at risk for radiation therapy of pancreatic cancer. *Pract Radiat Oncol*. (2017) 7:126–36. doi: 10.1016/j.prro.2016.10.006

11. Mostafaei F, Tai A, Omari E, Song Y, Christian J, Paulson E, et al. Variations of MRI-assessed peristaltic motions during radiation therapy. *PloS One*. (2018) 13:e0205917. doi: 10.1371/journal.pone.0205917

12. Martí-Bonmatí L, Graells M, Ronchera-Oms CL. Reduction of peristaltic artifacts on magnetic resonance imaging of the abdomen: a comparative evaluation of three drugs. *Abdom Imaging*. (1996) 21:309–13. doi: 10.1007/s002619900070

13. Tringale KR, Tyagi N, Reyngold M, Romesser PB, Wu A, O'Reilly EM, et al. Stereotactic ablative radiation for pancreatic cancer on a 1.5 Telsa magnetic resonance-linac system. *Phys Imaging Radiat Oncol*. (2022) 24:88–94. doi: 10.1016/j.phro.2022.10.003

14. Dice LR. Measures of the amount of ecologic association between species. *Ecology*. (1945) 26:297–302. doi: 10.2307/1932409

15. Uno T, Tsuneda M, Abe K, Fujita Y, Harada R, Saito M, et al. A new workflow of the on-line 1.5-T MR-guided adaptive radiation therapy. *Jpn J Radiol*. (2023) 41:1316–22. doi: 10.1007/s11604-023-01457-4

16. Werensteijn-Honingh AM, Kroon PS, Winkel D, Aalbers EM, van Asselen B, Bol GH, et al. Feasibility of stereotactic radiotherapy using a 1.5 T MR-linac: Multi-fraction treatment of pelvic lymph node oligometastases. *Radiother Oncol*. (2019) 134:50–4. doi: 10.1016/j.radonc.2019.01.024

17. Wagner M, Klessen C, Rief M, Elgeti T, Taupitz M, Hamm B, et al. High-resolution T2-weighted abdominal magnetic resonance imaging using respiratory triggering: impact of butylscopolamine on image quality. *Acta Radiol*. (2008) 49:376–82. doi: 10.1080/02841850801894806

18. Dosdá R, Martí-Bonmatí L, Ronchera-Oms CL, Mollá E, Arana E. Effect of subcutaneous butylscopolamine administration in the reduction of peristaltic artifacts in 1.5-T MR fast abdominal examinations. *Eur Radiol*. (2003) 13:294–8. doi: 10.1007/s00330-002-1500-5

19. Tanaka O, Komeda H, Tamaki M, Seike K, Fujimoto S, Yama E, et al. Efficacy of butylscopolamine in obtaining clear MR image for intensity-modulated radiotherapy for prostate cancer. *Tech Innov Patient Support Radiat Oncol*. (2017) 3–4:19–22. doi: 10.1016/j.tipsro.2017.08.001

frontiers | Frontiers in Oncology

TYPE Methods
PUBLISHED 28 May 2024
DOI 10.3389/fonc.2024.1358487

OPEN ACCESS

EDITED BY
Merav Ben-David,
Assuta Medical Center, Israel

REVIEWED BY
Maria F. Chan,
Memorial Sloan Kettering Cancer Center, United States
Sunyoung Jang,
The Pennsylvania State University, United States

*CORRESPONDENCE
Nema Bassiri
nemabassiri@gmail.com

RECEIVED 19 December 2023
ACCEPTED 07 May 2024
PUBLISHED 28 May 2024

CITATION
Bassiri N, Bayouth J, Chuong MD, Kotecha R, Weiss Y, Mehta MP, Gutierrez AN and Mittauer KE (2024) Quality assurance of an established online adaptive radiotherapy program: patch and software upgrade. *Front. Oncol.* 14:1358487. doi: 10.3389/fonc.2024.1358487

Quality assurance of an established online adaptive radiotherapy program: patch and software upgrade

Nema Bassiri[1,2]*, John Bayouth[3], Michael D. Chuong[1,2], Rupesh Kotecha[1,2], Yonatan Weiss[1,2], Minesh P. Mehta[1,2], Alonso N. Gutierrez[1,2] and Kathryn E. Mittauer[1,2]

[1]Department of Radiation Oncology, Miami Cancer Institute, Baptist Health South Florida, Miami, FL, United States, [2]Herbert Wertheim College of Medicine, Florida International University, Miami, FL, United States, [3]Department of Radiation Medicine, Oregon Health and Science University, Portland, OR, United States

Introduction: The ability to dynamically adjust target contours, derived Boolean structures, and ultimately, the optimized fluence is the end goal of online adaptive radiotherapy (ART). The purpose of this work is to describe the necessary tests to perform after a software patch installation and/or upgrade for an established online ART program.

Methods: A patch upgrade on a low-field MR Linac system was evaluated for post-software upgrade quality assurance (QA) with current infrastructure of ART workflow on (1) the treatment planning system (TPS) during the initial planning stage and (2) the treatment delivery system (TDS), which is a TPS integrated into the delivery console for online ART planning. Online ART QA procedures recommended for post-software upgrade include: (1) user interface (UI) configuration; (2) TPS beam model consistency; (3) segmentation consistency; (4) dose calculation consistency; (5) optimizer robustness consistency; (6) CT density table consistency; and (7) end-to-end absolute ART dose and predicted dose measured including interruption testing. Differences of calculated doses were evaluated through DVH and/or 3D gamma comparisons. The measured dose was assessed using an MR-compatible A26 ionization chamber in a motion phantom. Segmentation differences were assessed through absolute volume and visual inspection.

Results: (1) No UI configuration discrepancies were observed. (2) Dose differences on TPS pre-/post-software upgrade were within 1% for DVH metrics. (3) Differences in segmentation when observed were small in general, with the largest change noted for small-volume regions of interest (ROIs) due to partial volume impact. (4) Agreement between TPS and TDS calculated doses was 99.9% using a 2%/2-mm gamma criteria. (5) Comparison between TPS and online ART plans for a given patient plan showed agreement within 2% for targets and 0.6 cc for organs at risk. (6) Relative electron densities demonstrated comparable agreement between TPS and TDS. (7) ART absolute and predicted measured end-to-end doses were within 1% of calculated TDS.

Discussion: An online ART QA program for post-software upgrade has been developed and implemented on an MR Linac system. Testing mechanics and their respective baselines may vary across institutions, but all necessary components for a post-software upgrade QA have been outlined and detailed. These outlined tests were demonstrated feasible for a low-field MR Linac system; however, the scope of this work may be applied and adapted more broadly to other online ART platforms.

KEYWORDS

quality assurance, software upgrade, adaptive radiotherapy, treatment planning system, end-to-end testing, MR linear accelerator

1 Introduction

Online adaptive radiotherapy (ART) is an emerging paradigm that is becoming routine for MR Linacs and X-ray-based image-guided radiotherapy (RT) systems. The assessment of the accuracy and workflow validation is critical to the implementation and ongoing performance of ART platforms. Currently, there are many studies describing the commissioning of online adaptive radiotherapy through end-to-end testing and deformable image registration evaluation (1–4). However, there is limited literature to date on routine quality assurance (QA) for online adaptive RT, specifically regarding patch or software upgrades for established programs. Software upgrades affect the front-end of the patient workflow, specifically the treatment planning system (TPS) and its ability to function in the context of ART. Additionally, a software upgrade would also impact the delivery console, which includes a built-in TPS for online ART. Both the TPS and the delivery console are integrated in the ART workflow, and their performance needs to be tested (5). The need for QA recommendations pertaining to updating online ART platforms is important for the maintenance feasibility in addition to ongoing quality and safety.

The success of an online ART program relies on the ability of the delivery console to receive a baseline plan from the TPS, adapt the plan to the anatomy of the day, and create a new adaptive plan. As such, integral workflow steps include (1) propagate (deformably and/or rigidly) organs at risk (OARs) and target volumes to the anatomy of day (6); (2) recreate planning-dependent structures based on newly modified OARs and target volumes (7); (3) generate the ideal fluence and plan quality per the anatomy of the day; and (4) send over updated delivery instructions to the Linac. The purpose of this work is to describe the necessary tests to perform after a standard software patch installation and/or upgrade for an established online ART program. Specifically, the proposed set of tests are designed to evaluate the delivery console and TPS systems' integration with one another to ensure high-quality online ART after a system patch and/or software upgrade.

2 Materials and methods

2.1 Scope

It is assumed that the online ART system being upgraded is fully commissioned and has been treating patients prior to the upgrade and/or patch. The focus of the outlined tests was performed on the MRIdian system (ViewRay Systems Inc., Oakwood, OH). Note that figures and tables included in this work are specific to the MRIdian platform; user interface (UI)-specific details have been included for demonstration purposes. A patch installation refers to an update that resolves a software bug, and a software upgrade refers to a functionality update in the UI. Note that for this work, post-software upgrade refers collectively to both a patch installation and software upgrade.

2.2 Overview

2.2.1 ART platform overview

The MRIdian system (A3i, version: 5.5.4.14) has its own proprietary planning system which is bifurcated into two distinct platforms (1): the MRIdian TPS which is used during the initial planning stage and (2) the MRIdian treatment delivery system (TDS) which is a TPS integrated into the delivery console for online ART planning. Specifically, the initial plan is created on the TPS and is loaded to the TDS for use as the baseline plan for online ART. Details of the MRIdian ART workflow have been previously described (2, 6, 8).

2.2.2 Overview of tests

An overview of the tests performed for online adaptive post-software upgrade at our institution is outlined in Table 1. A brief overview of the QA procedure, materials utilized (i.e., UI or physical phantom), estimate of full time equivalent (FTE) hours, and type of results (i.e., functional or dosimetric) are presented for each test.

TABLE 1 Overview of the online adaptive radiotherapy post-software upgrade QA tests, materials required, anticipated hours, and description of results.

ART post-software upgrade QA procedure	Overview	Materials	FTE time (h)	Description of results
Configuration consistency	Checksum on UI configuration	TDS	0.5	System settings verification
TPS beam model consistency	Compare dosimetry of a clinical plan pre- and post-software upgrade	TPS	1.0	Dosimetric comparison for relevant DVH metrics
Sub-end-to-end: Segmentation consistency	Planning structures were created on a phantom and compared using TPS and TDS	MR phantom TPS, TDS	2.0	Comparison of contour volumes and visual agreement
Sub-end-to-end: Dose calculation consistency TPS vs. TDS	Compare dose of an SBRT plan calculated on the TPS vs. TDS	MR phantom TPS, TDS	1.0	Comparison of dose calculated by TPS and TDS for same fluence
Sub-end-to-end: Optimizer robustness consistency TPS vs. TDS	Run ART workflow with a phantom, and compare baseline TPS plan with a newly reoptimized ART plan	MR phantom TPS, TDS	1.5	Comparison of the modulation and dose differences of ART plan versus baseline TPS plan
Sub-end-to-end: CT density table consistency	Run ART workflow and compare electron density on TDS with TPS	MR phantom TPS, TDS	0.5	Comparison of electron density values from TPS and TDS
Full-end-to-end: Absolute dose motion phantom	Full end-to-end test with introduced target shifts	MR motion phantom ionization chamber TDS	5.0 (four end-to-end procedures at 1 h per procedure + simulation and initial plan generation)	Comparison of TDS calculated dose with measured dose from ionization chamber

2.3 QA procedures

2.3.1 Configuration consistency

It is important to evaluate the consistency of the UI settings after a software upgrade. For this evaluation, we generated a UI configuration report to evaluate the checksum differences between dates pre- and post-software upgrade. The UI settings generated from this report include all MRIdian system computers including TDS, TPS, MR host, Linac control computer (LCC), treatment delivery computer unit (TDCU), core, and database. Any differences are noted by the configuration value and are highlighted to indicate a difference.

2.3.2 TPS beam model consistency

For evaluating the consistency of the beam model and the dose calculation algorithm, it is recommended by MPPG 5a (section 9) to compare the dosimetry pre- and post-software upgrade on a benchmark plan (9). For this evaluation, we used an existing clinical case and recalculated the plan post-software upgrade. We then compared the relevant dose volume histogram (DVH) metrics (i.e., D0.5 cc, D95% etc.) of the clinical case to the pre-software upgrade respective DVH metrics.

2.3.3 Sub-end-to-end: segmentation consistency (rigid assessment)

The ability to accurately propagate rigid segmentation and contour dependent expansions and Boolean logic from the initial treatment plan onto the anatomy of the day is crucial for ART. Rigid propagation is important for delineation of the targets (gross tumor volume [GTV] and clinical target volume [CTV]) on the anatomy of the day as a starting point per our institutional ART workflow and planning technique (8, 10). As such, we used a rigid phantom with predefined Boolean segmentation logic to evaluate the segmentation consistency between the baseline plan and the adaptive plan.

To this end, we scanned an MR-compatible motion phantom (QUASAR, Modus Medical Devices Inc., Ontario, Canada) and followed our institutional MR simulation workflow. MR simulation was performed using the 3D true fast imaging with steady-state free precision (TrueFISP) imaging protocol. Since voxel size has dependency on how regions of interest (ROIs) are interpolated/expanded, we thought it was important to test all imaging protocols with the institutional segmentation technique. The imaging protocols evaluated included our institutional abdominal and thoracic protocol of $50 \times 50 \times 35.8$ cm^3 with a resolution of 1.5 mm^2 in-plane and slice thickness of 3 mm, and our pelvic protocol of $50 \times 50 \times 35.8$ cm^3 with isotropic 1.5-mm^3 resolution.

The institutional segmentation technique will be briefly described here for context for the ROI consistency verification test. Key features were segmented including OARs and a GTV. Our institutional planning approach utilizes a set of rules which creates dependent planning structures. The following target-derived planning ROIs were created based on these predefined rules in the TPS: (1) planning target volume (PTV) was created as a 0.3 cm uniform expansion of the GTV; (2) "Ring_2cm" was created as a 1 cm-diameter shell that is a 2 to 3 cm expansion of the PTV; (3) "LowDoseRing" was created by subtracting the 3 cm PTV expansion from the external contour; and (4) "GTV_core" was created to drive the hotspot in the optimizer and was a uniform contraction of the "GTVopt" by 0.3 cm. An identical set of planning structures should automatically be created when the registered phantom is loaded onto the TDS. Our institutional planning approach is based on summing then expanding OARs and subtracting the intersection between them and target structures using "rules". The OARs of interest were summed into a single structure ("AllOARs"). This large, contiguous structure was then uniformly expanded by 0.3 cm to create planning-at-risk volume ("AllPRVs") which was used to carve out any overlapping target structures. The remaining targets ("GTVopt" and "PTVopt") are used to direct the prescription dose when optimizing the plan, by subtracting "AllPRVs" from the respective GTV and PTV.

For this segmentation consistency check, all structures were set to rigid on the baseline plan in the TPS. The same TrueFISP MR scan from simulation was acquired in the adaptive workflow on the TDS, and the ROIs were then compared. Specifically, the geometric dimensions and locations of the contours and planning-dependent outputs were both visually and quantitatively evaluated between the TPS and the TDS. Figure 1 displays the axial, coronal, and sagittal planes of the MR motion phantom with all targets and OARs on the TPS baseline plan (A-C) and the TDS adaptive plan (D-F).

2.3.4 Sub-end-to-end: dose calculation consistency TPS vs. TDS

Note that since the online ART environment is a different UI than the initial plan creation, as previously described, evaluating the consistency between the dose calculation algorithm is important. For this measurement, we used the same phantom setup from the segmentation consistency test. A stereotactic body radiotherapy (SBRT) treatment plan was designed on the phantom setup using the TPS on the simulation dataset, as previously described.

We then evaluated the differences in the TPS baseline plan's dose distribution to the "predicted dose" calculation from the TDS' adaptive workflow. Since the geometry and ROIs of this evaluation were rigid, the DVH metrics can be simply evaluated to determine consistency of the dose calculation algorithm on the TDS to the TPS. Note that the predicted dose is the fluence of the simulation baseline plan from the MRIdian TPS recalculated onto the image acquired at the time of online ART. In short, the dose distribution from the "predicted plan" should match that of the initial TPS generated plan within Monte Carlo statistical uncertainty. Figure 2 displays an example of the dose statistics for the baseline plan in the TPS UI (left) and the predicted plan in the TDS UI (right) used to evaluate dose calculation consistency using identical beam fluence.

Furthermore, gamma analysis could be used to compare the consistency between two calculation-generated dose distributions. DICOM dose files of the TPS plan and the predicted plan from the TDS were exported to SNC Patient software (Sun Nuclear, Melbourne, FL). Gamma indices of 2%/2 mm and 1%/1 mm were used to assess the difference between the dose distributions generated from the TPS and TDS of the same fluence.

2.3.5 Sub-end-to-end: optimizer robustness consistency TPS vs. TDS

For online ART, evaluating the differences in the optimizer performance (i.e., reproducibility) between the TPS and TDS is important to benchmark. Any difference if not understood can lead

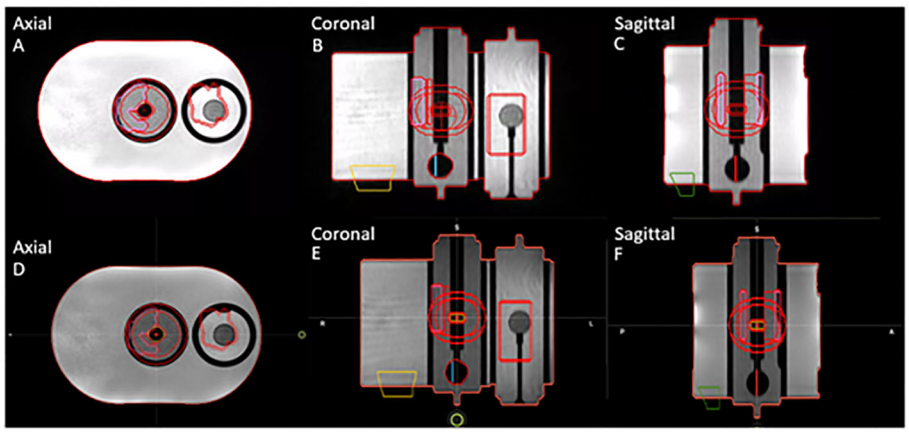

FIGURE 1
Segmentation consistency between baseline plan on TPS **(A–C)** and adaptive plan on TDS **(D–F)** for axial, coronal, and sagittal planes of QUASAR phantom and contours of targets and OARs.

TPS UI: Baseline Plan

TDS UI: Predicted Plan Dose

PRESCRIPTION STATS	CONSTRAINT	OP	DOSE	TOLERANCE VOLUME	TOLERANCE DOSE	VOL AT GY	GY AT VOL
PTV	95.00 %	≥	50.00 GY	3.00 %	1.00 GY	71.01 %	31.92 GY
CTV	99.00 %	≥	50.00 GY	3.00 %	1.00 GY	83.72 %	34.85 GY
CTV_opt	99.00 %	≥	50.00 GY	3.00 %	1.00 GY	97.55 %	47.05 GY
Esophagus	0.50 CC	≤	35.00 GY	1.00 CC	1.00 GY	0.00 CC	9.75 GY
Esophagus	0.03 CC	≤	40.00 GY	1.00 CC	1.00 GY	0.00 CC	13.00 GY
GTV	99.00 %	≥	50.00 GY	3.00 %	1.00 GY	90.02 %	39.26 GY
GTV_opt	99.00 %	≥	50.00 GY	3.00 %	1.00 GY	97.35 %	46.46 GY
Heart	0.03 CC	≤	56.00 GY	1.00 CC	1.00 GY	0.00 CC	53.56 GY
LargeBowel	0.50 CC	≤	38.00 GY	1.00 CC	1.00 GY	0.00 CC	14.72 GY
LargeBowel	0.03 CC	≤	43.00 GY	1.00 CC	1.00 GY	0.00 CC	17.55 GY
Liver-GTV	Dose Aver...	≤	13.00 GY		1.00 GY		2.88 GY

FIGURE 2
Example of dose calculation consistency check between the TPS (left) during the baseline planning, and the TDS (right) during the ART planning for the same plan/fluence.

to challenges in the online adaptive replanning quality and efficiency. As such, we evaluated the differences of the optimizer and leaf sequencer between the TPS and the TDS. Figure 3 displays the workflow/method for evaluating optimizer robustness between the TPS and TDS. Note that a clinical plan can be used following TPS preparation as outlined below; the ART workflow is then performed on an MR-compatible phantom.

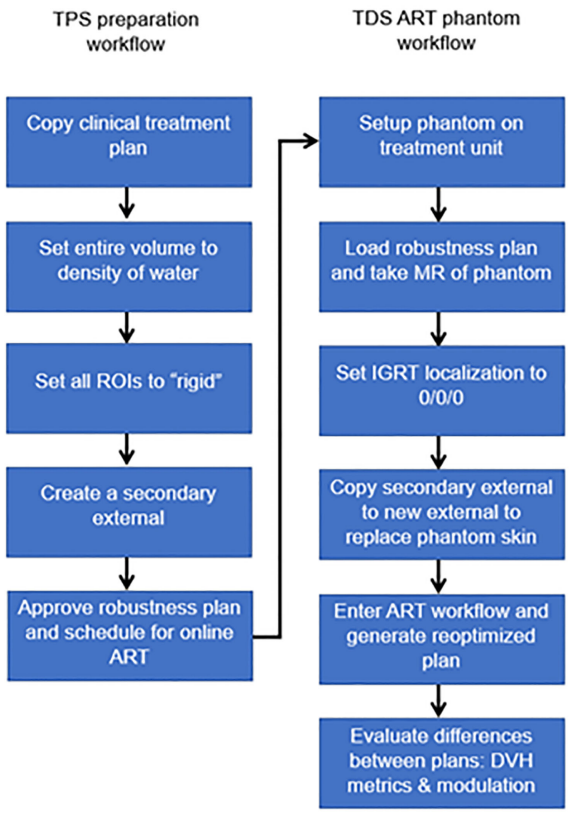

FIGURE 3
Overview of workflow to evaluate the optimizer robustness consistency between the baseline plan in the TPS and adaptive plan in the TDS.

Any previously treated clinical case can be selected for this exercise. All ROIs were set to a rigid propagation. The CT that was used to map the electron density for the clinical case was removed, and all densities were overridden to match that of water. Note that the accuracy of the electron density is not important for this test. What we are measuring is the ability to replicate a plan and creating a homogenous treatment volume simplifies this procedure. A separate external contour was created on the initial patient image and set as a rigid structure in the MRIdian TPS.

The multimodality abdominal phantom was then set up to the lasers and imaged using our standard institutional imaging protocol. Note that any MR-imageable phantom can be used for this assessment, since the density is already predefined as rigid ROI and the electron density is homogenous water. The skin generated by the TDS was replaced with the rigid external ROI created during treatment planning. The "fully reoptimized plan" on the TDS was then compared with the original plan (i.e., original fluence plan created by the TPS calculated on the simulation baseline anatomy). Robustness is evaluated based on the similarity between the original from the TPS generated dose distribution and the ART plan generated by the TDS optimizer. The MU and number of segments were compared with evaluate the leaf sequencer similarity.

2.3.6 Sub-end-to-end: CT density table consistency

To verify that the CT density table in the TDS is consistent with the density table of the TPS, the electron density propagation for relevant values should be verified. For this assessment, we used a heterogeneous phantom with known density plugs (CT Electron Density Phantom, Sun Nuclear, Melbourne, FL) that had been previously CT scanned. Since such CT density phantom is not capable of generating MR signal, we used an MR-imaging phantom

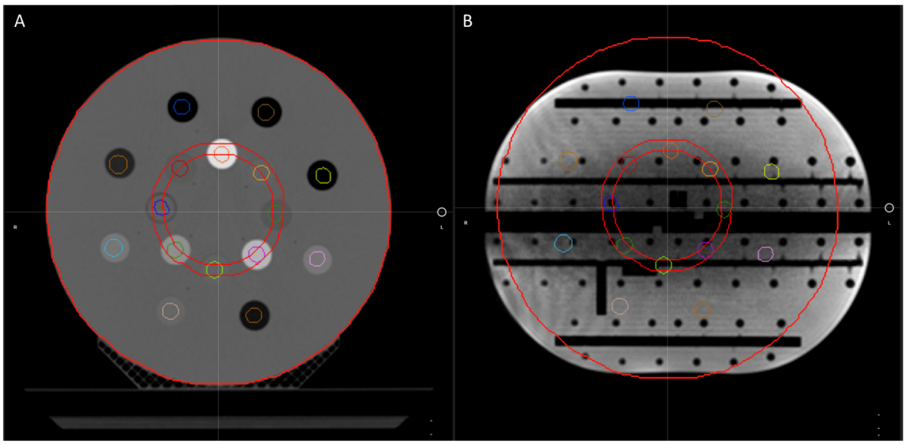

FIGURE 4
The CT electron density phantom as it appears on the TPS **(A)** and the CT electron density phantom projected onto the Magphan in the ART workflow for verification of image value consistency **(B)**.

(Magphan RT 820, Phantom Laboratory, Greenwich, NY) that approximated a similar size of the density phantom. The MR-imaging phantom was then used as the primary dataset of the initial plan for the TPS validation and for the primary dataset of the ART plan for TDS validation. Figure 4 displays the CT electron density phantom as it appears on the TPS (A), and the CT electron density phantom projected onto the MR-imaging phantom in the ART workflow (B). The electron density values relative to water as displayed in the UI were compared.

2.3.7 Full-end-to-end: absolute dose motion phantom

The ability to dynamically adjust target contours, derived Boolean structures, and ultimately the optimized fluence is the end goal of ART. We developed an end-to-end test to assess the dosimetric accuracy of an RT plan which had its target volume simulating interfractional motion. Our test was designed to enable statistical differences in the predicted dose compared with the reoptimized adaptive dose, by ensuring the motion of the target was beyond the original fluence (i.e., adapted target was positioned beyond the treatment volume of the original plan). We designed this test in the same manner as our ART workflow (i.e., fully reoptimized with normalization); this will vary based on the institutional ART technique. Plan design should reflect institutional technique and methods will vary.

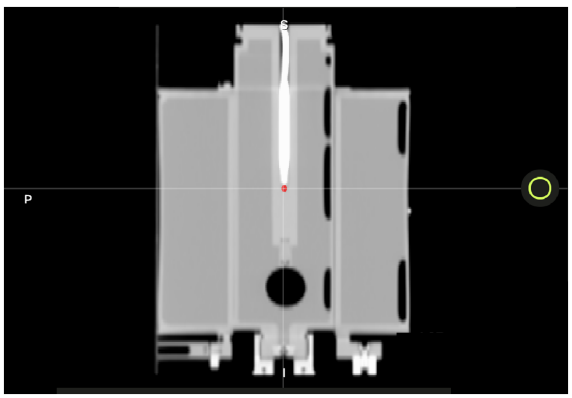

FIGURE 5
A CT image of the QUASAR with A26MR ionization chamber. The A26MR active volume is contoured in red.

We used an MR-compatible motion phantom (QUASAR) and an Exradin A26MR ionization chamber (0.015 cc, Standard Imaging Inc., Middleton, WI) to perform this test. The movable phantom plunger (i.e., chamber holder) was initially positioned at the positive peak position of its travel path, +19.9 mm. Our standard clinical imaging protocol was used, and a previously acquired CT scan of the phantom was imported into the TPS to map the electron density. Figure 5 displays the CT of the motion phantom with the A26MR chamber.

We created a treatment plan using the aforementioned planning technique by creating a GTV volume of 2 cm in diameter and centered on the active volume of the ionization chamber. The GTV was uniformly expanded, planning rings were generated, and custom OARs were used to create AllOARs, AllPRVs, GTVopt, and PTVopt structures.

The active volume of the chamber was contoured to compare the calculated dose to the measured dose. The generated plan was designed to deliver a homogenous dose distribution across the PTV to avoid large dose gradients and reduce measurement uncertainty. As such, for the baseline plan, the maximum/minimum/mean dose to the PTV and the contoured A26MR active volume on the TPS were 8.40/7.95/8.20 and 8.29/8.21/8.24 Gy per fraction, respectively.

Without moving or touching the phantom, the motion phantom's plunger was positioned to the other extreme position (−19.9 mm) using the phantom's software. Per the ART workflow, a new MR scan was acquired for the anatomy of the day and the GTV was adapted to the new location of the A26MR. Specifically, the

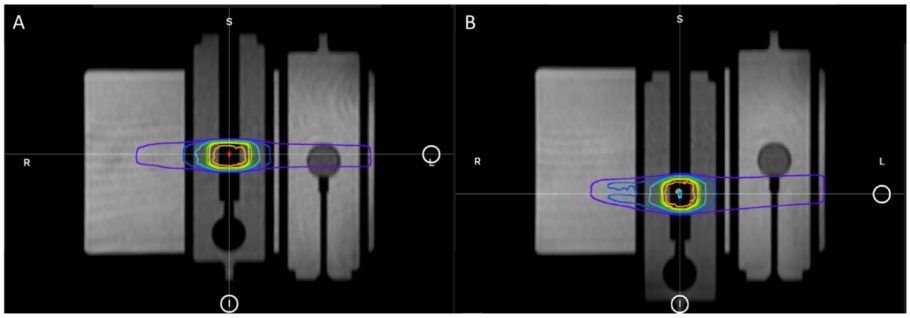

FIGURE 6
The plunger at its initial +19.9 mm position for baseline plan **(A)** and the shifted −19.9 mm position for adaptive plan **(B)**.

GTV and A26 active volume contour were shifted longitudinally by the fixed amount the motion phantom was translated (+19.9 mm to −19.9 mm). Figure 6 displays the motion phantom shifting between the two positions with respective dose distribution from the baseline plan (A) and adaptive plan (B).

All subsequent derived structures were recreated based on the adapted GTV through predefined Boolean logic and expansions. Note that the active volume contour of the A26MR was not a derived structure; it was created manually.

There are two treatment techniques that we tested: replicating the baseline plan onto the original geometry of +19.9 mm position (predicted plan) and adapting the baseline plan onto the new geometry of −19.9 mm position (ART plan). Both treatment techniques were delivered as a continuous treatment and an interrupted treatment, where the beam and MRI were completely turned off before the phantom was reimaged and treatment was set to resume. For each treatment, the measured and calculated dose to the A26MR was compared. For the predicted plan, we also compared the calculated statistics of the TPS and TDS to the delivered dose, as a secondary evaluation of the TPS to TDS dose calculation consistency.

3 Results

3.1 Configuration consistency

For the configuration consistency, no differences were observed in the UI configuration report. Figure 7 demonstrates an example of the MRIdian configuration report. Note that the UI configurations were maintained, and UI settings were confirmed pre-software upgrade to post-software upgrade.

3.2 TPS beam model consistency

For the TPS beam model consistency, the results between pre- and post-software upgrade dose distributions are shown in Table 2 for the same case. Note that both percentage of volume and absolute volume statistics were evaluated. The large percentage differences in point dose metrics (i.e., V40 Gy (cc) to small bowel) are inflated as the TPS calculates the 40 Gy dose to the small bowel as 0.03 cc (pre-software upgrade) versus 0.04 cc (post-software upgrade), a 33.33% increase which is equivalent to a 0.01 cc increase. The slight differences in point

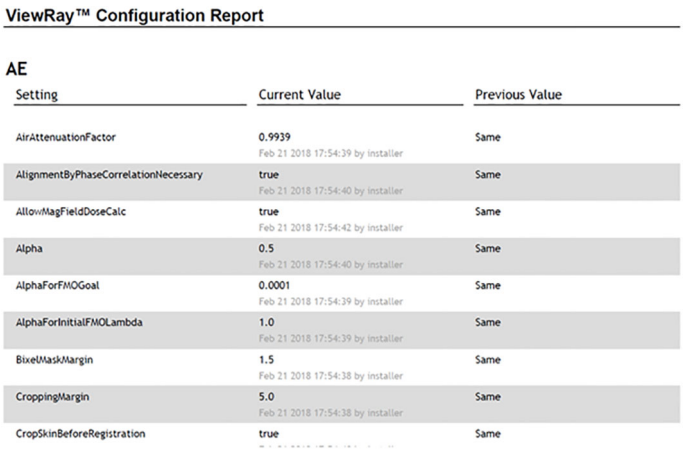

ViewRay™ Configuration Report

AE

Setting	Current Value	Previous Value
AirAttenuationFactor	0.9939 Feb 21 2018 17:54:39 by installer	Same
AlignmentByPhaseCorrelationNecessary	true Feb 21 2018 17:54:40 by installer	Same
AllowMagFieldDoseCalc	true Feb 21 2018 17:54:42 by installer	Same
Alpha	0.5 Feb 21 2018 17:54:40 by installer	Same
AlphaForFMOGoal	0.0001 Feb 21 2018 17:54:39 by installer	Same
AlphaForInitialFMOLambda	1.0 Feb 21 2018 17:54:39 by installer	Same
BixelMaskMargin	1.5 Feb 21 2018 17:54:38 by installer	Same
CroppingMargin	5.0 Feb 21 2018 17:54:38 by installer	Same
CropSkinBeforeRegistration	true	Same

FIGURE 7
An example of the MRIdian configuration report with post-software upgrade and pre-software upgrade UI settings shown in the "current value" and "previous value," respectively.

TABLE 2 TPS beam model consistency results pre- and post- software upgrade with relevant dose volume statistics.

ROI	Metric	Pre-software upgrade	Post-software upgrade	Difference
PTV	V40 Gy (%)	91.10	91.33	0.25%
PTVopt	V40 Gy (%)	98.41	98.72	0.32%
GTV	V50 Gy (%)	97.85	97.77	−0.08%
GTVopt	V50 Gy (%)	99.98	100	0.02%
Duodenum	V40 Gy (cc)	0.07	0.08	0.01 cc
Duodenum	V35 Gy (cc)	0.50	0.53	0.03 cc
Small bowel	V40 Gy (cc)	0.03	0.04	0.01 cc
Small bowel	V35 Gy (cc)	0.14	0.15	0.01 cc

doses receiving a given volume are not clinically significant and within the Monte Carlo dose calculation uncertainty.

3.3 Sub-end-to-end: segmentation consistency (rigid assessment)

For the segmentation consistency, the differences between the contour volumes of the TPS and TDS are shown in Table 3 for the same case. The results were consistent, and there were no clinically impactful differences. Of note, there were slight volume differences when structures were expanded.

3.4 Sub-end-to-end: dose calculation consistency TPS vs. TDS

For the dose calculation consistency between the TPS and TDS, a plan created by the TPS was compared with the predicted plan of the TDS. Figure 8 displays the gamma comparison between the two dose distributions using an index of 2%/2 mm and 1%/1 mm. The passing rates were 99.9% and 91.3% for the 2%/2 mm and 1%/1 mm indices, respectively.

TABLE 3 Segmentation consistency results of TPS versus TDS with relevant volumes statistics.

ROI	TPS volume (cc)	TDS volume (cc)	Absolute difference (cc)
PTV	6.39	6.39	0.00
PTVopt	5.43	5.43	0.00
GTV	2.86	2.86	0.00
GTVopt	2.58	2.58	0.00
Ring2cm	165.78	166.80	1.02
OAR1	104.27	104.27	0.00
OAR2	162.27	162.27	0.00
PTV+2cm	128.89	126.98	−1.91
PTV+3cm	294.67	293.78	−0.89

3.5 Sub-end-to-end: optimizer robustness consistency TPS vs. TDS

For the robustness check between the TPS and TDS, a patient case was applied through an online ART workflow to compare the TPS generated plan to the fully reoptimized online ART-generated plan. Table 4 contains the results of the robustness consistency with relevant clinical dose volume goals and modulation parameters displayed for both plans. Maximum percentage and absolute volume differences in dose were 2.01% and 0.56 cc for respective CTV V33 Gy and small bowel V35 Gy, demonstrating that online adaptive plan quality was upheld using the institutional planning technique on a rigid geometry.

3.6 Sub-end-to-end: CT density table consistency

The electron density value comparison of the deformed density phantom was performed in the TPS and TDS for the validation of the image value to density conversion in the initial plan workflow and online adaptive workflow, respectively. Table 5 displays the measured relative electron density values from the TPS and TDS comparison. Note that the maximum difference observed was the lung at 3.57%; however, 0.28 and 0.29 relative electron densities between TPS and TDS are negligible.

3.7 Full-end-to-end: absolute dose motion phantom

Simulated interfractional motion on an MR-compatible phantom was performed as an end-to-end absolute dose procedure. Four end-to-end permutations as shown in Table 6 were performed: (1) predicted dose, (2) predicted dose with interruption, (3) ART dose, and (4) ART dose with interruption. A predicted dose plan and the ART fully reoptimized plan were generated based on the nominal anatomy and induced anatomical change, respectively. Note that the predicted dose plan was performed in the adaptive workflow to confirm that the original fluence delivery parameters would maintain in an ART

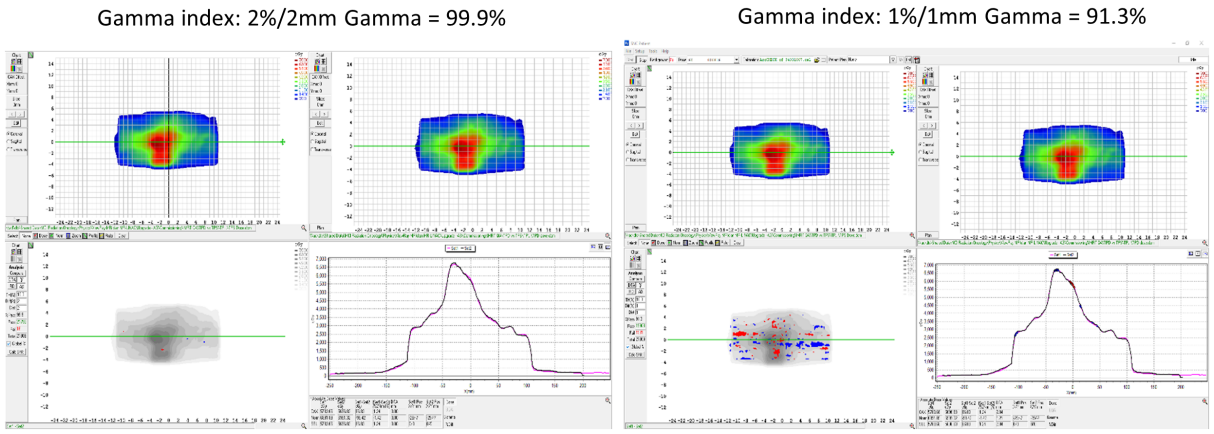

FIGURE 8
The dose calculation consistency between the TPS and TDS with gamma comparison using an index of 2%/2 mm and 1%/1 mm.

environment when the non-ART plan was selected for delivery. All dosimetric results (Table 6) were within 1% agreement of measured to calculated values. Note that for the interruption tests, approximately 60% of MU were delivered prior to the planned interruption.

4 Discussion

The purpose and key advantage of ART is the ability to adjust contours and their derived planning-dependent structures to the daily anatomy, such that a newly optimized fluence can maximize the therapeutic ratio. The aim of this work is to describe the necessary tests to perform after a software upgrade has been implemented to an ART-capable system. It is assumed that the system being upgraded is already commissioned and used in a clinical environment. Our tests were performed on a MRIdian system; however, the processes outlined in this work can be adapted and applied to other systems capable of online ART. Note that QA tests should be designed to validate elements of the UI that were impacted by the software upgrade in conjunction to online ART process and workflow procedures. As such, there may be QA elements outside the scope of this work that may be relevant in the QA of an online ART post-software upgrade (i.e., image quality).

The UI configuration report was generated in real-time after patch installation and was compared with institutional-specific approved configurations. It is expected that different systems and institutions will have different baseline parameters. The purpose of the UI configuration report is to ensure and verify to the user that all system settings are maintained. It is possible that not all system configurations are included in the vendor-supplied report, and

TABLE 4 Optimizer robustness consistency as shown through plan quality metrics of a clinical plan created by the TPS and compared with the fully reoptimized online ART plan on the TDS.

ROI/modulation	Metric	TPS initial plan	Online ART plan	Difference
PTV50	V50 Gy (%)	95	95	0.00%
PTV50opt	V50 Gy (%)	95.31	95.27	−0.04%
GTV	V50 Gy (%)	100	100	0.00%
PTV33	V33 Gy (%)	95.51	93.97	−1.61%
PTV33opt	V33 Gy (%)	96.53	95.83	−0.73%
CTV	V33 Gy (%)	99.52	97.52	−2.01%
Small bowel	V35 Gy (cc)	0.19	0.75	0.56
Stomach	V35 Gy (cc)	0	0	0
Large bowel	V38 Gy (cc)	0.03	0	−0.03
Modulation	# of beams	16	16	0
Modulation	# of segments	49	50	+1
Modulation	# MUs	2,883.5	3,925.4	136%
Modulation	MU/prescribed dose	2.88	3.93	136%

TABLE 5 Comparison of the relative electron density of known value, TPS, and TDS.

ROI	Known electron density relative to water	Relative electron density (TPS)	Relative electron density (TDS/Online ART)	% difference TPS to known density	% difference TPS to TDS
Air	0	0.05	0.05	–	0.00%
Lung	0.29	0.28	0.29	−3.45%	3.57%
Water	1	0.99	0.97	−1.00%	−2.02%
Bone	1.28	1.26	1.24	−1.56%	−1.59%
Dense Bone	1.69	1.67	1.66	−1.18%	−0.60%

users should work with their respective vendor to confirm if additional configuration files need to be manually verified for integrity.

When analyzing the segmentation consistency, we observed slight differences in the volumes for the output of the expansion-based rule dependent ROIs. These differences were observed at the interface of a voxel and likely due to the non-partial voxelization of the MRIdian system. The translation of rigid ROIs maintained the integrity between TPS and TDS during the online ART workflow.

When comparing the TPS's beam model before and after the software upgrade, dosimetric agreement (Table 2) was found to be consistent to the statistical uncertainty of 0.5% of the Monte Carlo histories. Note that the DVH metrics for large volumes such as target coverage metrics were within the accepted uncertainty of Monte Carlo. However, slight variations in dosimetric metrics to small volumes (i.e., D0.03 cc) appeared as skewed results in percentage differences, and therefore were taken as differences in absolute volume instead. This relationship is due to the sampling of the finite dose grid (2 mm^3) for smaller volume ROIs.

In addition to inherent uncertainties of Monte Carlo calculations, we found that slight differences in dose reporting also arise between the TPS and TDS during the dose calculation consistency validation, as a result of the lack of partial voxelization and differences in intravoxel interpolation. Currently, MRIdian TPS calculates dose statistics based on the dose grid and then extrapolates to the resolution of the image grid. MRIdian TDS is a finer representation of the dose statistics by sampling the dose solely based on the calculation grid and is therefore independent of the image grid (i.e., no downsampling or extrapolation is applied). While the differences are small, it is possible for dose statistics to report inconsistencies between the TDS and TPS for small volume metrics (i.e., D0.03 cc), which could result in pass/fail criteria to be different for the same fluence.

For the robustness evaluation, while no differences were observed in DVH metrics, there were some differences in the modulation between the TPS and TDS for the same geometry, such as CTV and its derived structure, PTV33 (Table 4). Of note, the TDS ART UI utilizes a more efficient leaf sequencer, in which segments are combined when disjointed fluence is present. Therefore, during ART optimization extra modulation often occurs due to the optimizer having a greater number of available unused segments. Since the optimization settings were set to 50 total segments, both TPS and TDS plans generated a resulting plan with roughly 50 segments—hence allowing the TDS ART UI to get more complex. As such, the modified leaf sequencer from the TDS may produce slightly different coverage for larger targets such as the CTV and PTV33. When we observed this during commissioning, we implemented a modulation check during online ART in which the planner reduces the segments until a similar modulation is achieved on the ART plan relative to the TPS baseline plan. For the image value to density validation, we found good agreement between the reported electron density between the TPS baseline plan and the TDS adaptive plan. The purpose of this test was to verify the consistency of electron density values between the two platforms, benchmarking them was not the objective. Of note, we took advantage of a previously acquired CT scan of a dedicated electron density phantom from commissioning for the image value to electron density verification test. Note that a patient scan could have been easily used to verify electron density consistency between the TPS and TDS.

The end-to-end test evaluated the system's ability to accurately deliver the planned dose in the ART workflow in a single, integrated test. Plan delivery accuracy was evaluated based on a measurement within 2% of the calculated adaptive TDS dose (11). Note that for this test, a large shift was applied to simulate a target interfraction motion beyond the irradiated volume. While an SBRT plan was used, the overall dosimetry was not representative of an ablative technique as intentional homogenous dose distribution was applied across the chamber active volume for statistics. Sharp dose gradients, found in SBRT plans, would lead to difficult measurement conditions in a finite

TABLE 6 The end-to-end results of calculated and measured dose for online adaptive workflow on initial and shifted anatomy.

End-to-end evaluation	Phantom geometry	TDS calculated dose (Gy)	Measured dose (Gy)	% difference (calculated to measured dose)
Predicted dose	Unshifted	8.22	8.22	0.00%
Predicted dose with interruption	Unshifted	8.22	8.20	−0.17%
ART dose	Shifted	13.82	13.74	−0.58%
ART dose with interruption	Shifted	13.95	13.82	−0.90%

chamber volume, hence the use of a homogenous dose distribution. Moreover, the rationale for the uniform dose distribution was to minimize the effect of sub-millimeter translations, which could result in spurious dose reporting and a failed test. Shifting dose distributions, which are routinely performed on patient QA software to account for sub-mm setup uncertainties, are not available when taking an ionization chamber measurement which are sensitive to a static dose gradient.

We believe that QA procedures should reflect the intervention performed; as such, the tests in this work were designed to be indicative of the UI changes and how the ART program is clinically utilized. Note that the tests and procedures outlined in this work may only need to be applied as a subset based on the specific changes in the UI. Users should work with their vendor to know what aspects of the system were modified in the patch for such evaluations.

One advantage of this work is the methodology of the tests can be implemented as part of an ongoing QA program for online ART. Specifically, the end-to-end tests can be utilized as part of an annual QA program. Furthermore, these tests can be part of the initial commissioning of the system, and baseline tests/plans can be reused during patch installation, which will reduce the estimated FTE hours needed to perform these tests. Other studies have addressed ongoing QA into daily practice; for example, Chen et al. demonstrated daily online QA procedure testing the integration of critical ART components (12).

There are various ways to evaluate the TPS vs. TDS beam model and dose calculation consistency. We performed a 3D gamma analysis between exported DICOM RT dose files of the baseline plan from the TPS and the same fluence calculated on rigid geometry during the ART workflow from the TDS. Not all institutions may have access to the same resources, but there are viable alternative methods available to evaluate beam consistency. Users could superimpose DVH curves on each other, evaluate individual DVH metrics, or run a gamma analysis comparing the dose distribution from the same plan generated by the TPS and TDS.

The scope of this work is related to UI (i.e., software), and not hardware modifications. As such, if hardware components were involved in the system patch and/or upgrade, then further system QA would need to be assessed, including but not limited to imaging and radiotherapy components. Patch and software upgrades influence an ART-capable system's treatment planning software and the data transfer capabilities between the TPS and TDS. As such, IMRT QA is not a necessary component of a patch upgrade, because the mechanical and beam components of the Linac remain unaltered. QA of radiation production, imaging, and mechanical functionality is recommended if their respective components are altered. Recommendations include performing monthly QA per institutional guidelines (i.e., TG142).

While the ability to accurately deliver adaptive RT is dependent on the gating (13), the QA of intrafraction motion management (14) is outside the scope of this work. Similarly, deformable image registration (DIR) accuracy is a key feature of the online ART workflow. This work assumes baseline performance commissioning of the DIR algorithm (2) has been performed and algorithm remains unaltered in the UI. Additional work related to online ART is the QA of dose accumulation (15), which is also outside the scope of this work.

After a software upgrade is performed, it is recommended that the therapists and qualified medical physicists mode up any active patients as well as confirm any other clinical functionality associated with their institution's specific ART workflow. If there is no change in the UI or clinical workflow (i.e., software patch for a bug), a re-training is not necessary. Furthermore, if UI or clinical workflow has changed, then it is recommend that therapists be involved with a dry run workflow on phantom. The onus of therapists' involvement post-QA lies with each ART program, as each institution has different methods of operation and divisions of labor.

There are several limitations to this work. First, this study is a single institution/machine reporting. Additionally, no longitudinal QA assessment was performed. Another limitation of this work is that QA procedures are specific to one ART modality. This study specifically does not outline daily, monthly, and annual QA for ART, although as previously stated, the proposed post-software upgrade ART QA procedures can be adopted and applied as routine QA (i.e., Annual). Future work will be on reporting implementation of routine QA for ART. Specifically, we envision daily QA consisting of a TPS checksum/integrity QA of ART TDS. For monthly QA, we envision a simplified approach to the end-to-end procedures previously described in this work.

Lastly as previously mentioned, QA procedures were developed around institutional workflow protocols (i.e., imaging protocol, planning technique). Another limitation of our study is that QA procedures may need to be adapted to institutional workflow. Specifically, different institutions will have different workflow protocols and will need to design QA procedures to reflect ART program use.

5 Conclusion

An online ART QA program for post-software upgrade has been developed and implemented on an MR Linac system. Tests were implemented to validate in online ART workflow: UI configuration, segmentation, beam model, dose calculation algorithm, optimizer robustness, relative electron densities, and end-to-end absolute dose. The practice of online ART continues to grow but remains an emerging paradigm, and currently there is no official standards established by AAPM and/or ASTRO to guide users on quality assurance for adaptive radiotherapy. As such, we have implemented the recommended QA procedures described here after a post-software upgrade. The outlined QA procedures were demonstrated feasible for a low-field MR Linac system. The scope of this work can be applied and adapted broadly to other online ART platforms.

Data availability statement

The original contributions presented in the study are included in the article/supplementary material. Further inquiries can be directed to the corresponding author.

Author contributions

NB: Conceptualization, Data curation, Formal analysis, Methodology, Writing – original draft, Writing – review & editing.

JB: Conceptualization, Methodology, Writing – review & editing, Supervision. MC: Resources, Writing – review & editing. RK: Writing – review & editing. YW: Writing – review & editing. MM: Supervision, Writing – review & editing. AG: Writing – review & editing, Resources, Supervision. KM: Conceptualization, Formal analysis, Investigation, Supervision, Writing – original draft, Writing – review & editing.

Funding

The author(s) declare that no financial support was received for the research, authorship, and/or publication of this article.

Conflict of interest

The listed authors have received past funding from ViewRay Inc. Mittauer, Chuong, Kotecha, Bayouth, Mittauer, Bassiri. The listed authors have received honoraria in the past from ViewRay Inc. Chuong, Kotecha, Mittauer. The listed authors have had ownership stakes in past in companies that provided consulting services in image guided radiation therapy Mittauer, Bayouth.

The author(s) declared that they were an editorial board member of Frontiers, at the time of submission. This had no impact on the peer review process and the final decision.

Publisher's note

References

1. Kisling K, Keiper TD, Branco D, Kim GG, Moore KL, Ray X. Clinical commissioning of an adaptive radiotherapy platform: Results and recommendations. *J Appl Clin Med Phys*. (2022) 23:e13801. doi: 10.1002/acm2.13801

2. Mittauer KE, Hill PM, Bassetti MF, Bayouth JE. Validation of an MR-guided online adaptive radiotherapy (MRgoART) program: Deformation accuracy in a heterogeneous, deformable, anthropomorphic phantom. *Radiother Oncol*. (2020) 146:97–109. doi: 10.1016/j.radonc.2020.02.012

3. Hoffmans D, Niebuhr N, Bohoudi O, Pfaffenberger A, Palacios M. An end-to-end test for MR-guided online adaptive radiotherapy. *Phys Med Biol*. (2020) 65:125012. doi: 10.1088/1361–6560/ab8955

4. Elter A, Dorsch S, Mann P, Runz A, Johnen W, Spindeldreier CK, et al. End-to-end test of an online adaptive treatment procedure in MR-guided radiotherapy using a phantom with anthropomorphic structures. *Phys Med Biol*. (2019) 64:225003. doi: 10.1088/1361-6560/ab4d8e

5. Okamoto H, Igaki H, Chiba T, Shibuya K, Sakasai T, Jingu K, et al. Practical guidelines of online MR-guided adaptive radiotherapy. *J Radiat Res*. (2022) 63:730–40. doi: 10.1093/jrr/rrac048

6. Mittauer K, Paliwal B, Hill P, Bayouth JE, Geurts MW, Baschnagel AM, et al. A new era of image guidance with magnetic resonance-guided radiation therapy for abdominal and thoracic Malignancies. *Cureus*. (2018) 10:e2422. doi: 10.7759/cureus.2422

7. Bohoudi O, Bruynzeel AME, Senan S, Cuijpers JP, Slotman BJ, Lagerwaard FJ, et al. Fast and robust online adaptive planning in stereotactic MR-guided adaptive radiation therapy (SMART) for pancreatic cancer. *Radiother Oncol*. (2017) 125:439–44. doi: 10.1016/j.radonc.2017.07.028

8. Chuong MD, Bryant J, Mittauer KE, Hall M, Kotecha R, Alvarez D, et al. Ablative 5-fraction stereotactic magnetic resonance-guided radiation therapy with on-table adaptive replanning and elective nodal irradiation for inoperable pancreas cancer. *Pract Radiat Oncol*. (2021) 11:134–47. doi: 10.1016/j.prro.2020.09.005

9. Smilowitz JB, Das IJ, Feygelman V, Fraass BA, Kry SF, Marshall IR, et al. AAPM medical physics practice guideline 5.a.: commissioning and QA of treatment planning dose calculations - megavoltage photon and electron beams. *J Appl Clin Med Phys*. (2015) 16:14–34. doi: 10.1120/jacmp.v16i5.5768

10. Mittauer KE, Yarlagadda S, Bryant JM, Bassiri N, Romaguera T, Gomez AG, et al. Online adaptive radiotherapy: Assessment of planning technique and its impact on longitudinal plan quality robustness in pancreatic cancer. *Radiother Oncol*. (2023) 31:109869. doi: 10.1016/j.radonc.2023.109869

11. Kim Ji, Park SY, Kim HJ, Ye SJ, Park JM. The sensitivity of gamma-index method to the positioning errors of high-definition MLC in patient-specific VMAT QA for SBRT. *Radiat Oncol*. (2014) 9:167. doi: 10.1186/1748–717X-9–167

12. Chen X, Ahunbay E, Paulson ES, Chen G, Li XA. A daily end-to-end quality assurance workflow for MR-guided online adaptive radiation therapy on MR-Linac. *J Appl Clin Med Phys*. (2020) 21:205–12. doi: 10.1002/acm2.12786

13. Chuong MD, Bryant JM, Herrera R, McCulloch J, Contreras J, Kotecha R, et al. Dose-escalated magnetic resonance image-guided Abdominopelvic reirradiation with continuous intrafraction visualization, soft tissue tracking, and automatic beam gating. *Adv Radiat Oncol*. (2021) 7:100840. doi: 10.1016/j.adro.2021.100840

14. Charters JA, Abdulkadir Y, O'Connell D, Yang Y, Lamb JM. Dosimetric evaluation of respiratory gating on a 0.35-T magnetic resonance-guided radiotherapy linac. *J Appl Clin Med Phys*. (2022) 23:e13666. doi: 10.1002/acm2.13666

15. Maraghechi B, Mazur T, Lam D, Price A, Henke L, Kim H, et al. Phantom-based quality assurance of a clinical dose accumulation technique used in an online adaptive radiation therapy platform. *Adv Radiat Oncol*. (2022) 8:101138. doi: 10.1016/j.adro.2022.101138

frontiers | Frontiers in Oncology

TYPE Original Research
PUBLISHED 11 June 2024
DOI 10.3389/fonc.2024.1401703

OPEN ACCESS

EDITED BY
Merav Ben-David,
Ramat-Hahayal, Israel

REVIEWED BY
Gage Redler,
Moffitt Cancer Center, United States
Yoichi Watanabe,
University of Minnesota Twin Cities,
United States

*CORRESPONDENCE
Joseph A. Miccio
jmiccio@pennstatehealth.psu.edu

†These authors have contributed equally to this work

RECEIVED 15 March 2024
ACCEPTED 20 May 2024
PUBLISHED 11 June 2024

CITATION
Miccio JA, Potter NJ, Showkat A, Yao M, Mahase S, Ferenci M, Sisley K, Dailey A, Knipple J, Blakely A, Tuanquin L and Machtay M (2024) Single institution experience of MRI-guided radiotherapy for thoracic tumors and clinical characteristics impacting treatment duty cycle.
Front. Oncol. 14:1401703.
doi: 10.3389/fonc.2024.1401703

Single institution experience of MRI-guided radiotherapy for thoracic tumors and clinical characteristics impacting treatment duty cycle

Joseph A. Miccio[1*†], Nicholas J. Potter[1†], Anaum Showkat[1,2], Min Yao[1], Sean Mahase[1], Michele Ferenci[1], Kaitlin Sisley[1], Amy Dailey[1], Jamie Knipple[1], Amy Blakely[1], Leonard Tuanquin[1] and Mitchell Machtay[1]

[1]Department of Radiation Oncology, Penn State Cancer Institute, Hershey, PA, United States, [2]Department of Arts and Letters, University of Notre Dame, South Bend, IN, United States

Introduction: MRI-guided radiotherapy (MRgRT) allows for direct motion management and real-time radiation treatment plan adaptation. We report our institutional experience using low strength 0.35T MRgRT for thoracic malignancies, and evaluate changes in treatment duty cycle between first and final MRgRT fractions.

Methods: All patients with intrathoracic tumors treated with MRgRT were included. The primary reason for MRgRT (adjacent organ at risk [OAR] vs. motion management [MM] vs. other) was recorded. Tumor location was classified as central (within 2cm of tracheobronchial tree) vs. non-central, and further classified by the Expanded HILUS grouping. Gross tumor volume (GTV) motion, planning target volume expansions, dose/fractionation, treatment plan time, and total delivery time were extracted from the treatment planning system. Treatment plan time was defined as the time for beam delivery, including multileaf collimator (MLC) motion, and gantry rotation. Treatment delivery time was defined as the time from beam on to completion of treatment, including treatment plan time and patient respiratory breath holds. Duty cycle was calculated as treatment plan time/treatment delivery time. Duty cycles were compared between first and final fraction using a two-sample t-test.

Results: Twenty-seven patients with thoracic tumors (16 non-small cell lung cancer and 11 thoracic metastases) were treated with MRgRT between 12/2021 and 06/2023. Fifteen patients received MRgRT due to OAR and 11 patients received MRgRT for motion management. 11 patients had central tumors and all were treated with MRgRT due to OAR risk. The median dose/fractionation was 50 Gy/5 fractions. For patients treated due to OAR (n=15), 80% had at least 1 adapted fraction during their course of radiotherapy. There was no plan adaptation for patients treated due to motion management (n=11). Mean GTV motion was significantly higher for patients treated due to motion management compared to OAR (16.1mm vs. 6.5mm, p=0.011). Mean duty cycle for fraction 1 was 54.2% compared to 62.1% with final fraction (p=0.004). Mean fraction 1 duty cycle was higher for patients treated due to OAR compared to patients treated for MM (61% vs. 45.0%, p=0.012).

Discussion: Duty cycle improved from first fraction to final fraction possibly due to patient familiarity with treatment. Duty cycle was improved for patients treated due to OAR risk, likely due to more central location and thus decreased target motion.

KEYWORDS

MRI guidance, radiotherapy, thoracic, SBRT, duty cycle

1 Introduction

Lung cancer is the third most common malignancy in the United States (1), and the lung is one of the most common sites of metastatic spread for from other primary cancers (2). The safe and effective delivery of radiotherapy to intrathoracic tumors is challenging due to critical organs at risk (OARs) such as the bronchial tree, esophagus, heart, and spinal cord as well as inherent respiratory motion leading to uncertainty in tumor position throughout the respiratory cycle (3). Even modern series evaluating radiotherapy for tumors near the bronchial tree have shown unacceptable grade 5 toxicity rates of up to 15% (4).

Magnetic Resonance Image Guided Radiotherapy (MRgRT) utilizing a 0.35T MR-Linac allows for direct visualization of targets during treatment and motion-management by way of patient breath hold gating (i.e. delivery of radiation at a particular position in the patient's respiratory cycle). Additionally, the system allows for online real-time dosimetric evaluation, and the ability to adapt the radiation plan based on daily anatomic changes to optimize target coverage while ensuring acceptable dose to OARs. MRgRT offers a unique solution to safely and effectively treat intrathoracic tumors by accounting for adjacent OARs and respiratory motion (5).

This manuscript describes our experience treating thoracic tumors with 0.35T MRgRT. Herein we describe our experience including patient demographics and the clinical reasoning for utilizing MRgRT for each case. We also evaluate the frequency of radiation plan adaptation and finally we evaluate the change in treatment duty cycle between first and final fractions of radiotherapy. Lastly, we explore duty cycle differences between patients treated before and after our department installed an in-bore viewing video display to provide visual feedback to patients to assist with breath hold gating.

2 Methods

All patients with intrathoracic tumors treated with MRgRT from December 2021 through June 2023 were included. Institutional Review Board approval was obtained for this analysis (Study 00021052). All patients were treated with respiratory gating, and 19 patients were treated after the visual feedback display installation. The primary reason for MRgRT (OAR vs. motion management vs. other) was recorded by the treating physician. Tumor location was classified as central (within 2cm of tracheobronchial tree) vs. non-central, and further classified by the Expanded HILUS grouping (A: ≤ 1 cm from the mainstem bronchus; B: ≤ 1 cm from the lobar bronchi but >1 cm from the mainstem bronchi; C: 1 - 2 cm around the tracheobronchial tree; D: ≤ 1 cm from the trachea but > 2 cm from the carina.) (6). Gross tumor volume (GTV) motion during free breathing, planning target volume (PTV) expansions, and radiation dose and fractionation were recorded for each patient. For each fraction, OARs were evaluated online and contours were adjusted as needed. The radiation plan was predicted on the anatomy of the day, and the decision to adapt the plan was at the treating physician's discretion. In general, plans were adapted to improve target coverage, decrease OAR dose, or both.

The treatment plan time (TPT) and total delivery time (TDT) were extracted from the treatment planning system for the first and final fractions of each patient's treatment course. Treatment plan time is defined as the time for beam delivery, including multileaf collimator (MLC) motion and gantry rotation (i.e. time for treatment delivery if target was always within the treatment boundary). If there was no plan adaptation, the first fraction's treatment plan time is equal to the final fraction's treatment plan time. Treatment delivery time was defined as the time from beam-on to fraction completion (i.e. treatment plan time plus time for patient to repeatedly breath-hold the target into the treatment boundary).

The ratio of time spent by the signal within the specific portion of the respiratory cycle ("gate") to the overall treatment time is referred to as the duty cycle (7). Beam gating for motion management on the 0.35T MR-Linear Accelerator is performed by having the patient hold their breath and tracking the physical location of the tumor on real-time cine MRI imaging. When the patient's target is within the correct positional window the machine delivers radiation. Duty cycle is a measure of efficiency of this method. It is important to note the user can select two parameters during tracking that have a significant impact on duty cycle, size of positional window and %ROI-threshold (the acceptable ROI percentage outside of the tracking positional window). The positional window for all patients treated in this study was

10.3389/fonc.2024.1401703

created by applying a 3 mm isotropic expansion on the tracking volume, and the %ROI-threshold was set between 5–8% for all patients, with majority utilizing 5%. A consistent definition of duty cycle for MRgRT is not well established (8–10). In the present study, Duty cycles (DC) were calculated for the first fraction (i), and final fraction (f) as:

$$DC_i = \frac{TPT_i}{TDT_i}$$

$$DC_f = \frac{TPT_f}{TDT_f}$$

Duty cycles were compared between first and final fraction, and between patients receiving MRgRT for primary reason of OAR vs. motion management using a two-sample t-test. The analysis was performed using STATA, version 13.1 (StataCorp LLC, College Station, TX) and P-values< 0.05 were considered statistically significant.

3 Results

Twenty-seven patients with thoracic disease were treated with a total of 169 fractions of MRgRT between December of 2021 and June of 2023 (Table 1). Patients treated with MRgRT had good to excellent performance status with 30% ECOG 0 and 70% ECOG 1. Sixteen patients had non-small cell lung cancer and 11 patients had metastatic disease to the chest from another primary site. The majority of treated lesions were within the lung parenchyma, however 4 patients were treated to mediastinal lymph nodes. Eleven patients met Expanded HILUS grouping definition (6 group A, 1 group B, 2 group C, and 2 group D). Fifteen patients were treated with MRgRT due to OAR proximity, 11 patients were treated primarily for respiratory motion management, and one patient was treated with MRgRT due to a variable pleural effusion. All 11 patients meeting HILUS grouping definition were treated with MRgRT primarily due to OAR proximity. Figure 1 shows an example for HILUS grouping B due to proximity to the left upper lobe bronchus.

The median dose/fractionation was 50 Gy/5 fractions and 30% (n=51) of fractions delivered were adapted (Table 2). Of the 51 adapted fractions, 19 (37.3%) were adapted due to OAR dose, 9 (17.6%) were adapted due to PTV coverage, and the remaining 23 fractions (45.1%) were adapted due to both PTV coverage and OAR dose considerations. For patients treated with MRgRT due to OAR proximity (n=15), 80% had at least 1 adapted fraction during their course of radiotherapy. There was no plan adaptation for patients treated due to motion management (n=11). Nine patients had adapted plans in either their first or final fraction, resulting in different treatment plan times thus impacting duty cycle. For these 9 patients, the average change in treatment plan time from first to final fraction was 0.29 minutes, with only 3 patients plan time changing by more than one minute.

Mean GTV motion was significantly higher for patients treated due to motion management compared to OAR (16.1mm vs. 6.5mm, p=0.011). Mean duty cycle for fraction 1 was 54.2% compared to 62.1% for the final fraction (p=0.0035). In the subset of 18 patients with identical treatment plan times in fraction 1 and final fraction (i.e. fraction 1 and final fraction were not adapted), mean duty cycle for fraction 1 was 52.6% compared to 60.9% for the final fraction (p=0.0075). Duty cycle was higher for patients treated due to OAR compared to patients treated for motion management in fraction 1 (61% vs. 45.0%, p=0.0124) and in the final fraction (69.5% vs. 52.7%, P=0.0146; Figure 2). The mean duty cycle for fraction 1 was 65.3% for patients treated before installation of the visual feedback display compared to 49.6% for patients treated after installation (p=0.0185). The mean duty cycle for final fraction was 68.0% for patients before visual feedback display installation compared to 59.6% for patients without (p=0.2657).

TABLE 1 Cohort characteristics.

Age (median and IQR)	71 (58–80)
ECOG	
0	8 (30%)
1	19 (70%)
Sex	
Male	12 (44%)
Female	15 (56%)
Histology	
NSCLC	16 (59%)
Other	11 (41%)
Stage	
I, II, III	11 (41%)
IV	16 (56%)
Concurrent Systemic Therapy	
None	18 (67%)
Immunotherapy	6 (22%)
Chemotherapy	1 (4%)
Biologic	2 (7%)
Expanded HILUS Classification	
A	6 (22%)
B	1 (4%)
C	2 (7%)
D	2 (7%)
NA	16 (60%)
Site	
Right lung	15 (55%)
Left lung	8 (30%)
Mediastinum	4 (15%)
Reason for MRgRT Treatment	
Adjacent OAR	15 (55.6%)
Motion Management	11 (40.7%)
Other	1 (3.7%)

4 Discussion

During our institution's MRgRT program, we delivered thoracic MRgRT to 27 patients over 169 fractions for a variety of intrathoracic tumors. We found that on average, treatment duty cycle improved by an average of 8% between fraction 1 and the final

10.3389/fonc.2024.1401703

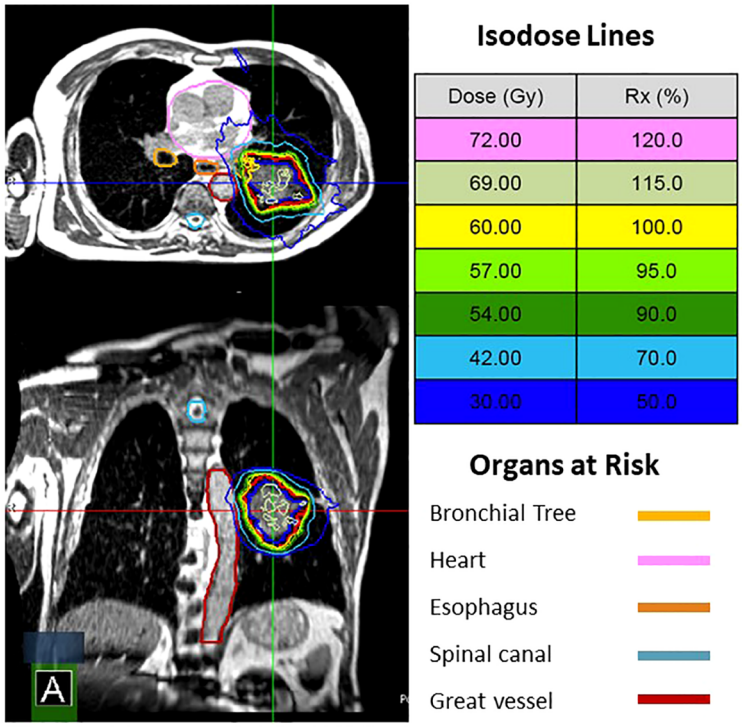

FIGURE 1
MRgRT plan for a patient with a cT3N0 NSCLC. He was not a surgical candidate. HILUS B due to proximity to the left upper lobe bronchus. The patient was treated with 60 Gy in 8 fractions with 1 of 8 fractions adapted.

fraction. Since the time for beam delivery, multileaf collimator (MLC) motion, and gantry rotation are mostly constant, the improvement likely correlates with patient breath hold performance between first and final fractions.

TABLE 2 Treatment characteristics (median and IQR).

Dose per fraction (Gy)	10 (7–10)
Fraction number	5 (5–5)
Total dose (Gy)	50 (50–50)
Hotspot in GTV (%)	122 (117–129)
GTV (cc)	10.3 (5.43 – 22.5)
GTV motion (mm)	9 (4–13)
PTV expansion (mm)	5 (5–5)
PTV volume (cc)	32.1 (14.0–48.3)
Number of Adapted Fractions	0 (0–3)
Plan Time Fraction 1 (minutes)	10.0 (8.7–12.5)
Delivery Time Fraction 1 (minutes)	17.3 (15.1–28.8)
Duty Cycle Fraction 1 (%)	55 (40.3–68.3)
Plan Time Final Fraction (minutes)	10.0 (8.7 – 12.5)
Delivery Time Final Fraction (minutes)	16.0 (13.5–21.5)
Duty Cycle Final Fraction (%)	64.1 (54.7 – 73.7)

The duty cycle plays a critical role in the overall efficacy of MRgRT respiratory gated treatments. Treatment times are significantly longer for patients undergoing real time tracking and breath-hold gating on MR-Linac when compared to conventional linac treatments. This leads to a higher probability for changes in patient positioning during treatment that may not be reflected in a 2D cine image, changes in patients breathing acumen due to duration and fatigue, and possibility of respiratory baseline shift during treatment, which may change target motion trajectory. The factors contributing to duty cycle are complex and include medical factors, (baseline cardiopulmonary function impacting breath hold duration), psychological factors (patient understanding and education), and technical factors (tumor, MLC, and gantry motion). Thus, patient selection and continual patient education is key to maximize the treatment duty cycle.

Our work adds to the literature describing the feasibility of using MRgRT for thoracic tumors and adds hypothesis-generating results about the improvement in duty cycle between first and final fraction. This likely reflects improved patient familiarity with the treatment and breath hold technique needed on subsequent fractions to accurately get the tumor into the target region. The therapist team debriefed the patient after each fraction to answer questions and offer suggestions to improve treatment efficiency. Additionally, a physics consult was offered to MRgRT patients prior to simulation, in which breath hold gating was discussed with visual aids. Further analysis is required to validate the impact of physics consultation on duty cycle efficiency.

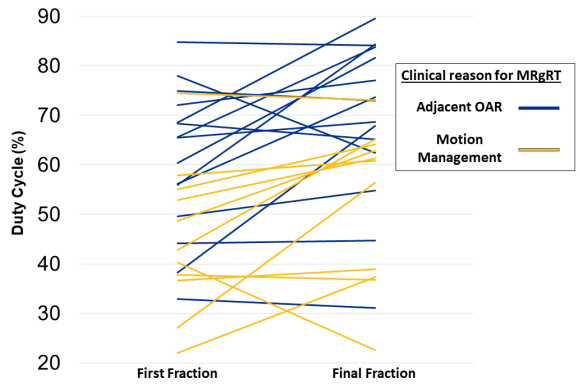

FIGURE 2
Change in duty cycle between first and final fraction. Each line represents a single patient and color denotes if a patient was treated primarily due to motion management or adjacent organ at risk.

Respiratory motion is complex and there is variability in the extent of craniocaudal and anteroposterior displacement between fractions (3). In our clinical observations, we noted that several patients have a striking change in target location as the patient relaxed into their breath hold, which necessitates them breathing their tumors past the region of interest prior to breath hold initiation (Appendix Video 1). This observation is not well-described in the current literature. This may confuse patients using visual feedback displays who are attempting to move their tumors into the region of interest. This observation is supported by the decreased duty cycle for patients treated after to installation of the visual feedback display. However, this association needs to be analyzed with a broader scope, as some patients chose not to fully utilize the visual feedback display and majority of patients in our cohort treated after visual feedback display installation were being treated due to complex motion management as opposed to OAR proximity. In the depicted patient in the Appendix Video 1, duty cycle was improved from first fraction (52.8%) to final fraction (61.3%).

There have been several published series utilizing MRgRT for thoracic tumors. One group evaluated "treatment process time efficiency" across multiple disease sites, calculated in a similar fashion to duty cycle in the present study, though the time for gantry rotation and MLC motion were not included. Two-hundred and sixty-eight fractions were treated with deep inspiration breath hold with a 42.4%treatment process time efficiency (8). Adjusting our calculations to exclude gantry rotation and MLC motion yields a similar value, with a 41.3% average duty cycle for all fractions, 37.0% average duty cycle for fraction 1 and 45.6% final fraction average duty cycle. Another study examined 15 patients treated with 87 fractions to lung, adrenal, and pancreatic tumors, and evaluated "duty cycle efficiency", defined as the total number of "beam-on" frames divided by the total number of MR cine frames acquired during treatment delivery (9). The mean duty cycle efficiency for lung tumors was 68.7%, which was significantly higher than our calculated duty cycle. We believe this is primarily due to differences in threshold region of interest (ROI), which is the maximum percentage of the target that can be out of the tracking volume without stopping radiation delivery. The threshold-ROI in the study varied from 10% - 20% for the patients with lung tumors, whereas all of the patients treated within our study utilized a threshold-ROI<8%, with majority utilizing 5%. The tighter threshold increases the difficulty of precisely breathing the tumor into the ROI, likely resulting in the decreased mean duty cycle comparatively seen in our study. Another study of 14 patients with 15 lung tumors treated with MRgRT reported a 53% median treatment duty cycle, though the duty cycle calculation method was not reported (10). Other studies in the thoracic MRgRT space evaluated general feasibility and potential benefits of adaptation (11), peripheral tumor motion in breath-hold vs. free breathing (12), safety and feasibility of single fraction SBRT with MRgRT (13), and MRI-based lung tumor motion. The aforementioned studies focus on evaluating overall tumor size and its effect on motion, validating tumor motion models, reproducibility, and surrogate and fiducial based tracking (14–20).

Several studies have been published on using MRgRT for higher risk treatment of intrathoracic tumors (21, 22). One study evaluated 50 patients receiving MRgRT for high risk tumors defined as centrally located, previous thoracic radiotherapy, or interstitial lung disease (21). Ablative radiation (BED ≥ 100) was delivered to over 90% of tumors and 12 month local control was 95.6%, with only 8% grade 3 toxicity and no grade 4 or 5 toxicities. Another study of 47 patients with central (n=21) or ultra-central (n=26) tumors were treated with MRgRT to a median dose of 60 Gy in 8 fractions. Reported 1 year local control was 87% with only 2 late grade 3 toxicities (4.3%) and no grade 4 or 5 toxicities in this high risk patient population (22). The therapeutic index described in these studies favorably compares to the recent Nordic HILUS study of CT-based radiation for central lung tumors, where 30% of patients experienced grade 3–5 toxicity with a treatment related death rate of 15% (4). Notably, the HILUS trial did not utilize breath-hold MRgRT and thus treatment volumes were inherently larger and without real-time tumor tracking. Additionally, lobar bronchi and great vessels were not contoured as avoidance OARs, walls of luminal OARs were not included, and hotspots in radiotherapy plans were 150%, which may have contributed to excessive radiation dose to critical OARs and observed toxicity rates (23). Future phase II studies should be conducted to prospectively validate MRgRT for high risk intrathoracic tumors.

Some limitations of our work should be discussed. First, we report 30% of fractions were adapted, but the decision to adapt was at the treating physician's discretion. This is in contrast to some series where all plans were adapted. Generally, plans may not have been adapted despite small differences in coverage or OAR dose that may have minimally exceeded pre-specified planning goals if not deemed clinically significant by the treating physician. Additionally, it is unclear how the addition of visual aid may have truly influenced duty cycle, requiring a more detailed data analysis outside the scope of this paper. Lastly, this report covers only the technical treatment data of our patient cohort; clinical outcomes such as tumor control and toxicity have not been collected.

5 Conclusions

MRgRT was utilized to treat 27 patients over 169 fractions for various intrathoracic tumors. There was a significant improvement in treatment duty cycle between the first and final fraction possibly due to continued patient education and familiarity with treatment. MRgRT is a feasible modality to treat intrathoracic tumors though future work should be conducted to further optimize duty cycle and thus improve treatment efficiency.

Data availability statement

The raw data supporting the conclusions of this article will be made available by the authors, without undue reservation.

Ethics statement

The studies involving humans were approved by Institutional Review Board (IRB). The studies were conducted in accordance with the local legislation and institutional requirements. Written informed consent for participation was not required from the participants or the participants' legal guardians/next of kin in accordance with the national legislation and institutional requirements.

Author contributions

JM: Conceptualization, Data curation, Formal analysis, Investigation, Methodology, Project administration, Resources, Software, Supervision, Validation, Visualization, Writing – original draft, Writing – review & editing. NP: Conceptualization, Data curation, Formal analysis, Investigation, Methodology, Software, Writing – original draft, Writing – review & editing, Supervision. AS: Data curation, Formal analysis, Investigation, Resources, Validation, Writing – review & editing. MY: Data curation, Formal analysis, Writing – review & editing. SM: Data curation, Formal analysis, Writing – review & editing. MF: Data curation, Formal analysis, Writing – review & editing. KS: Data curation, Formal analysis, Writing – review & editing. AD: Data curation, Formal analysis, Writing – review & editing. JK: Data curation, Formal analysis, Writing – review & editing. AB: Data curation, Formal analysis, Writing – review & editing. LT: Data curation, Formal Analysis, Writing – review & editing. MM: Conceptualization, Data curation, Formal analysis, Methodology, Project administration, Writing – review & editing.

Funding

The author(s) declare that no financial support was received for the research, authorship, and/or publication of this article.

Conflict of interest

The authors declare that the research was conducted in the absence of any commercial or financial relationships that could be construed as a potential conflict of interest.

Publisher's note

Supplementary material

The Supplementary Material for this article can be found online at: https://www.frontiersin.org/articles/10.3389/fonc.2024.1401703/full#supplementary-material

APPENDIX VIDEO 1

74-year-old former heavy smoker with a cT1bN0 NSCLC of the right lower lung. He received 50Gy in 5 fractions utilizing MRgRT due to motion management as GTV respiratory motion was 1.3cm. When he relaxes into his breath hold, the tumor drifts superiorly and sometimes out of the gating boundary. He was educated to breathe his tumor past the ROI for subsequent treatments. His duty cycle improved from first fraction (52.8%) to final fraction (61.3%).

References

1. American Cancer Society. Key Statistics for Lung Cancer . Available online at: https://www.cancer.org/cancer/lung-cancer/about/key-statistics.html (Accessed 12/27/2022).

2. Ripley RT, Rusch VW. 52 - Lung Metastases. In: Niederhuber JE, Armitage JO, Doroshow JH, Kastan MB, Tepper JE, editors. *Abeloff's Clinical Oncology (Fifth Edition)*. Philadelphia, PA: Churchill Livingstone (2014). p. 764–777.e4.

3. Thomas DH, Santhanam A, Kishan AU, Cao M, Lamb J, Min Y, et al. Initial clinical observations of intra- and interfractional motion variation in MR-guided lung SBRT. *Br J Radiol*. (2018) 91:20170522. doi: 10.1259/bjr.20170522

4. Lindberg K, Grozman V, Karlsson K, Lindberg S, Lax I, Wersäll P, et al. The HILUS-trial—a prospective nordic multicenter phase 2 study of ultracentral lung tumors treated with stereotactic body radiotherapy. *J Thorac Oncol*. (2021) 16:1200–10. doi: 10.1016/j.jtho.2021.03.019

5. Crockett CB, Samson P, Chuter R, Dubec M, Faivre-Finn C, Green OL, et al. Initial clinical experience of MR-guided radiotherapy for non-small cell lung cancer. *Front Oncol*. (2021) 11:617681. doi: 10.3389/fonc.2021.617681

6. Lindberg S, Grozman V, Karlsson K, Onjukka E, Lindbäck E, Jirf KA, et al. Expanded HILUS trial: A pooled analysis of risk factors for toxicity from stereotactic body radiation therapy of central and ultracentral lung tumors. *Int J Radiat Oncol Biol Phys*. (2023) 117:1222–31. doi: 10.1016/j.ijrobp.2023.06.246

7. Kissick MW, Mackie TR. Task Group 76 Report on 'The management of respiratory motion in radiation oncology' [Med. Phys. 33, 3874–3900 (2006)]. *Med Phys*. (2009) 12:5721–2. doi: 10.1118/1.3260838

8. Placidi L, Cusumano D, Boldrini L, Votta C, Pollutri V, Antonelli MV, et al. Quantitative analysis of MRI-guided radiotherapy treatment process time for tumor real-time gating efficiency. *J Appl Clin Med Phys*. (2020) 21:70–9. doi: 10.1002/acm2.13030

9. van Sörnsen de Koste JR, Palacios MA, Bruynzeel AME, Slotman BJ, Senan S, Lagerwaard FJ. MR-guided gated stereotactic radiation therapy delivery for lung, adrenal, and pancreatic tumors: A geometric analysis. *Int J Radiat Oncol Biol Phys*. (2018) 102:858–66. doi: 10.1016/j.ijrobp.2018.05.048

10. De Costa AMA, Mittauer KE, Hill PM, Bassetti MF, Bayouth J, Baschnagel AM. Outcomes of real-time MRI-guided lung stereotactic body radiation therapy. *Int J Radiat Oncol Biol Phys*. (2018) 102:e679–80. doi: 10.1016/j.ijrobp.2018.07.1835

11. Padgett KR, Simpson GN, Llorente R, Samuels MA, Dogan N. Feasibility of adaptive MR-guided stereotactic body radiotherapy (SBRT) of lung tumors. *Cureus*. (2018) 10:e2423. doi: 10.7759/cureus.2423

12. Finazzi T, Palacios MA, Haasbeek CJA, Admiraal MA, Spoelstra FOB, Bruynzeel AME, et al. Stereotactic MR-guided adaptive radiation therapy for peripheral lung tumors. *Radiother Oncol*. (2020) 144:46–52. doi: 10.1016/j.radonc.2019.10.013

13. Finazzi T, van Sörnsen de Koste JR, Palacios MA, Spoelstra FOB, Slotman BJ, Haasbeek CJA, et al. Delivery of magnetic resonance-guided single-fraction stereotactic lung radiotherapy. *Phys Imaging Radiat Oncol*. (2020) 14:17–23. doi: 10.1016/j.phro.2020.05.002

14. Koch N, Liu HH, Starkschall G, Jacobson M, Forster K, Liao Z, et al. Evaluation of internal lung motion for respiratory-gated radiotherapy using MRI: Part I—correlating internal lung motion with skin fiducial motion. *Int J Radiat OncologyBiologyPhysics*. (2004) 60:1459–72. doi: 10.1016/j.ijrobp.2004.05.055

15. Plathow C, Fink C, Ley S, Puderbach M, Eichinger M, Zuna I, et al. Measurement of tumor diameter-dependent mobility of lung tumors by dynamic MRI. *Radiother Oncol*. (2004) 73:349–54. doi: 10.1016/j.radonc.2004.07.017

16. Blackall JM, Ahmad S, Miquel ME, McClelland JR, Landau DB, Hawkes DJ. MRI-based measurements of respiratory motion variability and assessment of imaging strategies for radiotherapy planning. *Phys Med Biol*. (2006) 51:4147. doi: 10.1088/0031–9155/51/17/003

17. Cai J, Read PW, Altes TA, Molloy JA, Brookeman JR, Sheng K. Evaluation of the reproducibility of lung motion probability distribution function (PDF) using dynamic MRI. *Phys Med Biol*. (2007) 52:365. doi: 10.1088/0031–9155/52/2/004

18. Cai J, Read PW, Larner JM, Jones DR, Benedict SH, Sheng K. Reproducibility of interfraction lung motion probability distribution function using dynamic MRI: statistical analysis. *Int J Radiat OncologyBiologyPhysics*. (2008) 72:1228–35. doi: 10.1016/j.ijrobp.2008.07.028

19. Cai J, McLawhorn R, Read PW, Larner JM, Yin F, Benedict SH, et al. Effects of breathing variation on gating window internal target volume in respiratory gated radiation therapya). *Med Phys*. (2010) 37:3927–34. doi: 10.1118/1.3457329

20. Seregni M, Paganelli C, Lee D, Greer PB, Baroni G, Keall PJ, et al. Motion prediction in MRI-guided radiotherapy based on interleaved orthogonal cine-MRI. *Phys Med Biol*. (2016) 61:872. doi: 10.1088/0031–9155/61/2/872

21. Finazzi T, Haasbeek CJA, Spoelstra FOB, Palacios MA, Admiraal MA, Bruynzeel AME, et al. Clinical outcomes of stereotactic MR-guided adaptive radiation therapy for high-risk lung tumors. *Int J Radiat Oncol Biol Phys*. (2020) 107:270–8. doi: 10.1016/j.ijrobp.2020.02.025

22. Sandoval ML, Sim AJ, Bryant JM, Bhandari M, Wuthrick EJ, Perez BA, et al. Magnetic resonance-guided stereotactic body radiation therapy/hypofractionated radiation therapy for metastatic and primary central and ultracentral lung lesions. *JTO Clin Res Rep*. (2023) 4:100488. doi: 10.1016/j.jtocrr.2023.100488

23. Rosenberg SA, Mak R, Kotecha R, Loo BW Jr., Senan S. The nordic-HILUS trial: ultracentral lung stereotactic ablative radiotherapy and a narrow therapeutic window. *J Thorac Oncol*. (2021) 16:e79–80. doi: 10.1016/j.jtho.2021.06.030

frontiers | Frontiers in Oncology

TYPE Case Report
PUBLISHED 11 July 2024
DOI 10.3389/fonc.2024.1357916

OPEN ACCESS

EDITED BY
Enis Ozyar,
Acıbadem University, Türkiye

REVIEWED BY
Nadia Saeed,
Brigham/Dana Farber Cancer Institute, United States
Philipp Hoegen,
Heidelberg University Hospital, Germany

*CORRESPONDENCE
Kathryn Elizabeth Mittauer
kathrynm@baptisthealth.net

RECEIVED 18 December 2023
ACCEPTED 20 June 2024
PUBLISHED 11 July 2024

CITATION
Yarlagadda S, Weiss Y, Chuong MD, Bassiri N, Gutierrez AN, Kotecha R, Mehta MP and Mittauer KE (2024) Case report: Intrafraction dose-guided tracking for gastrointestinal organ-at-risk isotoxicity delivery on an MR-guided radiotherapy system.
Front. Oncol. 14:1357916.
doi: 10.3389/fonc.2024.1357916

Case report: Intrafraction dose-guided tracking for gastrointestinal organ-at-risk isotoxicity delivery on an MR-guided radiotherapy system

Sreenija Yarlagadda[1], Yonatan Weiss[1], Michael David Chuong[1,2], Nema Bassiri[1,2], Alonso N. Gutierrez[1,2], Rupesh Kotecha[1,2], Minesh P. Mehta[1,2] and Kathryn Elizabeth Mittauer[1,2]*

[1]Department of Radiation Oncology, Miami Cancer Institute, Baptist Health South Florida, Miami, FL, United States, [2]Herbert Wertheim College of Medicine, Florida International University, Miami, FL, United States

In the current era of high-precision radiation therapy, real-time magnetic resonance (MR)-guided tracking of the tumor and organs at risk (OARs) is a novel approach that enables accurate and safe delivery of high-dose radiation. Organ tracking provides a general sense of the need for daily online adaptation but lacks precise information regarding exact dosimetry. To overcome this limitation, we developed the methodology for monitoring intrafraction motion with real-time MR-guided isodose line-based tracking of an OAR in combination with anatomic tumor-based tracking and reported the first case treated with this approach. An isolated para-aortic (PA) nodal recurrence from carcinosarcoma of the endometrium was treated with an ablative dose of 50 Gy in five fractions using MR-guided radiotherapy (MRgRT). This report demonstrates the feasibility, workflow, dosimetric constraints, and treatment paradigm for real-time isodose line-based OAR tracking and gating to enable an isotoxicity delivery approach. This innovative treatment strategy effectively tracked the intrafraction motion of both the target and OAR independently and enhanced the accuracy of structure localization in time and space with a more precise dosimetric evaluation.

KEYWORDS

MRgRT, dose-guided tracking, SBRT, ablative dose, GI OAR

Introduction

Radiation dose escalation has been highly effective in achieving high rates of durable local control for several tumors, which can further cause improved overall survival (1–3). However, the delivery of ablative doses is often compromised by the proximity of certain organs at risk (OARs), and this has been a major limiting factor, especially when

intrafraction organ motion adds a layer of dosimetric uncertainty, as is frequently observed in the thorax and abdomen. Given the lack of correlation between surface changes and internal organ position, location, and movement, patient surface anatomy cannot be used as a reliable surrogate for the internal motion of the thorax and upper abdominal organs (4).

Real-time tracking and automatic gating of radiation delivery is an effective solution to spare the OARs and mitigate treatment-related toxicity. This enables the safe delivery of ablative doses to the gastrointestinal (GI)/pelvic structures, which was previously impractical due to limited visualization and intrafraction motion. Magnetic resonance-guided radiation therapy (MRgRT) enables online adaptation to customize the radiation to the anatomy of the day, addressing both intra- and interfraction anatomic variation while providing excellent soft tissue visualization. The ability to continuously track in real time with MR imaging addresses the uncertainty associated with intrafraction motion (5), while eliminating the need for invasive procedures such as internal fiducials (required for x-ray-based real-time tracking) or electromagnetic transponders (6). It also eliminates the need to expand the true target to account for motion using the concept of an internal target volume (ITV) and thereby reduces the required setup margin, therefore exposing less normal tissue to unnecessary radiation doses (7).

In contrast to conventional radiation therapy, where homogeneous target coverage is the primary objective, isotoxic dose escalation increases the dose to the target volume until the pre-selected adjacent OAR dose constraint is reached. An isotoxic approach is generally applied when certain OARs are in proximity to the target volume, and these OARs are constrained to a lower dose level than the target volume. As such, this isotoxicity approach is characterized by heterogeneous target coverage, with a higher dose covering the core of the target [usually the gross tumor volume (GTV)] (8). Furthermore, this approach necessitates ensuring a rapid dose falloff of the ablative doses from the core to the periphery of the target, so as to further minimize OAR doses in close proximity. Because of the anatomically constrained dosimetric gradients between the OARs and target volumes in such cases, it is essential to ensure that the motion of the OAR-target geometry is minimized and/or accounted for in isotoxicity planning and delivery.

Liu et al. implemented a multitarget MLC-based motion tracking system for MRgRT that can simultaneously track two independently moving structures and gate the radiation beam in real time, compensating for motion (9). This approach can be used to track the tumor and adjacent dose-limiting OARs concurrently. Such an approach makes isotoxic dose escalation in real time feasible, thus broadening the therapeutic window. MRgRT provides continuous real-time cine MR imaging of the radiation field and is deployed utilizing a simple target margin, i.e., a boundary, for standard anatomic tracking and gating. The addition of isodose line-based tracking can further enhance the intrafraction motion accuracy beyond the use of simple anatomic margin expansion, as has been used historically in MRgRT.

This is the first report to describe the feasibility and workflow of this innovative approach to dose-guided tracking of GI OAR using MRgRT. Additionally, we report the institutional dose constraints for abdominal and pelvic targets to ablative doses (50 Gy in five fractions) and time analysis for the current workflow.

Case description

A 63-year-old woman was initially diagnosed with stage IB carcinosarcoma of the endometrium in September 2020. She was treated with robotic total laparoscopic hysterectomy with bilateral salpingo-oophorectomy and bilateral pelvic sentinel lymph node dissection, followed by high-dose-rate intracavitary brachytherapy to the upper vagina (21 Gy in three fractions of 7 Gy prescribed to 0.5 cm depth), and completed six cycles of adjuvant carboplatin/paclitaxel chemotherapy in February 2021. A follow-up positron emission tomography–computed tomography (PET-CT) scan in June 2022 revealed an oligometastatic disease in the left para-aortic (PA) node (1.1 cm), which has further enlarged to 1.3 cm by October 2022, with an increase in maximum standardized uptake value (SUV_{max}) from 5.75 to 10.9.

A multi-disciplinary discussion at our institutional gynecology tumor board recommended treating isolated nodal recurrence with ablative radiation therapy. Clinically, she reported intermittent rectal pain and sporadic rectal bleeding, with the last occurrence 1 month before. She was also diagnosed with co-existing acute inflammatory bowel disease (IBD), which raised the concern of severe acute GI toxicity if treated with conventional abdominal and pelvic radiation fields. Therefore, online adaptive stereotactic body radiation therapy (SBRT) was recommended at a dose of 50 Gy in five fractions on the MRIdian system (ViewRay, Cleveland, OH, USA). The MRIdian system combines a 0.35-T MR scanner with a 6-MV flattening filter-free Linac and a double-stacked, double-focused MLC offset by half a leaf width, enabling a leaf resolution of 4.15 mm at the isocenter (10). The patient was included in an institutional review board (IRB)-approved protocol.

Treatment description

Simulation and initial planning

The simulation was performed under mid-inspiration breath hold in the supine position with both arms at her sides to ensure patient comfort. The planning MR scan was acquired on the MRIdian at 50 × 50 × 35.8 cm^3 field of view (FOV) with a resolution of 1.5 × 1.5 × 3.0 mm^3. The planning MR scan acquired for simulation and also the scan at each fraction for adaptive re-planning were a balanced steady-state free precession (TrueFISP) sequence with a maximum distortion of <1.0 mm and <2.0 mm within 5 cm and 17.5 cm of the isocenter, respectively (11). Patient devices included a foam pad and wing board since continuous MR imaging is available for motion management.

Segmentation and treatment planning were performed on the MR simulation scan. The GTV was defined as the tumor visualized on the TrueFISP MR, and the clinical target volume (CTV) was delineated as GTV with a 2-mm isotropic margin, excluding

extension into the vertebral body posteriorly, and then uniformly expanded by a 3-mm margin to create the planning target volume (PTV), which was prescribed to 50 Gy (PTV_{50}). A simultaneous integrated boost (SIB) technique was used, and a second CTV prescribed to 30 Gy (CTV_{30}) was delineated by the PA chain as defined from the renal vessels (superiorly) to the aortic bifurcation (inferiorly), following the RTOG consensus (12). A 3-mm uniform setup margin expansion of the CTV_{30} was used to create the PTV_{30}. Relevant OARs segmented included the duodenum, small bowel, large bowel, stomach, kidneys, liver, spinal canal, and cauda equina. Figure 1 depicts the simulation anatomy and dose distribution on the TrueFISP MR scan.

Our planning technique, which has been previously described in the literature, utilized subdivision of the PTV_{50} to differential dosing based on a nonoverlapping region of the PTV_{50} with a GI planning OAR volume (PRV) (8). To this end, a GI PRV was created as an optimization structure to define the dose falloff between the proximal GI OARs and the target. The GI PRV was defined by a 3-mm isotopic expansion of the union of the stomach, duodenum, small bowel, and large bowel. Any overlapping portion of the GTV and PTV_{50} by the GI PRV was optimized to achieve 25–35 Gy. The non-overlapping portion of the GTV and PTV_{50} with the GI PRV was defined as GTV_{opt} and PTV_{50opt}, respectively, and optimized to achieve at least 50 Gy. Further details on the optimization and adaptive robustness of this planning technique have been previously reported (8).

A 15-field step-and-shoot intensity-modulated radiation therapy (IMRT) arrangement with 40 segments was created with a Monte Carlo dose calculation algorithm using a 2-mm isotropic dose grid size. A deformed CT approach was used to map the electron density. Manual edits were applied as needed to correct for GI luminal gas as air and/or tissue. Note that the CT scan was performed in mid-inspiration breath hold and acquired on the same day as the simulation MR scan.

A recent hardware and software upgrade to the MRIdian system was released for clinical use (A3i, 510K approval, December 2021) and included an updated user interface with an online adaptive parallel workflow and updated gating protocols that enable multi-planar tracking capabilities. Specifically, the MR multi-planar tracking capabilities now include anatomical tracking and/or dose-guided tracking for real-time gating. With these novel A3i features, we chose to implement "two planar" tracking for this patient: dose-guided tracking of the GI luminal OAR and anatomical tracking of the target in the sagittal and coronal planes, respectively. Owing to the patient's history of IBD and its close proximity TO the target volume, duodenum was the prioritized OAR in this case to minimize the risk of acute inflammatory flare-ups or late effects like ulceration, perforation, or fibrosis.

Online adaptation and isotoxicity planning

Our institutional online adaptive MRgRT workflow has been reported previously (1). Target volumes were rigidly registered, and OARs were deformably registered from the simulation MR to the daily volumetric MR scan. All OARs within 2 cm axially and 3 cm craniocaudally of the PTV were reviewed and manually edited by the radiation oncologist. Manual electron density edits were performed on the deformed CT to match the anatomy of the daily MR scan.

Following segmentation, a predicted plan was calculated using the original plan, generated using the simulated anatomy, and superimposed on the current anatomy and contours of the day to

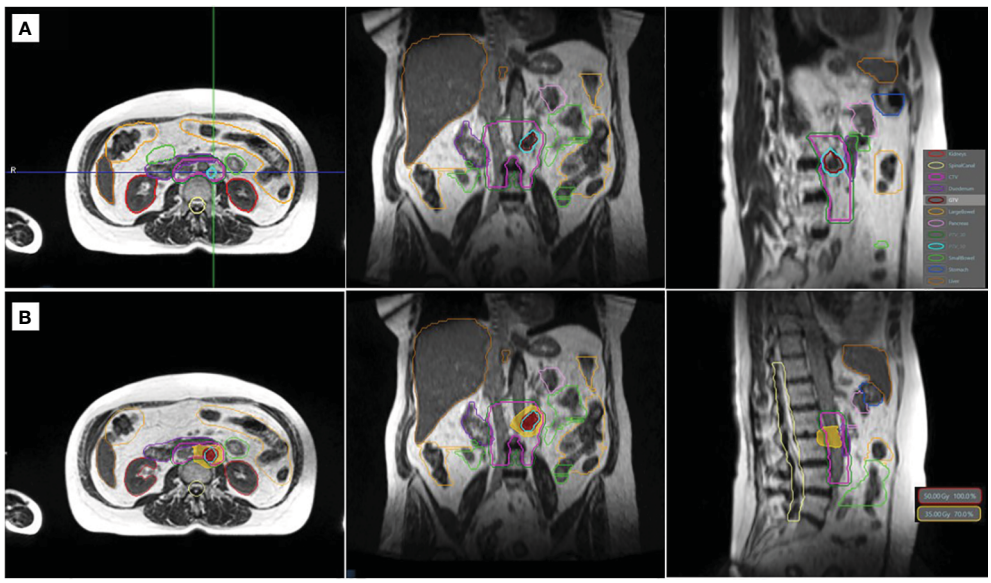

FIGURE 1
TrueFISP MR scan showing the simulation anatomy **(A)** and the dose distribution of the original plan **(B)**. Relevant organs at risk and targets are shown in outline **(A)**. The isodose lines of the prescription (50 Gy) and gastrointestinal organ-at-risk constraint (35 Gy) are shown in colorwash **(B)**.

evaluate the indication for adaptation. The predicted plan was considered sufficient if all OARs and target coverage metrics were achieved based on the individualized treatment planning directive. If the predicted plan failed for any metric (i.e., under-coverage of the target volume or overdose to any OAR), an adaptive plan was then generated to meet OAR constraints and/or improve target coverage. The first priority was to ensure that the OAR constraints were met, and target coverage was a secondary goal for isotoxic planning.

Gated treatment

Real-time tracking was performed on the coronal and sagittal planes. For this particular patient, a novel gating scheme of dose-guided tracking utilized the MRIdian A3i features. To this end, we chose to track the duodenum, the most proximal GI OAR, in the sagittal plane, since it seemed ideal to track the OAR with respect to the pre-specified border of the selected isodose line. Meanwhile, the coronal plane was used to track and ensure the target coverage.

Specifically for the sagittal plane tracking, a boundary was defined such that the gating threshold would be that no more than 5% of the duodenum overlapping within the 35-Gy isodose line. This technique was selected for this case since we utilized a dose escalation approach with isotoxicity normalization to the proximal GI luminal OAR, i.e., the duodenum. Figure 2 demonstrates the intrafraction gating with respiration tracked in the sagittal plane with an earlier overlap between the 35-Gy isodose line and the duodenum (A), and a later separation is observed when the patient is in an adequate breath hold (B).

Additionally, we tracked the gross target on the coronal plane through a tracking structure that approximated the GTV. The target tracking region of interest (ROI) was contoured daily based on the contrast differences of the daily MR to enable the highest accuracy for the deformable image registration algorithm during cine imaging. The sagittal target tracking ROI had a 3-mm boundary margin such that when the deformed tracking ROI moved outside the boundary more than 5%, the beam would automatically be withheld.

The cine image acquisition was selected as a cartesian sequence at a nominal 4 frames per second (FPS). Note that the cine-temporal resolution is dependent on the FOV. For this case, the achieved frame rate was 3 FPS after FOV adjustments. An FOV of 27.5 × 42 × 0.70 cm and a spatial resolution of 0.35 × 0.35 cm were used, which enabled a frame rate of at least 3 FPS during treatment for each respective plane. Cine imaging was acquired in repeated sequential order between sagittal and coronal orientations. The treatment delivery was a step-and-shoot IMRT, and as such, continuous MR cine imaging occurred for each gantry treatment position. Note that in this isotoxic gating approach, the treatment beam is automatically gated on/off based on the tumor position and duodenum position relative to the high dose gradient. No real-time intra-fraction adaptation was performed based on the duodenum position during treatment delivery. Online adaptation was only performed once per fraction based on the daily volumetric MR scan prior to delivery. Figure 3 demonstrates the timeline for this patient for each fraction. The median total in-room time was 58 min [range (R): 46–76 min] with the longest on fraction 1 and the shortest on fraction 5. The multi-planar tracking and the breath hold did not substantially increase the treatment time compared to prior literature, with the observed median duration of radiation delivery being 15 min (R: 13–20 min).

Follow-up

She completed the planned treatment course, with Common Terminology Criteria for Adverse Events (CTCAE) grade 1 nausea being the only acute toxicity. The follow-up PET-CT 3 at months and 6 months post-treatment confirmed complete metabolic and anatomic resolution of the node. With a follow-up at 12 months post-radiation, the patient had durable local control of the treated

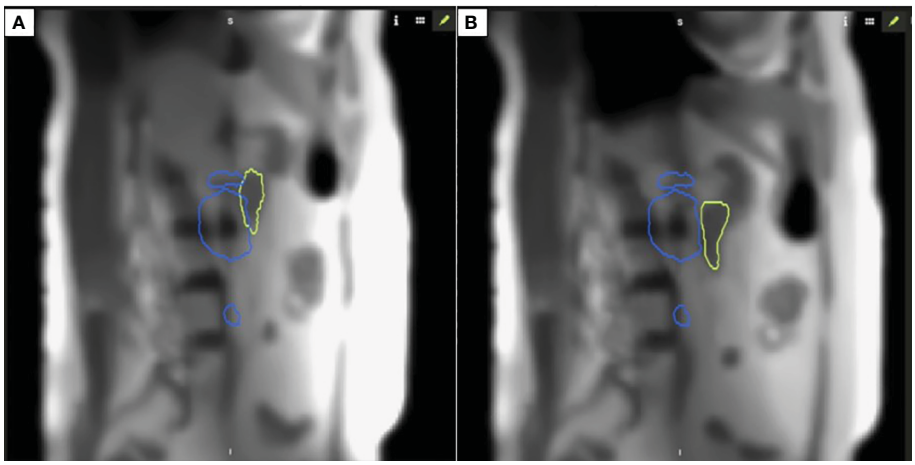

FIGURE 2
Intrafraction motion with respiration **(A)** demonstrates an overlap between 35 Gy isodose line and duodenum; **(B)** demonstrates separation between the organ-at-risk and respective constraint isodose line when patient is in appropriate breath hold for isotoxic delivery.

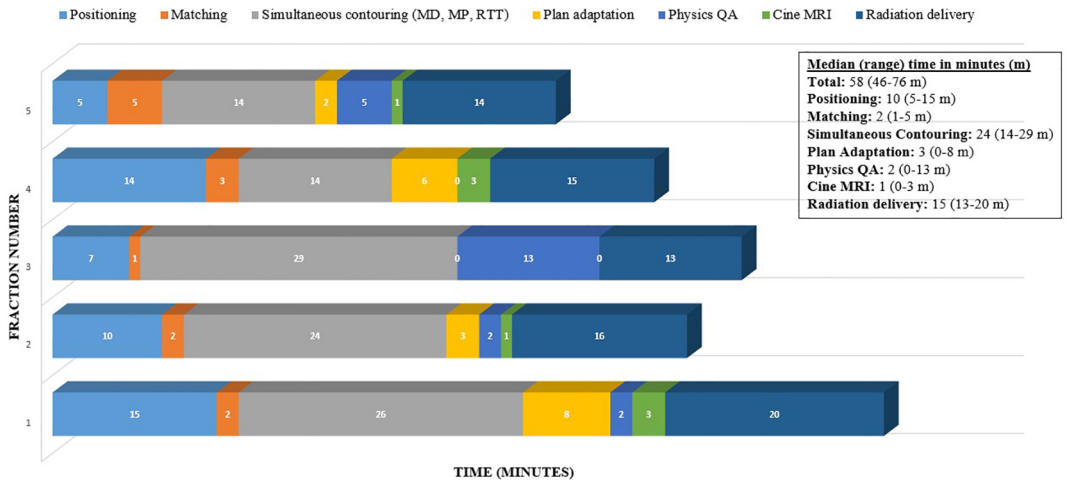

FIGURE 3
Time (minutes) taken through the workflow for online adaptive MRgRT for this patient case example (5 fractions).

lesion and the entire PA chain. She has not developed any further late GI toxicity but had one out-of-field failure (left external iliac lymph node). This was also treated with SBRT using MRIdian; however, owing to its quite posterior position and the absence of any abutting GI OAR with respiratory-induced motion, no GI OAR management was needed during cine tracking, and only multi-planar anatomical tumor tracking was used. She continues to have no late toxicity and no evidence of disease on the latest scans in November 2023.

Discussion

Although multi-object tracking has been technically described, to our knowledge, this is the first report that describes the clinical workflow, successful implementation, and treatment timeline of an isotoxicity approach with dose-guided tracking of a GI OAR (9, 13). With the MRIdian A3i 510K approved for clinical use, several features now facilitate modern SBRT, including multi-planar tracking (up to three planes simultaneously at 4 FPS), dose-guided and anatomical tracking capabilities, and a parallel adaptive workflow that significantly reduces the on-table treatment times. This novel technology was applied to this patient's case, in which a high-risk OAR was in close proximity to the target in a patient who had a higher predisposition for GI toxicity due to active IBD. The challenge of delivering an ablative dose in this case was that the intrafraction motion of the GI luminal OAR was not synchronous with the target motion. This approach was deemed successful because the patient did not have any significant GI toxicity (only grade 1 nausea), despite being at higher risk and she had complete resolution of the tumor after treatment.

Radiotherapy in the setting of IBD may be at increased risk of severe toxicity, with estimates upwards of 40%–50% in some series (14). In this cohort, 21% of patients required cessation of treatment due to toxicity, which, in the context of curative intent therapy, may result in suboptimal overall survival. There are other cohorts, including a systematic review, suggesting lower rates of toxicity, similar to the baseline risk following pelvic radiation, and some showed a similar risk of toxicity in the setting of IMRT vs. 3D-CRT techniques (15, 16). There is a paucity of data reporting dose constraints for the SBRT technique in the setting of IBD, and for consistency within our institution, similar OAR constraints were used as compared to other indications for adaptive abdominal radiotherapy.

As previously detailed, real-time tracking was performed for the target on the coronal plane and the duodenum, with dose-guided

TABLE 1 Institutional target coverage and dose constraints for abdominal targets to ablative dose schedule (50 Gy in five fractions).

Target coverage		
Target	**Parameter**	**Constraint**
GTV	$D_{99\%}$	≥50 Gy
PTV_{50} (GTV + 3 mm margin)	$D_{95\%}$	≥50 Gy
CTV_{30}	$D_{99\%}$	≥30 Gy
PTV_{30} (CTV + 3 mm margin)	$D_{95\%}$	≥30 Gy
OAR constraints		
Organ at risk	**Parameter**	**Constraint**
Duodenum	$D_{0.5cc}$	≤35 Gy
	$D_{0.03cc}$	≤38 Gy
Small bowel	$D_{0.5}$	≤35 Gy
	$D_{0.03}$	≤38 Gy
Large bowel	$D_{0.5}$	≤38 Gy
	$D_{0.03}$	≤40 Gy

(Continued)

10.3389/fonc.2024.1357916

TABLE 1 Continued

Target coverage		
Target	Parameter	Constraint
Organ at risk	Parameter	Constraint
Stomach	$D_{0.5}$	≤35 Gy
	$D_{0.03}$	≤38 Gy
Spinal canal	$D_{0.03}$	≤20 Gy
Kidneys	D_{mean}	≤10 Gy
Liver	D_{mean}	≤13 Gy
	$V_{21\ Gy}$	≤700 cc
Cauda equina	$D_{0.03}$	≤20 Gy

tracking on the sagittal plane. The institutional target coverage and dose constraints for abdominal targets at ablative doses (50 Gy in five fractions) are presented in Table 1. A prophylactic dose of 30 Gy was selected in line with the SPARTACUS protocol for elective lymph node coverage (17). With the duodenum adjacent to the target in this case and considering its independent intrafraction motion with respiration, an isotoxicity approach was implemented with the 35-Gy isodose line selected for the dose-guided tracking.

An in-room patient monitor was installed to guide patients regarding the adequacy of their breath hold (Figure 4). The monitor displays the real-time motion of the target volume on the right and the OAR on the left. Note that the user has the option to display all planes, a subset of planes, or none. A smiling emoji is displayed on the monitor as real-time feedback to the patient when the breath hold is adequate, and all gating parameters are satisfied.

In our case, we chose gating settings that required both planes to be satisfied for beam-on delivery. As the target and OAR motion are independent of each other with respiration, at times there can be good target coverage but not a separation with the OAR, and *vice versa*. This non-synchronous motion is also demonstrated in Figure 4, emphasizing the need for independent, simultaneous tracking of the target and OAR. The treatment beam is automatically gated off at such moments and delivered only when the target is inside and the OAR is outside of the defined boundary.

An increase in the gating events is generally expected, but note that in this case, the target was relatively static, improving the treatment delivery duty cycle. The in-room monitor that provides the visual position of the tumor in real time and feedback to the patient greatly enhanced the adequacy of the breath hold. Moreover, the patients felt actively involved in the treatment process, resulting in improved patient satisfaction, which might have compensated for the treatment time.

AAPM TG 76 recommends the use of appropriate respiratory motion management whenever the motion is >5 mm (18). In clinical practice, image-guided tracking and motion management are restricted to the target, while the OAR is considered secondary;

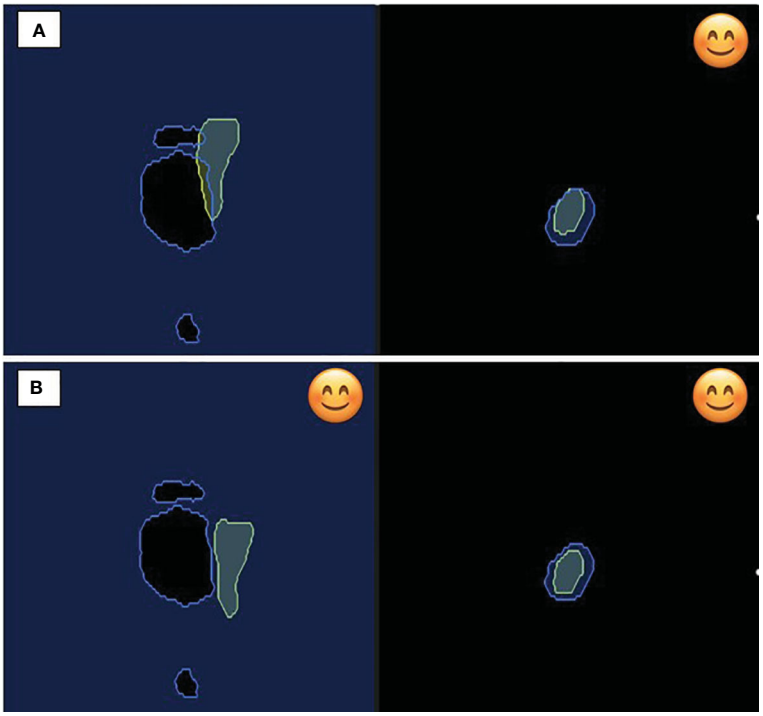

FIGURE 4
In-room patient monitor demonstrating on the left **(A)** free breathing with overlap between 35 Gy isodose constraint and duodenum; **(B)** breath hold demonstrating appropriate geometry for isotoxic delivery. On the right, figure displays the static target volume demonstrating favorable positioning during both respiration and breath hold. The smile emoji is the feedback to the patient during delivery that the patient is in the correct breath hold position for treatment delivery. Note both the organ-at-risk (left) and the target volume (right) have to be in the correct position for the beam to gate on.

there is no ideal solution to track two ROIs simultaneously in real time. However, SBRT for ablative doses relies on geometric accuracy even when the OAR and target are observed to have independent motion. The technique of multitarget tracking was demonstrated by Liu et al. to simultaneously track targets such as multiple primary lung tumors, prostate, and pelvic lymph nodes (9).

We have adapted this technique to track a target and the adjacent OAR, which have independent respiratory motion to enhance the accuracy of treatment delivery. Conventionally, abdominal and thoracic sites are treated using ITV and PRV, which can lead to inferior target coverage and/or a higher dose to the OAR. While our technique used a GI PRV to define the gradient of the ablative dose of 50 Gy, we performed plan normalization based on the isotoxicity to the nominal GI OAR wall rather than the GI PRV. Without adaptive planning and/or dose-guided tracking, performing isotoxicity to the GI PRV is recommended over the GI OAR wall. Therefore, our approach would rather allow tighter margins for both target and OAR without compromising on target coverage or OAR constraints. The median treatment time of 15 min was equivalent to other MRIdian A3i deliveries of tumor tracking only (19). MRIdian A3i parallel workflow efficiency gains of 30% reduction in online adaptive replanning times have been previously reported (19). The workflow presented here can be adopted for the definitive treatment of any thoracic, abdominal, or pelvic target with dose-limiting OAR in close proximity to ablative doses with an isotoxicity approach.

Beyond this case report, we have implemented dose-guided tracking for all MRgRT patients who have asynchronous motion between the proximal OAR and the tumor. In practice, we have found that the majority of applicable clinical sites are pelvic nodes, in which the target remains static with respiratory motion but the surrounding GI OARs have respiratory-induced motion. Criteria for the section are performed at the time of MRgRT simulation, upon which the geometry of the OAR and target motion is assessed in both the sagittal and coronal cine MR planes. Our future aim is to assess the toxicity profile of patients treated with tumor-based track alone versus dual tumor and isodose-based OAR tracking to quantify the potential reduced toxicity of this method.

Conclusion

Dose-guided tracking of a GI OAR for isotoxicity delivery is feasible on the MRIdian system for SBRT delivery of a target with an adjacent OAR having non-synchronous respiratory motion to ablative doses. This approach takes advantage of the soft tissue visualization of MR and the real-time multi-planar tracking capabilities of an MR Linac and aids in reducing toxicity while maintaining target coverage.

Data availability statement

The datasets presented in this article are not readily available because this is a case report. Requests to access the datasets should be directed to the corresponding author.

Ethics statement

This research was conducted as part of an institutional review board (IRB)-approved retrospective chart review of MR-guided radiotherapy that does not require prospective informed consent. There were no potentially identifiable images or data included in the article.

Author contributions

SY: Conceptualization, Data curation, Formal analysis, Investigation, Methodology, Writing – original draft, Writing – review & editing. YW: Conceptualization, Investigation, Methodology, Supervision, Writing – review & editing. MC: Investigation, Methodology, Supervision, Validation, Writing – review & editing. NB: Conceptualization, Supervision, Validation, Writing – review & editing. AG: Conceptualization, Supervision, Writing – review & editing. RK: Writing – review & editing. MM: Supervision, Writing – review & editing. KM: Conceptualization, Data curation, Formal analysis, Investigation, Methodology, Software, Supervision, Validation, Writing – original draft, Writing – review & editing.

Funding

The author(s) declare that no financial support was received for the research, authorship, and/or publication of this article.

Conflict of interest

NB: grants from ViewRay Inc. MC: Honoraria from ViewRay, Sirtex, IBA, and institutional research funding from ViewRay, Novocure, and StratPharma. AG: Honoraria from ViewRay, Inc., Elekta AB, IBA AB. Ownership interest of Atlantic Health Solutions uPlanÔ. RK: Honoraria from Accuray Inc., Elekta AB, ViewRay Inc., Novocure Inc., Elsevier Inc., Brainlab, Kazia Therapeutics, Castle Biosciences, and institutional research funding from Medtronic Inc., Blue Earth Diagnostics Ltd., Novocure Inc., GT Medical Technologies, AstraZeneca, Exelixis, ViewRay Inc., Brainlab, Cantex Pharmaceuticals, and Kazia Therapeutics. MM: Consulting Fees from Karyopharm, KAzia Therapeutics, Sapience, Zap, Mevion, Xoft; BOD Oncoceutics; Stock in Chimerix. KM: reports ownership interest in a company that provides consulting services on image guided radiation therapy technology MR Guidance, LLC.. She received travel reimbursement/consulting fees/speaking fees/grants from ViewRay Inc.

The remaining authors declare that the research was conducted in the absence of any commercial or financial relationships that could be construed as a potential conflict of interest.

The author(s) declared that they were an editorial board member of Frontiers, at the time of submission. This had no impact on the peer review process and the final decision.

Publisher's note

References

1. Chuong MD, Bryant J, Mittauer KE, Hall M, Kotecha R, Alvarez D, et al. Ablative 5-fraction stereotactic magnetic resonance–guided radiation therapy with on-xxx adaptive replanning and elective nodal irradiation for inoperable pancreas cancer. *Pract Radiat Oncol*. (2021) 11:134–47. doi: 10.1016/j.prro.2020.09.005

2. Spratt DE, Pei X, Yamada J, Kollmeier MA, Cox B, Zelefsky MJ. Long-term survival and toxicity in patients treated with high-dose intensity modulated radiation therapy for localized prostate cancer. *Int J Radiat Oncol Biol Phys*. (2013) 85:686–92. doi: 10.1016/j.ijrobp.2012.05.023

3. Gerard J-P, Barbet N, Schiappa R, Magné N, Martel I, Mineur L, et al. Neoadjuvant chemoradiotherapy with radiation dose escalation with contact x-ray brachytherapy boost or external beam radiotherapy boost for organ preservation in early cT2–cT3 rectal adenocarcinoma (OPERA): a phase 3, randomised controlled trial. *Lancet Gastroenterol Hepatol*. (2023) 8:356–67. doi: 10.1016/S2468-1253(22)00392-2

4. Dhont J, Harden SV, Chee LYS, Aitken K, Hanna GG, Bertholet J. Image-guided radiotherapy to manage respiratory motion: lung and liver. *Clin Oncol*. (2020) 32:792–804. doi: 10.1016/j.clon.2020.09.008

5. Chuong MD, Bryant JM, Herrera R, McCulloch J, Contreras J, Kotecha R, et al. Dose-escalated magnetic resonance image–guided abdominopelvic reirradiation with continuous intrafraction visualization, soft tissue tracking, and automatic beam gating. *Adv Radiat Oncol*. (2022) 7(2):100840. doi: 10.1016/j.adro.2021.100840

6. Bohoudi O, Bruynzeel AME, Senan S, Cuijpers JP, Slotman BJ, Lagerwaard FJ, et al. Fast and robust online adaptive planning in stereotactic MR-guided adaptive radiation therapy (SMART) for pancreatic cancer. *Radiother Oncol J Eur Soc Ther Radiol Oncol*. (2017) 125:439–44. doi: 10.1016/j.radonc.2017.07.028

7. Mittauer K, Paliwal B, Hill P, Bayouth JE, Geurts MW, Baschnagel AM, et al. A new era of image guidance with magnetic resonance-guided radiation therapy for abdominal and thoracic Malignancies. *Cureus*. (2018) 10:4. doi: 10.7759/cureus.2422

8. Mittauer KE, Yarlagadda S, Bryant JM, Bassiri N, Romaguera T, Gomez AG, et al. Online adaptive radiotherapy: Assessment of planning technique and its impact on longitudinal plan quality robustness in pancreatic cancer. *Radiother Oncol J Eur Soc Ther Radiol Oncol*. (2023) 188:109869. doi: 10.1016/j.radonc.2023.109869

9. Liu PZY, Dong B, Nguyen DT, Ge Y, Hewson EA, Waddington DEJ, et al. First experimental investigation of simultaneously tracking two independently moving targets on an MRI-linac using real-time MRI and MLC tracking. *Med Phys*. (2020) 47:6440–9. doi: 10.1002/mp.14536

10. Mittauer KE, Yadav P, Paliwal B, Bayouth JE. Characterization of positional accuracy of a double-focused and double-stack multileaf collimator on an MR-guided radiotherapy (MRgRT) Linac using an IC-profiler array. *Med Phys*. (2020) 47:317–30. doi: 10.1002/mp.13902

11. Ginn JS, Agazaryan N, Cao M, Baharom U, Low DA, Yang Y, et al. Characterization of spatial distortion in a 0.35 T MRI-guided radiotherapy system. *Phys Med Biol*. (2017) 62:4525. doi: 10.1088/1361-6560/aa6e1a

12. Small W, Mell LK, Anderson P, Creutzberg C, De Los Santos J, Gaffney D, et al. Consensus guidelines for delineation of clinical target volume for intensity-modulated pelvic radiotherapy in postoperative treatment of endometrial and cervical cancer. *Int J Radiat Oncol Biol Phys*. (2008) 71:428–34. doi: 10.1016/j.ijrobp.2007.09.042

13. Dhont J, Vandemeulebroucke J, Cusumano D, Boldrini L, Cellini F, Valentini V, et al. Multi-object tracking in MRI-guided radiotherapy using the tracking-learning-detection framework. *Radiother Oncol*. (2019) 138:25–9. doi: 10.1016/j.radonc.2019.05.008

14. Willett CG, Ooi CJ, Zietman AL, Menon V, Goldberg S, Sands BE, et al. Acute and late toxicity of patients with inflammatory bowel disease undergoing irradiation for abdominal and pelvic neoplasms. *Int J Radiat Oncol Biol Phys*. (2000) 46:995–8. doi: 10.1016/S0360-3016(99)00374-0

15. Trotta M, Patel KR, Singh S, Verma V, Ryckman J. Safety of radiation therapy in patients with prostate cancer and inflammatory bowel disease: A systematic review. *Pract Radiat Oncol*. (2023) 13:454–65. doi: 10.1016/j.prro.2023.04.006

16. White EC, Murphy JD, Chang DT, Koong AC. Low toxicity in inflammatory bowel disease patients treated with abdominal and pelvic radiation therapy. *Am J Clin Oncol*. (2015) 38:564–9. doi: 10.1097/COC.0000000000000010

17. Leung E, Gladwish AP, Davidson M, Taggar A, Velker V, Barnes E, et al. Quality-of-life outcomes and toxic effects among patients with cancers of the uterus treated with stereotactic pelvic adjuvant radiation therapy: the SPARTACUS phase 1/2 nonrandomized controlled trial. *JAMA Oncol*. (2022) 8:1–9. doi: 10.1001/jamaoncol.2022.0362

18. Keall PJ, Mageras GS, Balter JM, Emery RS, Forster KM, Jiang SB, et al. The management of respiratory motion in radiation oncology report of AAPM Task Group 76. *Med Phys*. (2006) 33:3874–900. doi: 10.1118/1.2349696

19. Votta C, Iacovone S, Turco G, Carrozzo V, Vagni M, Scalia A, et al. Evaluation of clinical parallel workflow in online adaptive MR-guided Radiotherapy: A detailed assessment of treatment session times. *Tech Innov Patient Support Radiat Oncol*. (2024) 29:100239. doi: 10.1016/j.tipsro.2024.100239

frontiers | Frontiers in Oncology

TYPE Case Report
PUBLISHED 16 September 2024
DOI 10.3389/fonc.2024.1411474

OPEN ACCESS

EDITED BY
Enis Ozyar,
Acıbadem University, Türkiye

REVIEWED BY
Nadia Saeed,
Brigham/Dana Farber Cancer Institute, United States
Lijun Zeng,
Sichuan University, China

*CORRESPONDENCE
Jinzhong Yang
jyang4@mdanderson.org

†These authors share first authorship

‡These authors share senior authorship

RECEIVED 03 April 2024
ACCEPTED 11 June 2024
PUBLISHED 16 September 2024

CITATION
Chen X, Weng JK, Sobremonte A, Lee BM, Hughes NW, Mohammedsaid M, Zhao Y, Wang X, Zhang X, Niedzielski JS, Shete SS, Court LE, Liao Z, Lee PP and Yang J (2024) Case report: Cardiac neuroendocrine carcinoma and squamous cell carcinoma treated with MR-guided adaptive stereotactic radiation therapy.
Front. Oncol. 14:1411474.
doi: 10.3389/fonc.2024.1411474

Case report: Cardiac neuroendocrine carcinoma and squamous cell carcinoma treated with MR-guided adaptive stereotactic radiation therapy

Xinru Chen[1,2†], Julius K. Weng[3†], Angela Sobremonte[4], Belinda M. Lee[4], Neil W. Hughes[4], Mustefa Mohammedsaid[4], Yao Zhao[1], Xiaochun Wang[1,2], Xiaodong Zhang[1,2], Joshua S. Niedzielski[1,2], Sanjay S. Shete[2,5], Laurence E. Court[1,2], Zhongxing Liao[3], Percy P. Lee[6‡] and Jinzhong Yang[1,2*‡]

[1]Department of Radiation Physics, The University of Texas MD Anderson Cancer Center, Houston, TX, United States, [2]The University of Texas MD Anderson Cancer Center UTHealth Houston Graduate School of Biomedical Sciences, Houston, TX, United States, [3]Department of Radiation Oncology, The University of Texas MD Anderson Cancer Center, Houston, TX, United States, [4]Department of Radiation Therapeutic Physics, The University of Texas MD Anderson Cancer Center, Houston, TX, United States, [5]Department of Biostatistics, The University of Texas MD Anderson Cancer Center, Houston, TX, United States, [6]Department of Radiation Oncology, City of Hope Orange County, Lennar Foundation Cancer Center, Irvine, CA, United States

We present two cases of cardiac metastases adjacent to the right ventricle in a 55-year-old male and a 61-year-old female, both treated with magnetic resonance (MR)-guided adaptive stereotactic radiation therapy (SBRT). The prescribed regimen was 30Gy delivered in 3 fractions using a 1.5 Tesla magnetic resonance linear accelerator (MR-linac). Patients exhibited favorable tolerance to the treatment, with no observed acute toxicity.

KEYWORDS

cardiac tumor, cardiac metastasis, MR-guided radiotherapy, SBRT, MR-Linac

1 Introduction

Cardiac tumors, though rare in incidence, present substantial challenges in both diagnostic and therapeutic treatment options. The incidence of primary cardiac tumors is reported to range from 0.002% to 0.3%, whereas secondary cardiac tumors, or cardiac metastases, exhibit a markedly higher frequency, being 22 to 132 times more common (1, 2). Although biopsy remains the gold standard for diagnosing cardiac tumors, the integration of multimodality imaging, encompassing transthoracic echocardiography, cardiovascular magnetic resonance (MR), cardiac computed tomography (CT), and positron emission

tomography (PET/CT), enables accurate diagnosis and treatment strategy formation, often obviating the need of invasive biopsy (3). Notably, primary lung cancer, breast cancer, and hematologic malignancies have elevated propensities for cardiac involvement (4). In contrast to the imperative for complete resection in many primary cardiac tumors, the management of cardiac metastasis is highly individualized and contingent upon the nature of the primary tumor (3). Surgical debulking is reserved for instances involving intracavitary metastases causing cardiac decompensation or solitary disease with a favorable prognosis. Nevertheless, the overall survival rate for patients with malignant cardiac tumors remains bleak. Historically, radiation therapy has served as a palliative treatment to alleviate symptoms and improve the quality of life for patients (5). In recent years, stereotactic body radiation therapy (SBRT) has emerged as an alternative definitive treatment method, particularly for patients that are inoperable, delivering higher and more definitive dose (6, 7). Moreover, the advent of MR-guided radiotherapy has significantly advanced treatment precision through superior soft-tissue/tumor visualization and the ability for daily plan adaptation. This report presents two cases of cardiac metastases treated at our institution on a high-field 1.5T MR-Linac using adaptive SBRT.

2 Methods and materials

This study was approved by the local Institutional Review Board (protocol # 2022-0521). Eligible patients with cardiac metastases were enrolled in the treatment protocol following a comprehensive discussion by a multi-disciplinary team, which considered the treatment history, the benefits and risks of potential interventions. A 4DCT simulation scan was conducted in the supine position, arms raised up, using a Wing Board and Vac-lock bag. This scan served to estimate the respiratory and cardiac motion, acquire electron density data, and delineate organs-at-risk (OARs). MR simulation was executed the same day of 4DCT simulation on a 1.5 Tesla Unity MR-linac system, using T2-weighted transverse scanning under free-breathing conditions. The internal gross target volume (iGTV) was contoured based on the T2-weighted scans to account for cardiac motion. To verify the contour integrity, contrast CT images were fused with the T2-weighted MR image. Semi-automatic tools were used to contour OARs on 4DCT scans, and both OAR contours and electron densities were subsequently transferred to the MR image. The synthetic CT generated from the MR image underwent subjective verification. The planning target volume (PTV) was generated through isotropic expansion of the iGTV with a margin based on the estimated respiratory motion. Demonstration of iGTV and PTV on MR and CT scans is shown in Figure 1. A reference plan, prescribing 30 Gy to 95% of the PTV, was created on the simulation T2-weighted image. Patients received treatment on consecutive days with free-breathing conditions. Daily adaptation of the reference plan employed the adapt-to-position (ATP) technique, where an isocenter shift is made on the reference plan based on rigid registration followed by plan re-optimization (8), given minor anatomical changes observed during the whole treatment course.

3 Case presentation

The first case is a 55-year-old male initially diagnosed with bulky stage II T2N0M0 laryngeal cancer in May 2018. The patient underwent chemoradiation treatment, receiving a total dose of 70Gy (2Gy per fraction) with concomitant cis-platinum. In 2020, he presented with left arm subcutaneous nodules and metastatic recurrence in the larynx. Subsequent biopsy of the subcutaneous nodules indicated poorly differentiated neuroendocrine carcinoma. Palliative radiation was then administered to multiple subdermal sites in 2020 in conjunction with chemo- and targeted therapy (carboplatin/etoposide/atezolizumab) and immunotherapy (Durvalumab) in 2021. By October 2021, the patient progressed with an intracardiac mass. A chest CT with contrast revealed an enlarging nodule in the right ventricle. Multi-sequence multiplanar cardiac MR imaging, acquired with and without intravenous contrast, identified a mass in the right ventricle lumen measuring 34 mm in greatest diameter. The patient claimed generalized pains in previously treated sites but no cardiovascular symptoms. Following consultation with the multi-disciplinary team, the patient was referred to the Department of Radiation Oncology for treatment with SBRT on MR-linac in November 2021. The iGTV is 12.45 cm^3 with the consideration of cardiac and respiratory motion. The PTV was created by expanding the iGTV by 5mm in all directions. The total dose of 30 Gy was prescribed in 3 fractions, targeting at least 95% of the PTV volume. Detailed patient and treatment characteristics are shown in Table 1. The dosimetric criteria are demonstrated in Table 2. Throughout the treatment course, the patient continued to take Xarelto 10mg orally once daily to prevent blood clots. The daily plan was re-optimized using ATP technique. The dose distribution and dose-volume histograms (DVH) of the third fraction are shown in Figure 2. After the SBRT treatment of the cardiac mass, the patient received chemotherapy (carboplatin/docetaxel) for subcutaneous metastases in January 2022. Three months post the SBRT treatment, the patient reported subdermal pains and moderate fatigue, with no chest pain and tightness. Four months post the treatment, a PET/CT scan suggested a reasonable response to SBRT for his cardiac metastasis. Follow-up cardiac MR with and without contrast, along with chest CT with contrast after 5 months, indicated a reduction in size of the cardiac mass, as shown in Figure 3. Another PET/CT scan acquired 7 months later suggested a stable response at the treatment site. However, he had further progression of existing pulmonary, intramuscular, and subcutaneous metastases.

The second case involved a 61-year-old female diagnosed with thymic squamous cell carcinoma of the anterior mediastinum in May 2020. In August 2020, the patient underwent chemoradiotherapy, receiving a total dose of 66 Gy (2.2 Gy per fraction), followed by immunotherapy. A subsequent PET/CT scan in the follow-up identified an anterior pericardial mass, further confirmed by echocardiogram and contrasted cardiac MR images in November 2021. Contrasted CT indicated the pericardial mass increased from 26 mm x 18 mm in November to 36 mm x 23 mm in December. Given the high risks associated with surgery

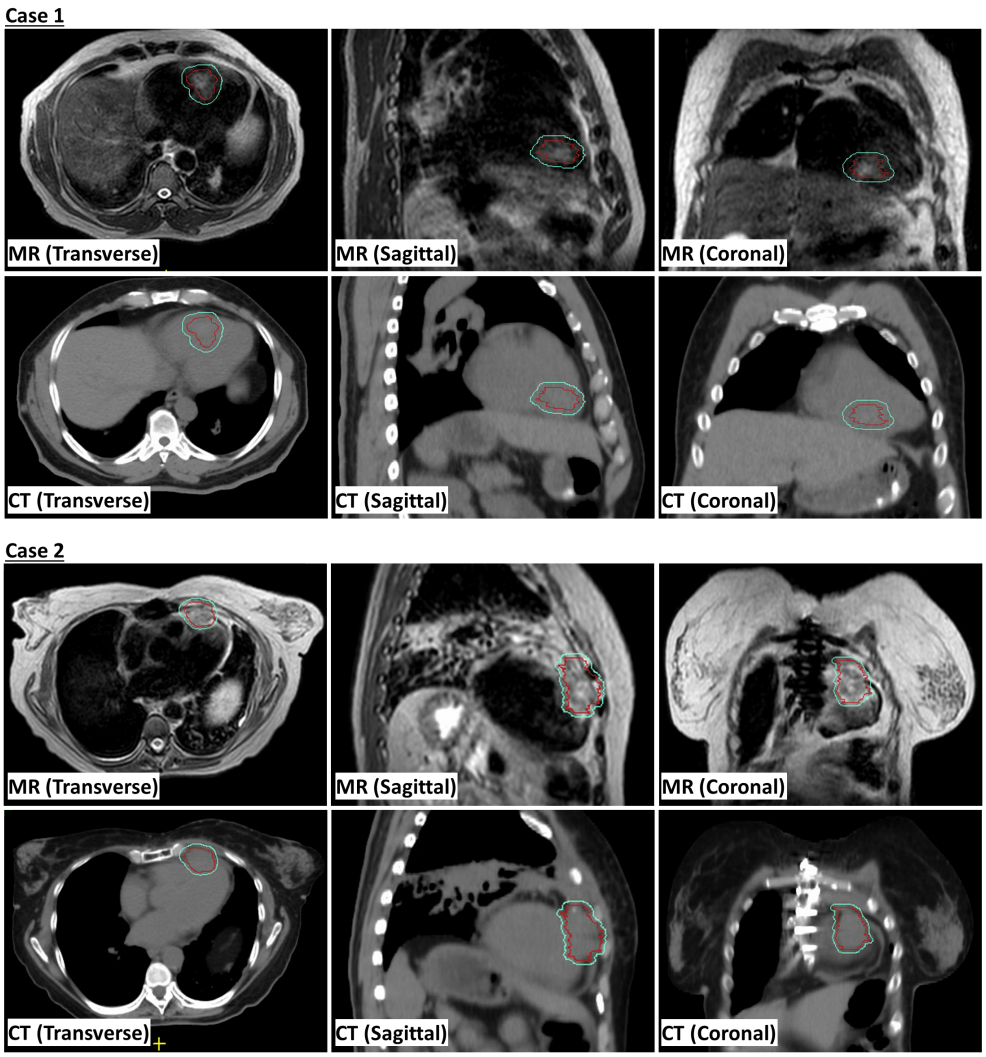

FIGURE 1
Magnetic resonance (MR) and computed tomography (CT) scans showing internal gross tumor volume (iGTV) in red and planning risk volume (PTV) in cyan.

in the tumor location, the patient was recommended for SBRT treatment on the MR-Linac in January 2022. The SBRT treatment plan was designed accounting for the prior thymic radiation. Three months post-treatment, the patient's chest pain was resolved. A CT chest with contrast suggested responsiveness of the pericardial mass and no progression of the original thymic carcinoma, as indicated in Figure 3. The centrally located anterior pericardial presumed metastasis remained controlled, along with the primary treatment-related changes in the anterior mediastinum, without evidence of local recurrence. A PET/CT scan acquired 6 months post-treatment revealed a reduction in size of the anterior pericardial metastasis, together with increased superior pericardial thickening. However, she was found to have recurrences outside of the SBRT field including a new 12 mm anterior pericardial and a 11 mm left lower lobe lung nodule. The new pericardial mass was separate from the treated cardiac metastasis. Both of new nodules were found to be within the radiation field of the primary mediastinum treatment. She also developed radiation pneumonitis and was treated with a long taper of high dose prednisone. Unfortunately, the patient had an acute myocardial infarction and died 8 months after her radiation treatment. This was felt to be unrelated to her SBRT treatment given her significant pre-existing significant coronary artery disease with history of coronary artery bypass surgery, stenting, and angioplasty.

4 Discussion

While cardiac metastases exhibit a higher incidence than primary cardiac tumors, they remain a rare disease. Currently, there is no standard for the treatment of cardiac metastases, and cardiac resection is infrequently recommended due to associated high risks and poor outcomes. Palliative interventions, chemotherapy, or radiotherapy (e.g., 24 Gy in 8 fractions) have been considered as treatment options (9, 10), yet these approaches demonstrate suboptimal prognosis. The emergence of SBRT and

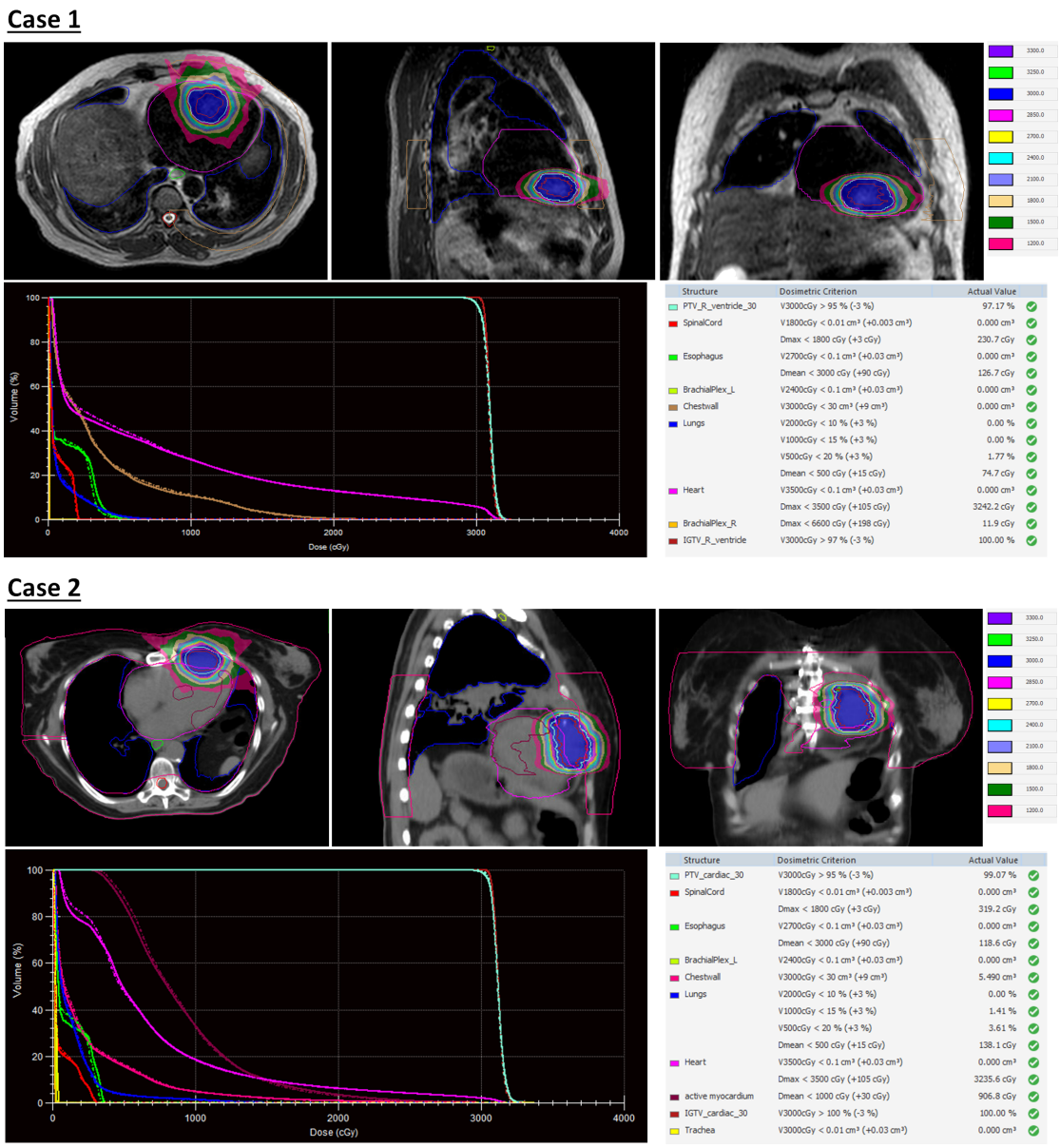

FIGURE 2
Dose distribution and dose-volume histograms (DVH) of the third fraction of stereotactic body radiation therapy (SBRT) treatment. In the DVH, solid curves represent the adapted plan and dash curves represent the reference plan created on simulation MR images.

MR-guided adaptive radiotherapy (MRgRT) has positioned radiotherapy as a curative option, providing patients with precise and highly conformal radiation treatments. Conventional CT scans lack sufficient imaging capabilities for accurate identification of cardiac tumors and surrounding cardiac structures. In contrast, the MR-linac system offers superior soft-tissue contrast, reducing uncertainties in target delineation and enhancing sparing of adjacent tissues. In addition, the daily verification of patient anatomy and adaptability of treatment plans enable dose escalation with acceptable acute toxicities. Further gains in the image quality and cardiac motion management can be made by the application of breath holding or beam gating techniques. MR-guided SBRT has found application in several cases involving primary (11–13) or metastatic cardiac tumors (14), with dose regimens ranging from 30-40 Gy in 5 fractions to 60 Gy in 12 fractions, achieving promising treatment responses and no acute adverse events. The reported histology includes angiosarcoma, primary and recurrent sarcoma, uveal, desmoplastic, and cutaneous melanoma, as well as breast intraductal carcinoma. Notably, both undifferentiated carcinoma (19.5%) and squamous cell carcinoma (18.2%) have high rates of cardiac metastasis (2). To the best knowledge of the authors, this study presents the first instance of patients with neuroendocrine carcinoma and squamous cell carcinoma cardiac metastases being treated using SBRT on a 1.5 Telsa MR-Linac. Although follow up for our patients was limited, MR-guided SBRT was delivered successfully with tumor regression and minimal acute toxicity suggesting that this may be a feasible treatment approach for cardiac metastases.

TABLE 1 Patient and treatment characteristics.

	Case 1	Case 2
Age	55	61
Gender	Male	Female
Histology	Neuroendocrine carcinoma	Squamous cell carcinoma
Site of tumor	Right ventricle septa wall	Anterior right ventricle
Prescription dose (Gy)	30	30
Number of fractions	3	3
Isodose prescription (PTV)	95%	95%
iGTV volume (cc)	12.45	21.59
Minimum iGTV dose	29.89	30.12
Max iGTV dose	32.14	32.99
PTV margin (mm)	5	3
PTV volume (cc)	38.53	40.07
Minimum PTV dose	28.64	29.21
Max PTV dose	32.38	32.99
PTV coverage	96.99%	99.57%
Monitor units	2267.4	2632.15
Beams	11	11
Segments	62	82

TABLE 2 Dosimetric criteria of targets and organs-at-risk (OARs) for the two cases.

Structure	Case 1		Case 2	
	Constraint	Planned	Constraint	Planned
iGTV	V3000cGy > 97%	99.98%	V3000cGy > 100%	100.00%
PTV	V3000cGy > 95%	96.99%	V3000cGy > 95%	99.57%
Spinal Cord	V1800cGy < 0.01 cm^3	0.0 cm^3	V1800cGy < 0.01 cm^3	0.0 cm^3
	Dmax < 1800 cGy	225.0 cGy	Dmax < 1800 cGy	301.8 cGy
Esophagus	V2700cGy < 0.1 cm^3	0.0 cm^3	V2700cGy < 0.1 cm^3	0.0 cm^3
	Dmean < 3000 cGy	121.0 cGy	Dmean < 3000 cGy	118.0 cGy
BrachialPlex_L	V2400cGy < 0.1 cm^3	0.0 cm^3	V2400cGy < 0.1 cm^3	0.0 cm^3
Chestwall	V3000cGy < 30 cm^3	0.0 cm^3	V3000cGy < 30 cm^3	4.939 cm^3
Lungs	V2000cGy < 10%	0.00%	V2000cGy < 10%	0.00%
	V1000cGy < 15%	0.01%	V1000cGy < 15%	1.23%
	V500cGy < 20%	1.45%	V500cGy < 20%	3.30%
	Dmean < 500 cGy	76.8 cGy	Dmean < 500 cGy	139.5 cGy
Heart	V3500cGy < 0.1 cm^3	0.0 cm^3	V3500cGy < 0.1 cm^3	0.0 cm^3
	Dmax < 3500 cGy	3237.7 cGy	Dmax < 3500 cGy	3246.6 cGy
BrachialPlex_R	Dmax < 6600 cGy	12.5 cGy	—	—
Active myocardium	—	—	Dmean < 1000 cGy	910.6 cGy
Trachea	—	—	V3000cGy < 0.01 cm^3	0.0 cm^3

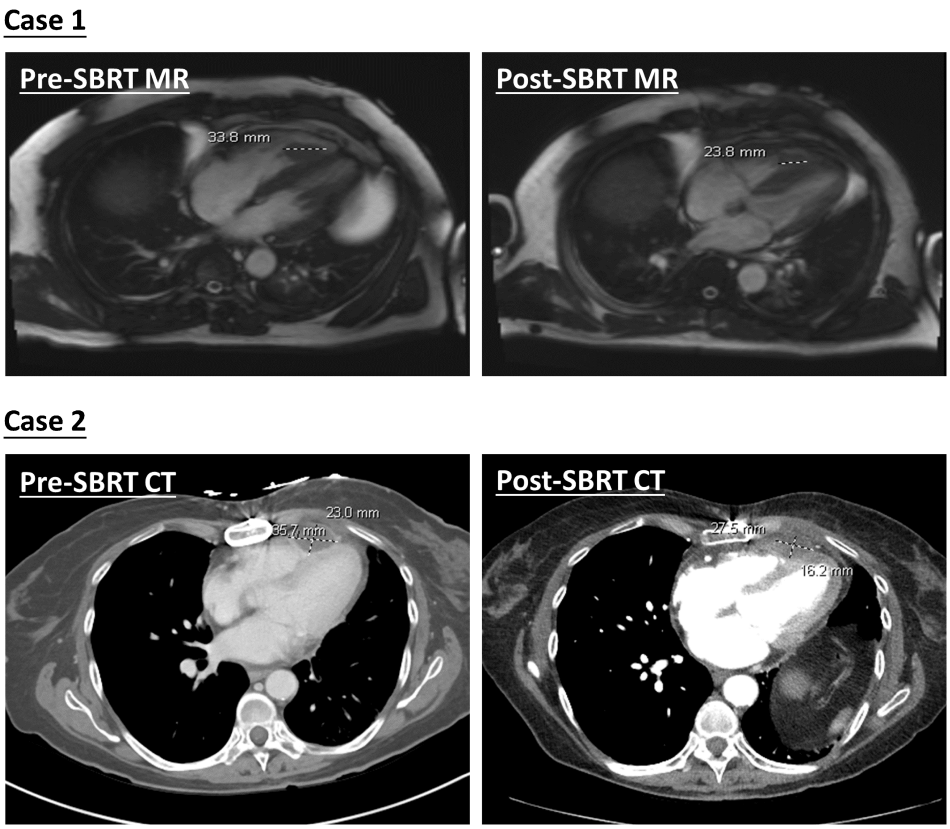

FIGURE 3
Demonstration of pre- and post-SBRT cardiac lesions. Diagnostic MR and CT images were both acquired with contrast agents.

5 Conclusions

We demonstrate the feasibility of using an MR-guided workflow for the treatment of cardiac metastases, yielding well-tolerated toxicities accompanied by symptomatic relief. Nevertheless, a more extensive dataset and extended follow-up periods are imperative for a comprehensive exploration of treatment efficacy. The growing interest and ongoing trials in the realm of hypo-fractionated SBRT delivered via MR-Linac promise avenue for addressing inoperable cardiac metastases. Continued research in this direction holds potential for refining treatment strategies and advancing patient outcomes.

Data availability statement

The raw data supporting the conclusions of this article will be made available by the authors, without undue reservation.

Ethics statement

The studies involving humans were approved by UT MD Anderson Cancer Center Institutional Review Board. The studies were conducted in accordance with the local legislation and institutional requirements. Written informed consent for participation was not required from the participants or the participants' legal guardians/next of kin in accordance with the national legislation and institutional requirements. Written informed consent was not obtained from the individual(s) for the publication of any potentially identifiable images or data included in this article because This is a retrospective study covered by an institutional review board (IRB)-approved protocol (2022-0521). Informed patient consent is waived in this protocol due to the nature of a retrospective study.

Author contributions

XC: Conceptualization, Data curation, Investigation, Methodology, Validation, Visualization, Writing – original draft. JW: Conceptualization, Data curation, Investigation, Methodology, Validation, Visualization, Writing – review & editing. AS: Data curation, Investigation, Validation, Writing – review & editing. BL: Data curation, Investigation, Writing – review & editing, Validation. NH: Data curation, Investigation, Validation, Writing – review & editing. MM: Data curation, Investigation, Validation, Writing – review & editing. YZ: Data curation, Investigation, Validation, Writing – review & editing. XW: Validation, Writing – review & editing. XZ: Validation, Writing – review & editing. JN: Validation, Writing – review & editing. SS: Validation, Writing – review & editing. LC: Supervision, Validation, Writing – review &

editing. ZL: Supervision, Validation, Writing – review & editing, Funding acquisition. PL: Writing – review & editing, Funding acquisition, Resources, Supervision, Validation. JY: Writing – review & editing, Funding acquisition, Resources, Supervision, Validation.

Funding

The author(s) declare financial support was received for the research, authorship, and/or publication of this article. This work was supported in part by the National Institutes of Health through Research Project Grant R01HL157273-03 and Cancer Center Support (Core) Grant P30016672, start-up funds from MD Anderson Cancer Center, and a grant from the Radiation Oncology Institute (ROI2022-9133).

Conflict of interest

The authors declare that the research was conducted in the absence of any commercial or financial relationships that could be construed as a potential conflict of interest.

Publisher's note

References

1. Rahouma M, Arisha MJ, Elmously A, El-Sayed Ahmed MM, Spadaccio C, Mehta K, et al. Cardiac tumors prevalence and mortality: A systematic review and meta-analysis. *Int J Surg*. (2020) 76:178–89. doi: 10.1016/j.ijsu.2020.02.039

2. Bussani R, Castrichini M, Restivo L, Fabris E, Porcari A, Ferro F, et al. Cardiac tumors: diagnosis, prognosis, and treatment. *Curr Cardiol Rep*. (2020) 22:169. doi: 10.1007/s11886-020-01420-z

3. Tyebally S, Chen D, Bhattacharyya S, Mughrabi A, Hussain Z, Manisty C, et al. Cardiac tumors. *JACC CardioOncology*. (2020) 2:293–311. doi: 10.1016/j.jaccao.2020.05.009

4. Goldberg AD, Blankstein R, Padera RF. Tumors metastatic to the heart. *Circulation*. (2013) 128:1790–4. doi: 10.1161/CIRCULATIONAHA.112.000790

5. Fotouhi Ghiam A, Dawson LA, Abuzeid W, Rauth S, Jang RW, Horlick E, et al. Role of palliative radiotherapy in the management of mural cardiac metastases: who, when and how to treat? A case series of 10 patients. *Cancer Med*. (2016) 5:989–96. doi: 10.1002/cam4.619

6. Bonomo P, Cipressi S, Desideri I, Masi L, Doro R, Iermano C, et al. Stereotactic body radiotherapy with cyberknife for cardiac Malignancies. *Tumori J*. (2015) 101:294–7. doi: 10.5301/tj.5000280

7. Bonomo P, Livi L, Rampini A, Meattini I, Agresti B, Simontacchi G, et al. Stereotactic body radiotherapy for cardiac and paracardiac metastases: University of Florence experience. *Radiol Med (Torino)*. (2013) 118:1055–65. doi: 10.1007/s11547-013-0932-0

8. Winkel D, Bol GH, Kroon PS, Van Asselen B, Hackett SS, Werensteijn-Honingh AM, et al. Adaptive radiotherapy: The Elekta Unity MR-linac concept. *Clin Transl Radiat Oncol*. (2019) 18:54–9. doi: 10.1016/j.ctro.2019.04.001

9. Maebayashi A, Nagaishi M, Nakajima T, Hata M, Xiaoyan T, Kawana K. Successful surgical treatment of cardiac metastasis from uterine leiomyosarcoma: A case report and literature review. *J Obstet Gynaecol Res*. (2020) 46:795–800. doi: 10.1111/jog.14231

10. Hiroi S, Miguchi M, Ikeda S, Nakahara H, Shinozaki K, Nishisaka T, et al. Capecitabine plus bevacizumab for cardiac metastasis of sigmoid colon cancer: case report and literature review. *In Vivo*. (2020) 34:3413–9. doi: 10.21873/invivo.12180

11. Noyan A, Yavas G, Efe E, Arslan G, Yavas C, Onal C. Cardiac angiosarcoma treated with 1.5 Tesla MR-guided adaptive stereotactic body radiotherapy – Case report and review of the literature. *Int J Surg Case Rep*. (2022) 98:107521. doi: 10.1016/j.ijscr.2022.107521

12. Corradini S, Von Bestenbostel R, Romano A, Curta A, Di Gioia D, Placidi L, et al. MR-guided stereotactic body radiation therapy for primary cardiac sarcomas. *Radiat Oncol*. (2021) 16:60. doi: 10.1186/s13014-021-01791-9

13. Pomp J, Van Asselen B, Tersteeg RHA, Vink A, Hassink RJ, van der Kaaij NP, et al. Sarcoma of the heart treated with stereotactic MR-guided online adaptive radiation therapy. *Case Rep Oncol*. (2021) 14:453–8. doi: 10.1159/000513623

14. Sim AJ, Palm RF, DeLozier KB, Feygelman V, Latifi K, Redler G, et al. MR-guided stereotactic body radiation therapy for intracardiac and pericardial metastases. *Clin Transl Radiat Oncol*. (2020) 25:102–6. doi: 10.1016/j.ctro.2020.10.006

Frontiers in Oncology

Advances knowledge of carcinogenesis and tumor progression for better treatment and management

The third most-cited oncology journal, which highlights research in carcinogenesis and tumor progression, bridging the gap between basic research and applications to imrpove diagnosis, therapeutics and management strategies.

Discover the latest Research Topics

See more →

Frontiers

Avenue du Tribunal-Fédéral 34
1005 Lausanne, Switzerland
frontiersin.org

Contact us

+41 (0)21 510 17 00
frontiersin.org/about/contact